A Machine Vision System for the Real-Time Fiber Orientation Measurement of Tubular Braided Preforms

by

Alexander Jeffrey Hunt

A thesis submitted in partial fulfillment of the requirements for the degree of

Master of Science

Department of Mechanical Engineering
University of Alberta

Abstract

Braided composite materials are a class of fiber reinforced composite materials which obtain their unique material properties from the interlaced fiber structure. The fiber orientation has a critical impact on the resulting material properties of the composite component and as a result, the quality assurance of the braid angle should be an essential step in the production process. To improve the braiding process, a non-intrusive and automated braid angle measurement technique was developed using machine vision principles. The use of a CCD camera and frequency domain image processing allowed the braid angle of stationary and dynamic tubular braid preforms to be measured. This technique was found to have lower uncertainty when compared to currently used manual measurement techniques with the additional benefit of allowing measurements to be made in real-time without user interaction.

Dedication

This thesis is dedicated to my parents, Ralph and Wendy Hunt, brother, Edward Hunt, and my fiancée Cristina Castillo for their unwavering love and support.

Table of Contents

List of figures

List of tables

Chapter 1 Introduction

1.1 Motivation

Braided composite materials have numerous applications in automotive [1], structural [2] and aerospace industries [3]. Two dimensional braided composites are often produced on a maypole braider. The braided fiber structure, called the braid preform, is produced atop a shape giving mandrel. The braid angle, which is a measure of the fiber orientation of the braided structure, has been shown to strongly influence the material properties of the composite part. Predictive models have shown that a 3° change in braid angle causes a 19% change in elastic modulus of a biaxial braided composite [4]. Due to the importance of the fiber orientation, it is often measured post production to ensure that the desired fiber orientation has been produced. The braid angle is most often measured using manual measurement techniques; however, the manual measurement techniques are prone to human error, resulting in uncertainties ranging from ±1° to ±2° degrees [5, 6]. This makes fiber orientation quality assurance a time consuming and error prone process which should be improved to improve the confidence in the material properties of braided composites.

To address this issue, a non-intrusive and automated braid angle measurement technique was developed using machine vision principles. A non-intrusive technique will allow the system to be applied to different braiding setups and will allow measurements to be made during the braiding process. An automated measurement system will remove human error from the measurement process and reduce the time taken to produce a braided preform.

1.2 Thesis objectives

For this thesis, a single camera machine vision system will be developed to measure the braid angle of tubular braided preforms in real-time during the manufacturing process. The image processing measurement system using the two-dimensional discrete Fourier transform is developed and an image preprocessing method will be validated for measuring tubular braided samples. The error associated with the single camera system will be considered and the measurement technique will be applied to an in-line braiding application where braid angle measurement will be made of preforms with a constant braid angle and a transient braid angle.

1.3 Thesis scope

This thesis work develops an optical braid angle measurement technique capable of measuring the braid angle of biaxial braids in real-time. Such a system has the potential for further automating the braiding process. This system will eventually be used in a control system to adapt braid angle during production. Several types of braiding machines are capable of producing biaxial braids, however, this work has been developed for a 36-carrier horizontal maypole braiding machine. 2D braided fibers can be deposited onto many different mandrel shapes due to the conformability of the structure and the ability for the fibers to lie on non-geodesic yarn paths [7]. Tubular braided preforms are simple structures which take advantage of the axis of symmetry of the braiding machine and can be produced in a continuous fashion which would benefit from automated visual inspection processes. Examples are braided composite rebar [2] and braid tubes. The tubular mandrel geometry is also a simple geometry which can be used to validate the accuracy of the measurement system. Once the machine vision system has been validated for measuring the fiber orientation of static tubular preforms, the process can be tested in-line on braided preforms that are produced with constant and non-constant braid angles.

1.4 Thesis outline

This thesis consists of 5 chapters. A discussion on the shortcomings of 2D braiding is given in Chapter 2. These topics are focused on the current limitations of the production of the fiber preform, which are the current measurement techniques used to measure the fiber orientation and the inaccuracies and difficulties associated with predicting the braided fiber structure. In Chapter 3, the image processing scheme is developed and validated for the measurement of tubular braided preforms. This begins with a discussion on the integration of visual inspection systems with textile and fiber reinforced composite production. The error associated with the image collection is discussed and is compared to a fiber distribution model to predict perspective error. In Chapter 4, the image processing technique is used in a machine vision system to measure the fiber orientation of tubular braided preforms during the braiding process. Preforms with constant braid angles are measured to determine the accuracy of the measurement technique. Preforms with non-constant braid angles are compared to a well-known 2D braiding model [8]. A summary of the work, as well as a discussion about the limitations and future work can be found in Chapter 5.

The appendices consist of additional information to supplement the methods used in this work. Appendix A consists of additional information regarding the periodicity of the two-dimensional discrete Fourier transform in which the effect of image boundaries influences the frequency spectrum. Spatial techniques used to compensate for this periodicity are discussed and applied to braid images. Appendix B consists of a mathematical validation showing the preserved angular orientation between the spatial and frequency domains. Additional results regarding spatial image preprocessing techniques can be found in Appendix C. The results of the braiding speed and puller speed calibrations are shown in Appendix D.

1.5 References

[1] B. Schmitt, "The Making of the Lexus LFA Supercar. An inside report, chapter 2, The Clean Room," .

[2] M.A. Ivey, J.P.R. Carey and C. Ayranci, "Braid reinforced polymeric rebar production and characterization," in International SAMPE Technical Conference, 2014.

[3] A.D. Kelkar, J.S. Tate and R. Bolick, "Structural integrity of aerospace textile composites under fatigue loading," Materials Science and Engineering: B, vol. 132, pp. 79-84, 2006.

[4] C. Ayranci, "Predicting the Elastic Properties of Two Dimensionally Braided Tubular Composite Structures Towards the Design of Braid-Reinforced Polymer Medical Catheters," ProQuest Dissertations and Theses, 2010.

[5] A.J. Hunt and J.P. Carey, "Geometry Measurement of Tubular Braided Composite Materials for Real-Time Applications," in CANCOM 2015 - Canadian International Conference on Composite Materials, 2015.

[6] J.H. Van Ravenhorst and R. Akkerman, "Circular braiding take-up speed generation using inverse kinematics," Compos Part A Appl Sci Manuf, vol. 64, pp. 147-158, 2014.

[7] W. Michaeli, U. Rosenbaum and M. Jehrke, "Processing strategy for braiding of complex-shaped parts based on a mathematical process description," Composites Manuf., vol. 1, pp. 243-251, 1990.

[8] G.W. Du and P. Popper, "Analysis of a circular braiding process for complex shapes," Journal of the Textile Institute, vol. 85, pp. 316-337, 1994.

Chapter 2 Literature Review

The design process requires, among a number of other variables, a concrete understanding of the material properties of all materials and components used in the structure. The same is true when using braided composite materials. The material properties of braided composite materials are highly tailorable and are strongly influenced by a number of factors. Multiple works have shown the importance of braid angle, fiber volume percent, crimp angle and braid pattern [1-5] when forming these composite materials. Additionally, the position of the mandrel relative to the braiding machine affects fiber deposition [6], which influences the braid angle of the fibers. Fiber position has been shown to influence all mechanical properties and material behavior including moduli [7-10], strength [11, 12], fatigue loading [13-15] and deflection [16]. Thus, to ensure that the braided composite component adheres to the predicted materials properties from the design process, precise control and quality control of the fiber position during production is required for the successful and economical production of these materials.

In this chapter, the strong relationship between fiber placement and material properties is discussed. This is followed by a discussion on modelling techniques used to generate fiber preforms. Finally, a discussion regarding the ability to use machine vision to bridge the quality gaps seen in the modelling techniques in the braided composite industry is presented.

2.1 Shortcomings in braiding and manufacturing of braided composites

The multi-step manufacturing process required to produce braided composite materials induces a level of material property variation between samples [17-19]. This variation negatively affects the confidence of predicted material properties and is undesirable for high performance applications. Chen et al [6] investigated the effects of small changes in braid angle with respect

to several defining characteristics of triaxial braided components finding that small changes in braid angle strongly influenced the transverse properties of triaxial braids. Chen et al. [20] also reported being able to produce flat triaxial panels with a braid angle within ±3 degrees. These unwanted braid angle distributions have been reported in other studies. Lomov et al [18] reported such distributions when measuring their flat glass fiber composite samples which were produced on a flat braiding machine. They found that the average braid angle across the sample was always less than the central braid angle. Birkefeld et al. [17] also reported a braid angle variation along their flat braided composite samples. Tate and Kelkar [11, 15] found braid angle variations across a sample to be between ±1° and ±2° for flat biaxial braided samples made from braided tubes. This suggests that manipulating the fiber structure prior to fiber consolidation adversely affects the braid angle within a braided sample. These variations in braid angle are not known until a series of braid angle measurements are taken for each sample. This can be time consuming, especially when multiple measurements must be made of each samples [17, 18] and measuring the braid angle manually is prone to human error when either aligning the measurement tool or selecting the landmarks in an image. However, it is unclear at what stage of the manufacturing process these variations occurs.

Apart from the fiber structure being produced, as noted above, there are shortcomings also related to the manual impregnation process used to produce tubular braided composites. Melenka et al [21] found that tubular braided composite materials can possess a significant void content introduced during the impregnation process. The presence of voids has been shown to affect fiber breakage and failure of braided composites [22]. Manual impregnation can also distort the fiber architecture prior to curing.

As it can be seen, unforeseen consequences of the manufacturing process can introduce flaws or contribute to phenomena in braided composite materials that can influence their material properties in ways which are not accounted for in predictive design models. The scope of this work lies with focusing on the issues related to fiber placement during the two dimensional (2D) braiding process. There are two aspects related to the production and inspection of braided composite materials to be discussed in this chapter. The first of which will be a discussion of the current modelling approaches that have been developed to relate fiber orientation to braiding machine speeds. The second will be a review of the techniques that are currently used to measure fiber orientation in braided composites, as well as other types of fiber reinforced composites.

2.2 2D braids and the 2D braiding process

2.2.1 The production of 2D braids

2D braids encompass a number of different braid architectures including biaxial, triaxial and flat braids. To produce the desired braid pattern, maypole, flat, radial and rotary braiding machines can be used to suit the application. This work focuses on the production of 2D biaxial braids with a horizontal maypole braider as one case study of the production process.

The maypole braiding machine and all critical components are shown in Figure 2-1. To produce the braided structure, the maypole braiding machine has two sets of yarn carriers which rotate in opposing sinusoidal paths around the mandrel. The sinusoidal path is achieved by the horn gears, which consist of a slotted plate connected to a spur gear. The rotation of the horn gears propels the yarn carriers around the track plate of the braiding machine. To control the convergence point of the braid, a guide ring is used [23] and the reduction of the size of the guide

ring relative to the size of the mandrel can reduce the time taken to reach steady state [24] The geometry of the maypole braiding machine, such as the radius of the track plate, size of the guide ring and the shape of the mandrel, affect the resulting braid pattern. However, all geometric features held constant, the braiding machine speeds are the critical process parameters which are varied to produce the desired braid pattern.

Figure 2-1: Annotated image of a horizontal maypole braiding machine showing the various components of the machine

The production parameters of the maypole braiding machine are the take up and yarn carrier speeds. The braiding schematic in Figure 2-2 shows how each of these process parameters affects the braiding process. Variation of these process parameters will allow the designer to control the fiber orientation of the braided fibers on the mandrel which, as previously discussed, has a significant impact on the material properties of the composite part. Like all fiber reinforced composite materials, the fiber orientation has the strongest influence on the resulting material properties.

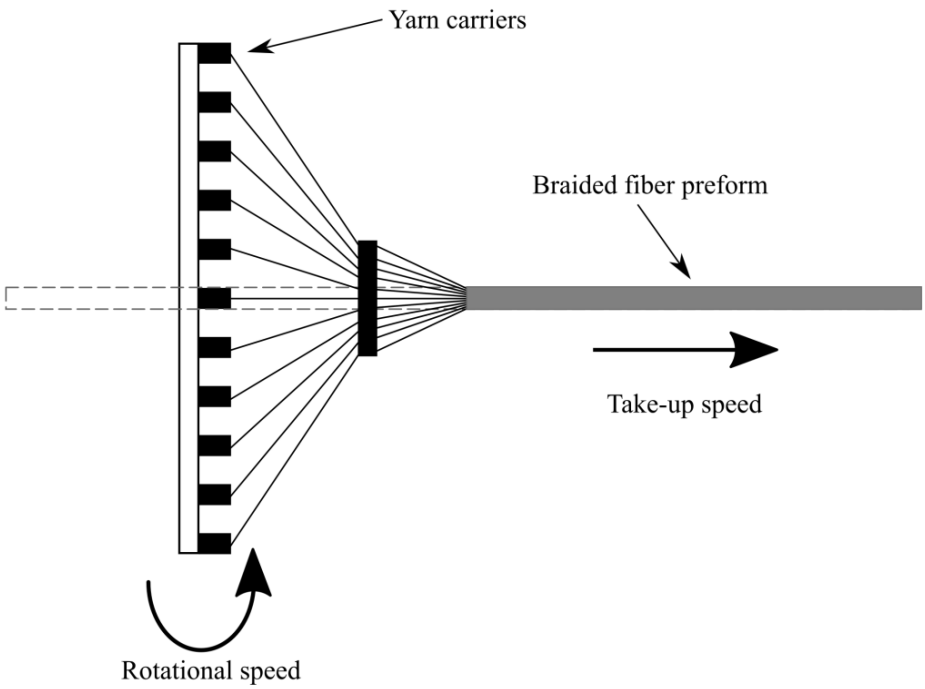

Figure 2-2: Schematic of a maypole braiding machine showing the rotational speed of the yarn carriers and take up speed of the fiber preform

The braid angle is used to quantify the fiber orientation of braided fiber structures. This is a measure of the orientation of the fibers relative to the longitudinal axis of the mandrel, as shown in Figure 2-3. The braid angle has been identified in multiple ways in literature. The most common way is the direct measurement of the superficial angle on the surface of the braided structure. The second way is to infer the braid angle from the length of the preform and pick spacing of the braid. This method has been developed in ISO 10122 for determining the braid angle of braided tubes [25]. By comparing the length of a single braid yarn, L_v to the length of the preform, L_t, the braid angle can be determined with Equation 2.1. This relation assumes that a perfect helical path is followed by the yarn. Due to the requirement of removing a yarn from the preform for measurement, this process may not be suitable for all applications.

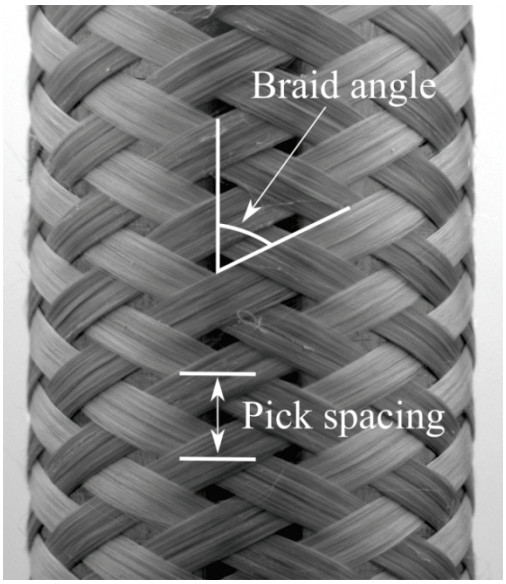

Figure 2-3: Annotated braid preform showing the braid angle and pick spacing on a tubular braid preform

$$\cos\theta_t = \frac{L_t}{L_v} \tag{2.1}$$

2.2.2 Braiding process models

The critical step in the design process of a braided composite is the determination of the required fiber geometry to achieve the desired material properties. To produce the desired braid geometry, a relationship between the process parameters and the fiber structure must be established. This is done with braiding process models which relate the braider geometry and mandrel geometry to the braided fiber structure. This work has a significant impact on the braiding process as they provide the tools to design and manufacture specific fiber structure relations between manufacturing process parameters and final braid geometry. There are two main approaches used to derive braiding process models. The first technique approaches the problem with geometric relations that map the fiber path onto the mandrel surface to predict the final yarn geometry. The second approach takes advantage of finite element techniques to model the final braid structure.

2.2.2.1 Geometry based kinematic models

Geometry based kinematic models derive vectors to represent the yarn path from the yarn carrier to the surface of the mandrel. These vectors can be mapped onto the surface of the mandrel, producing the predicted fiber preform. A large majority of models that use this approach rely entirely on braid kinematics and geometry, which makes the models simpler at the expense of neglecting some phenomenon which occurs during the braiding process. Geometry based kinematic models make a number of assumptions, the effects of which become more pronounced for braiding machines with a large number of yarns [11].

These types of models began with work done by Michaeli et al [6] who aimed to develop a generalized model of the tubular braiding process for design purposes. They discussed some of the process limitations of the circular braiding process, such as the maximum allowable mandrel eccentricity and fiber slippage on complex mandrel shapes, which can lead to adverse changes in braid angle and built the based framework of a machine control strategy, as well as a processing strategy to determine the feasibility of the desired braid pattern.

Du and Popper [26, 27] developed a series of equations to predict the fiber orientation on simple and complex axisymmetric mandrel shapes. A common assumption in the derivation of these kinematic models is neglecting frictional effects. This eliminates the need to consider any yarn interactions and allows the assumption that the yarn remains straight in the convergence zone to be made [2, 5, 26, 28-30]. Additional to this nearly universal straight yarn assumption, Du and Popper also assumed negligible friction between the yarns and the mandrel and that there is no yarn slippage once the yarns make contact with the mandrel. Their experimental work involved braiding over a number of different mandrels, including cylindrical and tapered mandrels. They found an accurate calculation of the convergence plane; however, the expected braid angle at

steady state was consistently 5° less than the measured value. This issue is believed to indicate that the yarns do not remain straight in the convergence zone. For tests with a more complex mandrel shape, the braid angle discrepancy between the measured and predicted reached a maximum of 10°.

Using a different geometry based approach, Ravenhorst and Akkerman [28] developed a set of kinematic braiding equations for predicting the braid geometry for complex mandrel shapes. Here, they neglect the friction between the yarn and the guide ring. They reported a braid angle error of 3° in non-tapered regions, and approximately 10° in tapered regions which is attributed to the bias yarn interactions which are not accounted for. They also found that having an eccentric mandrel relative to the braiding machine caused a maximum scatter of 7° when comparing different circumferential locations of the braid mandrel. The negative effect of mandrel eccentricity was also reported in Michaeli et al [6].

Mazzawi [24] used braiding equations from Ko's work [31], as well as developed a new model for predicting the braid structure on cylindrical and conical mandrels respectively. They found that when over braiding cylindrical mandrels, the measured value of the convergence length was between 12 and 25mm of the predicted value. Due to the relationship between convergence length and braid angle in these equations, this will lead to inaccurate braid geometry predictions. To braid over a conical mandrel, Mazzawi [24] used a stepwise procedure where to reduce the transient motion of the deposit plane, at specified intervals, the process was stopped and the mandrel was displaced to adjust the convergence length to the new steady state value prior to braiding the next section. This method was deemed unsuccessful in accurately producing conical braids with a 100% cover factor.

Guyader et al [2] used the common assumptions including no slippage on the mandrel and straight yarns in the convergence zone to derive a set of equations capable of predicting yarn slippage and relaxation of yarns during the braiding operation. To validate their model, a transient braid pattern was obtained by accelerating the mandrel linear velocity from 5 mm/s to 15 mm/s. The results from their model are compared to the speed of the convergence plane and the change in the braid angle along the mandrel. For tests performed by accelerating and decelerating the mandrel speed, maximum deviation between expected and measured braid angle was approximately 3° for a tubular mandrel.

Nishimoto et al [32] developed a model to allow the generation of tubular braids with a circumferentially varying braid angle. Their work depended on assuming that the inter-yarn forces and interactions can be neglected, thus leading to the conclusion that the yarns will remain straight in the convergence zone. They modelled the use of an elliptical guide ring to achieve a desired circumferential braid angle distribution on the tubular mandrel. Differences of up to 3° between their model and experimental results were attributed to variations in fiber speed, which could be caused by friction between the yarns or the guide ring, as well as motion of the fell point of the fibers due to the elliptical guide ring.

Rawal et al [33] assume no frictional effects between yarns, no slippage once the fibers make contact with the mandrel, no friction between the yarns and the mandrel and there is no yarn crimp. They modelled sparse, open mesh braids with cover factors less than 25% for a number of different mandrel shapes including cylindrical, square prism and conical. Their experimental braid angle measurements deviated from the predicted model results from 1°-4° of error for tubular mandrels. A second study by Rawal et al [5] was done to again model the braiding process of open mesh braids over axisymmetric mandrels. In this work, the undulating yarn path

was taken into account. These results show a much better agreement between the simulation and experimental results, with a maximum error between measured and predicted values of approximately 1 degree. However, the strand path equations are not related to machine process parameters, and as a result, may not be the first choice for manufacturing or design.

Nishimoto et al [30, 34] explored the transient nature of the braiding process by developing a model to predict the change in braid angle accompanied by a stepwise change in braiding machine speeds. The model relies on the assumption that the yarns remain straight in the convergence zone. Their work accurately predicts the transient change in braid angle due to a stepwise change in machine speeds. However, they do not explore the model results once they reach the steady state geometry. Nishimoto et al. relate the braid angle to the convergence zone length in the same way as Mazzawi [24] inferred the braid angle from the half cone angle which he measured during the braiding process.

2.2.2.2 Yarn Interaction Models

Mechanics based approaches

The presence of inter-yarn forces in the braiding process has been discussed by Brunschweiler [23], Zhang et al. [4], Rawal et al. [35], and Ravenhorst and Akkerman [36]. Kinematic braiding models have been developed through mechanics based approached. The work done by Zhang et al. [37] used a static force analysis to analyze the interlacing points. They produced braids at a range of braid angles using both glass fiber and cotton yarns to study the effect of interyarn friction. They showed that the use of their mechanics based model was capable of providing a better prediction for braids produced with cotton yarns. The high inter-yarn friction seen in cotton yarns resulted in a 10.4° error between the measured and predicted values from a geometric kinematic model. The use of the mechanics based model reduced this error by 59%.

Inaccuracies in this model arise from the inability to model the stick slip behavior and to not consider the serpentine path of the yarn carriers [37]. Ravenhorst and Akkerman [36] developed a model, building upon their past work [28] to include yarn interactions. In this work, emphasis was placed on determining the importance of yarn interactions on the braiding process. Yarn paths in the convergence zone were modelled using the developed yarn interaction model for varying inter-yarn coefficients of friction. Tracking of the true yarn paths using close range photogrammetry allowed the experimental yarn paths to be matched with the simulated curves. For the case of a radial braider, the true convergence length was found to be 25% of the frictionless condition, which is commonly assumed. This shows the effect that inter-yarn friction has on the braiding process.

Finite element approaches

Finite element approaches have been shown to have an increased level of accuracy over kinematic models at the expense of computational time, required user knowledge and complexity. The model developed by Pickett et al [38, 39] used finite element techniques to model the strand path during two-dimensional braiding. When compared to the analytical kinematic models discussed in the previous section, finite element techniques allow the modelling of inter-yarn friction, mechanical properties of the yarns during the braiding process, and friction at all points of contact on the yarns at the expense of high computational time [39]. 2D braiding simulations using finite element techniques can take two days of computation time on high performance computers. However, in order to obtain accurate results, numerous parameters must be known and validated for an each unique braiding scenario and mandrel type. Yarn properties including magnitude of inter-yarn forces, yarn bending stiffness, inter-yarn friction, yarn bobbin tension as well as friction between the yarns and guide ring [38, 39] are

required and an extensive knowledge in finite element techniques may be required to perform a predictive braiding simulation. A series of experiments must be conducted prior to the simulation process to quantify many the required values for the simulation [39].

2.2.3 Summary of modelling techniques

Geometric kinematic models rely on representing the fibers as vectors and determining the orientation of these vectors based on braiding machine geometry. These models can range in complexity, from considering the cross-sectional yarn shape [5] to modelling only a single yarn [4, 26, 27]. These types of models are useful because they are capable of producing empirical equations that relate the braiding process parameters to the braid geometry. These types of models contrast finite element techniques for modelling braid geometry. The successful application of these models requires an understanding of finite element principles, experimentally determined yarn properties and processing times which can span several days. The setup and validation of these approaches requires specialized knowledge and may not be the first choice for many textile composite engineers.

For manufacturing applications, geometric models have the advantage of the inverse solution [26, 28, 36] which allows the computation of a machine speed profile for a desired geometry profile. The inverse solution is useful for automatic braiding applications [26, 40] as it utilizes a similar methodology to the inverse kinematics of robotics motion [28].

The primary advantage of these geometric models is their simplicity. This simplicity comes at the expense of absolute model accuracy due to the neglection of phenomena that occurs during the braiding process. There are, however, scenarios where these assumptions are valid; for braiding setups with a small number of low friction yarns, the yarn interaction effects may not be as severe [37]. However, as was previously discussed, the possibility for these models to

inaccurately predict the braid angle reduces the confidence in the ability to produce the desired fiber structure. As a result, braid angle must be meticulously verified to ensure that the braid structure is of acceptable quality. Even with these shortcomings, these modelling approaches are still widely used for braid production applications. To increase the confidence in these currently used predictive models, the method in which the braid angle is measured can be improved. Rather than assessing the fiber geometry after the braiding process has been completed, the braid angle can be measured in-line with the braiding process as a quality control system. This gives the user the flexibility of using the previously used predictive models, as well as the ability to immediately compare the predicted and measured braid angles in real-time. The development of such a measurement system can also be applied to the development of a feedback loop to automatically adjust machine speeds to compensate for any undesirable braid geometry.

2.3 Braid angle measurement techniques

The kinematic braiding models discussed in Section 2.2.2.1 are widely used to calculate appropriate braiding process parameters for specified braid geometry. However, due to the possibility for inaccuracies in the production of the fiber structure with these models, the braid angle is often measured manually to ensure that the fiber orientation is within acceptable limits. The following section outlines many of the currently used measurement techniques and how they apply to the braided composite manufacturing process.

2.3.1 Manual measurement techniques

Handheld measurement tools suffer from error associated with alignment of the tool and reading the correct angle. The minimum increment on these tools is 1°, and combined with human error, these methods have a minimum error of ±1°. Repeat measurements of a unit cell were made using a protractor and a deviation of ±1° was reported [41].

Mazzawi [24] measured the braid angle of fiber preforms with a 100% cover factor by using a transparency wrapped around the preform and tracing the path of a single, pre-coloured fiber and measuring the braid angle from the unwrapped transparency [24]. This similar technique was used by Ayranci [42] where the yarn path was traced onto transparent paper, unwrapped and measured with a protractor. Zhang et al [37] used a flexible plastic protractor held by hand up to the braided specimen. They took 5 to 10 measurements per sample in their work. A goniometer was used by Ravenhorst and Akkerman [36] to measure the braid angle.

In each of these techniques, direct contact with the sample must be made, meaning that the fiber orientation can be altered by tracing or the placement of measurement tools. Additionally, the braided preform must be taken out of the production line for measurement, which is undesirable for an automated system.

2.3.2 Optical/image based measurement techniques

Optical and image based techniques offer the advantage of being non-contact measurement methods. However, image based measurements can still be affected by human error through landmark identification and boundary tracing. For such methods, uncertainties of ±2° are expected [28]. Due to the ability to accurately place landmarks in an image, repeatability of image based measurements was shown to be improved over manual techniques. For a digital image correlation approach, repeat measurements of a unit cell showed an uncertainty of ±0.54° [19]. These optical and image based techniques range from simple methods using basic software, such as imageJ [35, 43]. This software allows the used to trace vectors overtop of significant features in the image (fibers) and to compute the angle between these fibers, giving the braid angle. In a similar fashion, Lomov et al [18] also measured the fiber direction using an

image based method. X-ray CT images were taken of the flat glass fiber composite which allowed the central braid angle to be measured from the image.

Apart from these types of techniques, there are also a series of more complex image based methods used to capture the 3D shape of woven and braided fiber structures. For tubular samples, more advanced measurement methods using digital image correlation (DIC) was used [8, 19, 44]. This allows the 3D shape of the tubular surface and the curvature of the yarns to be taken into account and this provided braid angle measurements to within ±0.37° when measuring the change in braid angle due to the application of a tensile load. Ravenhorst and Akkerman [28] have used a multi-image photogrammetry technique which allows the study of a 3D fiber orientation. In this method, the fiber is selected by choosing the start and end landmarks and as a result, is accurate to ±2°. The photometric stereo technique to determine the fiber orientation of woven carbon fiber surfaces by Zambal et al [45]. This method requires several images to be captured with different lighting conditions. This allows the surface normals of a 3D surface to be estimated with the multiple irradiance values at each point. This measurement technique relies on knowing the reflectance behavior for the specific material; in cases where the reflectance properties are known, low measurement error, ranging between 0.37° to 0.55° is achieved. However, due to the dependence on an accurate reflectance model, error can significantly increase with incorrect material reflectance properties [46]. Another limitation of this technique is the sample cannot be moved in-between frames [47].

While these methods have been successful in allowing measurements of braid geometry to be made, they are both strongly dependent on user input to align the measurement tools, or to select the landmarks in the images. For the case of the 2D DIC technique, the computation time associated with the image processing method is also significant, and for the photogrammetry

approach, the user must select landmarks from the images, which makes these more advanced techniques ill-suited for real-time applications.

2.3.3 Real-time/in-line techniques

Mazzawi et al [24] developed an inline braid geometry measurement technique which does not use optical techniques, but uses a unique mechanical device. Their technique relies on the relationship between the convergence length of the fibers and the braid angle of the preform, which is commonly derived for simple shaped mandrels with a uniform cross section [26]. As the convergence zone increases or decreases in length, the cone angle changes, and the mechanical mechanism consisting of a pinned bar and a potentiometer attached to the guide ring is able to measure this cone angle. By knowing the fiber point of contact on both the guide ring and the mandrel, the length of the convergence zone can be obtained, which allows calculation of the braid angle.

2.3.4 Summary of fiber orientation measurement techniques

The importance of the braid angle and potential of obtaining undesired braid geometry from the predictive models means that a quality assurance step is required to verify that the proper fiber orientation is being produced. To improve the manufacturing process, the braid angle measurement should be automated to reduce the time and labour required to produce a composite part, which both would reduce the cost of a large scale production process.

The majority of braid angle measurement techniques are manual methods, meaning that the accuracy of these techniques is limited by human error. When using protractors or goniometers, error can occur from misalignments between the tool and the longitudinal direction of the component and from reading the measurement from the tool itself. These techniques require

contact with the sample, which makes it impossible to perform these measurements on moving samples or in an automated fashion. By using image based measurements, the data collection can be done in-line with the braiding process; however, many image based techniques still require human input. Techniques which require manual landmark selection or boundary tracing will be less repeatable than an automated measurement method. Automation of the process is not possible when human interaction is required, which is a major disadvantage of these braid angle measurement techniques.

There are other, more advanced measurement techniques which have been used, including digital image correlation and photometric stereo. These measurement techniques increase the level of accuracy due to their abilities to measure three dimensional surfaces however; each technique has requirements which may not be compatible with automated braid angle measurements. Digital image correlation requires a speckle pattern to correlate the set of stereo images and photometric stereo requires multiple images to be collected under different lighting conditions and post processing to form the height map. As a result, these more advanced methods may not be suitable for automated measurement applications.

2.4 Conclusions

The production of a 2D braid requires the selection of braiding machine speeds to produce the desired braid geometry. A number of predictive modelling techniques exist to relate the machine speeds and braider geometry to produced braid geometry. The complexity of these models ranges from the geometric kinematic models capable of predicting the braid structure through the use of differential equations, to finite element models can require two days of simulation time to predict appropriate braiding speeds.

Geometric braiding models are advantageous due to their simplicity and the ability to solve the inverse solution to these models, which allows for the direct calculation of machine speed profiles for desired braid pattern along the length of the mandrel [26, 28, 36]. The ability to directly calculate machine speeds based on a desired braid geometry profile with the inverse solution is also an advantage for the application of automated braiding. However, the same assumptions that are used to simplify the geometric models also cause them to inaccurately predict the braid pattern for certain scenarios. However, these models are still commonly used because of the relatively low error, between 1° and 5°, for simple mandrel shapes, such as tubular mandrels. This level of error matches the uncertainty associated with currently used braid angle measurement techniques due to human measurement error.

The potential of improperly predicting the braid geometry requires that the braid angle be measured after the braiding process for quality assurance purposes. Automating this quality assurance process would greatly benefit the manufacturing process of braided structures. An automated braid angle measurement system would allow the adverse effects of human error to be removed from the measurement process. This will allow for more accurate braid angle measurements to be made to better understand the accuracies and inaccuracies in the commonly used geometric models for fiber structure prediction. An automated and real-time braid angle measurement system will supplement the geometric braid models by being able to immediately detect undesirable braid angles. Rather than checking the fiber orientation after the completion of the braiding process, the user will get immediate feedback of the braid angle.

In order for this to be accomplished, a non-contact braid angle measurement technique will be developed which is capable of obtaining fully automated braid angle measurements of fiber preforms. A successful measurement technique will be capable of providing real-time braid

angle feedback to evaluate the accuracy of the kinematic model and with a level of uncertainty which is comparable to currently used manual measurement techniques. The real-time capabilities of the successful system will allow the braiding process to be further automated by eliminating the need to stop the production process to make manual braid angle measurements.

2.5 References

[1] J.-. Byun, "The analytical characterization of 2-D braided textile composites," Composites Sci.Technol., vol. 60, pp. 705-716, 2000.

[2] G. Guyader, A. Gabor and P. Hamelin, "Analysis of 2D and 3D circular braiding processes: Modeling the interaction between the process parameters and the pre-form architecture," Mechanism and Machine Theory, vol. 69, pp. 90-104, 2013.

[3] A.A. Head, F.K. Ko and C.M. Pastore, Handbook of Industrial Braiding, Atkins and Pearce, 1989, .

[4] Q. Zhang, D. Beale and R.M. Broughton, "Analysis of circular braiding process, Part 1: theoretical investigation of kinematics of the circular braiding process," J.Manuf.Sci.Eng.Trans.ASME, vol. 121, pp. 345-350, 1999.

[5] A. Rawal, S. Gupta, H. Saraswat and A. Sibal, "Geometrical modeling of near-net shape braided preforms," Text.Res.J., vol. 85, pp. 1055-1064, 2015.

[6] W. Michaeli, U. Rosenbaum and M. Jehrke, "Processing strategy for braiding of complex-shaped parts based on a mathematical process description," Composites Manuf., vol. 1, pp. 243-251, 1990.

[7] C. Ayranci, D. Romanyk and J.P. Carey, "Elastic properties of large-open-mesh 2D braided composites: Model predictions and initial experimental findings," Polymer Composites, vol. 31, pp. 2017-2024, 2010.

[8] G.W. Melenka, D.S. Nobes and J.P. Carey, "3D DIC Measurement of Tubular Braided Composites," in 19th International Conference on Composite Materials, 2013.

[9] C. Ayranci and J.P. Carey, "Experimental validation of a regression-based predictive model for elastic constants of open mesh tubular diamond-braid composites," Polymer Composites, vol. 32, pp. 243-251, 2011.

[10] J. Carey, M. Munro and A. Fahim, "Regression-based model for elastic constants of 2D braided/woven open mesh angle-ply composites," Polymer Composites, vol. 26, pp. 152-164, 2005.

[11] A.D. Kelkar, J.S. Tate and R. Bolick, "Structural integrity of aerospace textile composites under fatigue loading," Materials Science and Engineering: B, vol. 132, pp. 79-84, 2006.

[12] J.S. Tate and A.D. Kelkar, "Stiffness degradation model for biaxial braided composites under fatigue loading," Composites Part B: Engineering, vol. 39, pp. 548-555, 2008.

[13] A. Kelkar and J.D. Whitcomb, "Characterization and Structural Behavior of Braided Composites," U.S. Department of Transportation., Tech. Rep. DOT/FAA/AR-08/52, 2009.

[14] T. Liao and S. Adanur, "3D structural simulation of tubular braided fabrics for net-shape composites," Text.Res.J., vol. 70, pp. 297-303, 2000.

[15] J.S. Tate, A.D. Kelkar and J.D. Whitcomb, "Effect of braid angle on fatigue performance of biaxial braided composites," Int.J.Fatigue, vol. 28, pp. 1239-1247, 2006.

[16] S. Nasu, A. Ohtani, A. Nakai and H. Hamada, "Deformation behavior and mechanical properties of braided rectangular pipes," Composite Structures, vol. 92, pp. 752-756, 2010.

[17] K. Birkefeld, M. Röder, T. Von Reden, M. Bulat and K. Drechsler, "Characterization of biaxial and triaxial braids: Fiber architecture and mechanical properties," Appl Compos Mater, vol. 19, pp. 259-273, 2012.

[18] S.V. Lomov, R.S. Parnas, S.B. Ghosh, I. Verpoest and A. Nakai, "Experimental and theoretical characterization of the geometry of two-dimensional braided fabrics," Text.Res.J., vol. 72, pp. 706-712, 2002.

[19] C. Leung, "Examination of Braided Composite Geometric Factors Using Three Dimensional Digial Image Correlation Measurement Techniques," MSc. Thesis, 2012.

[20] J. Chen, T.M. McBride and S.B. Sanchez, "Sensitivity of Mechanical Properties to Braid Misalignment in Triaxial Braid Composite Panels," J.Compos.Technol.Res., vol. 20, pp. 13-17, 1998.

[21] G.W. Melenka, E. Lepp, B.K.O. Cheung and J.P. Carey, "Micro-computed tomography analysis of tubular braided composites," Compos.Struct., vol. 131, pp. 384-396, 2015.

[22] A.E. Scott, I. Sinclair, S.M. Spearing, M.N. Mavrogordato and W. Hepples, "Influence of voids on damage mechanisms in carbon/epoxy composites determined via high resolution computed tomography," Compos.Sci.Technol., vol. 90, pp. 147-153, 2014.

[23] D. Brunschweiler, "Braids and Braiding," Journal of the Textile Institute Proceedings, vol. 44, pp. 666-686, 1953.

[24] A. Mazzawi, "The Steady State and Transient Behaviour of 2D Braiding, PhD Thesis," Ottawa-Carleton Institute for Mechanical and Aerospace Engineering, University of Ottawa, 2001.

[25] ISO 10122:2014, "ISO 10122:2014 Reinforcement Materials - Tubular Braided Sleeves - Basis for Specification
," 2014.

[26] G.W. Du and P. Popper, "Analysis of a circular braiding process for complex shapes," Journal of the Textile Institute, vol. 85, pp. 316-337, 1994.

[27] G.W. Du, P. Popper and T.W. Chou, "Process Model of Circular Braiding for Complex Shaped Preform Manufacturing," in Proc. Symp. on Processing of Polymers and Polymeric Composites, 1990.

[28] J.H. Van Ravenhorst and R. Akkerman, "Circular braiding take-up speed generation using inverse kinematics," Compos Part A Appl Sci Manuf, vol. 64, pp. 147-158, 2014.

[29] H. Nishimoto, A. Ohtani, A. Nakai and H. Hamada, "Generation for circumferential distribution of braiding angle on cylindrical tubular braided fabrics," in Proceedings of the 9th International Conference on Textile Composites - TEXCOMP9: Recent Advances in Textile Composites, pp. 471-480, 2008.

[30] H. Nishimoto, A. Ohtani and A. Nakai, "Prediction method for temporal change in fiber bundle orientation on cylindrical braided preforms," Sen'i Gakkaishi, vol. 68, pp. 27-32, 2012.

[31] F.K. Ko, "Braiding," in Engineered Materials Handbook, Metals Park, OH: ASM International, 1987, pp. 519-528.

[32] H. Nishimoto, A. Ohtani, A. Nakai and H. Hamada, "Generation and prediction methods for circumferential distribution changes in the braiding angle on a cylindrical braided fabric," Proc.Inst.Mech.Eng.Part L J.Mat.Des.Appl., vol. 224, pp. 71-78, 2010.

[33] A. Rawal, P. Potluri and C. Steele, "Geometrical modeling of the yarn paths in three-dimensional braided structures," Journal of Industrial Textiles, vol. 35, pp. 115-135, 2005.

[34] H. Nishimoto, A. Ohtani, A. Nakai and H. Hamada, "Prediction method for temporal change in fiber orientation on cylindrical braided preforms," Text.Res.J., vol. 80, pp. 814-821, 2010.

[35] A. Rawal, A. Sibal and H. Saraswat, "Tensile behaviour of regular triaxial braided structures," Mech.Mater., vol. 91, pp. 277-289, 2015.

[36] J.H. Van Ravenhorst and R. Akkerman, "A yarn interaction model for circular braiding," Compos Part A Appl Sci Manuf, vol. 81, pp. 254-263, 2016.

[37] Q. Zhang, D. Beale, R.M. Broughton and S. Adanur, "Analysis of circular braiding process, part 2: Mechanics analysis of the circular braiding process and experiment," J.Manuf.Sci.Eng.Trans.ASME, vol. 121, pp. 351-357, 1999.

[38] A.K. Pickett, J. Sirtautas and A. Erber, "Braiding simulation and prediction of mechanical properties," Applied Composite Materials, vol. 16, pp. 345-364, 2009.

[39] A. Pickett, A. Erber, T. Von Reden and K. Drechsler, "Comparison of analytical and finite element simulation of 2D braiding," Plast.Rubber Compos., vol. 38, pp. 387-395, 2009.

[40] P. Monnot, J. Lvesque, O. Vermeersch and L.L. Lebel, "Automated braiding of dry preforms for aerospace structural components," in International SAMPE Technical Conference, 2016.

[41] A.J. Hunt and J.P. Carey, "Geometry Measurement of Tubular Braided Composite Materials for Real-Time Applications," in CANCOM 2015 - Canadian International Conference on Composite Materials, 2015.

[42] C. Ayranci, "Predicting the Elastic Properties of Two Dimensionally Braided Tubular Composite Structures Towards the Design of Braid-Reinforced Polymer Medical Catheters," ProQuest Dissertations and Theses, 2010.

[43] A. Rawal, A. Sibal, H. Saraswat and V. Kumar, "Geometrically controlled tensile response of braided sutures," Mater.Sci.Eng.C, vol. 48, pp. 453-456, 2015.

[44] C.K. Leung, G. Melenka, D.S. Nobes and J.P. Carey, "Validation of DIC as an Effective Tool for Composite Tubular Braid Characterization," in CSME International Congress, 2012.

[45] S. Thumfart, W. Palfinger, M. Stöger and C. Eitzinger, "Accurate fibre orientation measurement for carbon fibre surfaces," Lecture Notes in Computer Science (Including Subseries Lecture Notes in Artificial Intelligence and Lecture Notes in Bioinformatics), vol. 8048 LNCS, 2013.

[46] S. Zambal, W. Palfinger, M. Stger and C. Eitzinger, "Accurate fibre orientation measurement for carbon fibre surfaces," Pattern Recogn., vol. 48, pp. 3324-3332, 2015.

[47] B. Jahne, H. Haussecker and P. Grissler, "Reflectance-Based Shape Recovery," in Handbook of Computer Vision and Applications, San Diego, CA: Academic Press, 1999, pp. 532-590.

Chapter 3 Frequency domain measurement technique for the measurement of tubular braid preforms

3.1 Introduction

Braided composite materials have medical [1], aerospace [2] and structural applications [3]. Two-dimensional braided composite materials are produced on a maypole braiding machine and consist of a single layered braided fiber structure atop of a shape giving mandrel; a tubular mandrel is used for tubular braided composites. Similar to other types of fiber reinforced composites, the fiber orientation strongly influences the material properties of the composite part. The braid angle is the most important factor in determining the material properties of a braided composite and the effect of braid angle on various material properties has been shown in a number of experimental and analytical studies [4-10]. The braid angle is the only readily measurable geometric feature on the braided fiber structure, which makes an accurate braid angle measurement technique valuable for the production of braided composite materials for both material property characterization and quality assurance purposes. Braiding process models are used to relate the braiding machine geometry and process parameters to the geometry of the braided structure and have been derived in many different ways ranging from geometric models [11-15] to finite element and yarn interaction models [12, 16, 17]. These models play a crucial role in determining the required braiding machine speeds for a specific fiber orientation. Simple geometric models are commonly used. However, the assumptions made to develop the geometric relationships have been shown to be inaccurate [16] in certain cases. As a result, error of between 3° and 5° has been reported for constant cross-section mandrels [11, 12, 18].

Currently, the braid angle is measured manually after the production of the dry, braided fiber structure, also called the preform. The manual measurement techniques require a significant amount of time to make and are affected by human error, which leads to an uncertainty in the material properties of the braided composite part. To improve the consistency of the braid angle characterization, an automated, optical technique should be used rather than manual techniques. Such a technique will remove the need for human interaction when visually inspecting the braided fiber structure and will reduce the human error in measuring the braid angle. The majority of reported manual [19] and image based [20, 21] braid angle measurement techniques require constant user input, or extensive post-processing, making these unsuitable for real-time implementation. Thus, the development of an automated non-contact optical measurement technique will allow this system to be integrated into a production line to provide real-time feedback of the fiber orientation. The measurement accuracy should be within a comparable range compared to other previously developed measurement techniques. Uncertainty due to human error in fiber orientation measurements lies between ±1° and ±2 [18, 22].

Herein, such a system will be developed to measure the braid angle of tubular braided preforms. Images of braided preforms will be collected and measured to test the optical measurement technique. The measurement technique will be discussed and validated with a series of static, tubular braid samples produced with the two-dimensional (2D) braiding process. The effect of image preprocessing methods and the effect of perspective error from imaging the tubular surface on the measurement result will be discussed. A comparison of the error levels found with the new system and those with other existing measurement techniques will be provided. A successful braid angle measurement system will address issues associated with manual measurement techniques by providing an automated and real-time alternative.

3.1.1 Optical fiber orientation measurements with image processing techniques

The braid angle measurement is done by determining the fiber orientation from the features in the image. This can be done manually by tracing vectors overtop of images; however, this time-consuming process can be replaced through the development of an image processing algorithm. There are two classes of image processing techniques that have been used to measure various properties of fiber reinforced composites and textiles: spatial techniques, which modify or analyze the pixel values of the input image, and frequency domain techniques, which use transforms (commonly the Fourier transform) to study the frequency components of the image.

3.1.1.1 Spatial image processing techniques

The interpretation of scan line data is a computationally simple machine vision technique. Matela [23] and Creighton et al. [24] used scan lines to characterize faults in rope and to determine the fiber alignment in unidirectional fiber reinforced composites respectively. Rather than a scan line, Shi et al [25] located the position of sewed carbon fibers through filtering and Hough transforms.

Texture analysis techniques were used by Schmitt et al. [26, 27] to measure the fiber orientation of a local texture region. This was done by using the structure tensor to determine the local orientation of a grayscale pattern. The local orientation is the direction which exhibits the lowest change in grayscale value [28, 29]. Their work also used basic spatial image processing techniques such as filters, segmentation and thresholding to preprocess the images prior to measuring the orientation of the fibers.

Most the aforementioned spatial techniques were applied to flat samples. However, for cases where surface features sit atop of a curved, or three-dimensional surface, optical measurement techniques can be used to take the 3D surface profile into consideration. Such techniques consist

of multi-image photogrammetry, used by Ravenhorst and Akkerman [18] to measure the braid angle of 2D braided preforms, 3D digital image correlation used by Leung et al. [30, 31] to measure tubular braided composites and photometric stereo [32]. However, these imaging techniques either require manual selection of image landmarks, significant post-processing time or the collection of multiple frames with different lighting conditions which do not agree with the automated and real-time requirement.

3.1.1.2 Frequency domain image processing techniques

Frequency domain techniques have been used for a variety of measurement applications on both short fiber and continuous fiber samples. For short fiber samples, the Fourier transform is most commonly used to compute the orientation distribution function (ODF) of the fibers in the image [33-36]. Redon et al. [37] used a similar approach, combined with an inverse Fourier transform to isolate short fibers within a specific range of angles. For textile production applications, frequency domain approaches have been used for fault detection, [38-41] feature identification [42] and yarn density measurement [43]. The use of the Fourier transform takes advantage of the repeating textile pattern in these samples to detect defects and to make measurements of different parameters [44].

These techniques have also been applied to images of continuous fiber composites and preforms. Lian et al. [45] used the frequency transform to analyze flat and triaxial braids, while Wan et al. [46, 47] measured the outer surfaces of rectangular 3D braided preforms with the Fourier transform.

3.1.2 Machine vision

The primary advantage of implementing optical measurements is that they are non-intrusive and are not in physical contact with the sample. It is possible to make measurements of features directly from the images by manually tracing vectors and either measuring vector length, or the angle between vectors. These methods may be beneficial for a specific application. However, to fully take advantage of the image data, an automated image processing routine can be used to obtain the desired information. A machine vision process combines and accomplishes the tasks of image collection, image processing and image analysis in real time [48] allowing results to be extracted from images instantaneously.

Developing an optical measurement technique suitable for implementation in a machine vision application will allow the quality assurance braid angle measurement to be performed in-line with the braiding process, rather than being done manually at the end of the production cycle. In order to be suitable for a machine vision application, the measurement technique must not require constant user input, such as land mark identification or vector tracing. The images must also be processed in real-time. This real-time requirement eliminates methods such as digital image correlation [30, 31] due the need for extensive post processing of the images. The development of a low-cost solution is the final motivation for this work. This low-cost solution manifests itself as developing a system using a standard desktop computer, standard imaging equipment and user written software.

3.2 Methods and materials

3.2.1 The Fourier transform

The Fourier transform applied to an image connects the spatial (or time) domain, where pixel values correspond to spatial changes in the x and y directions, and the frequency domain, where image data is plotted corresponding to directionality and the rate at which pixel values change [49]. The two-dimensional discrete Fourier transform (2D DFT), shown in Equation 3.1, allows an image of size MxN with values *f(x,y)* to be transformed into a frequency spectrum, *F(u,v),* of size MxN. Where *x* and *y* are the spatial coordinates of the image and *u* and *v* are the frequency variables in the *x* and *y* directions respectively [50]. The reverse operation is performed using Equation 3.2. The frequency spectrum is a complex valued array representing the magnitude and direction of the frequencies in an image. Each pixel of the frequency spectrum corresponds to a specific frequency, and the magnitude of each pixel represents the significance of this particular frequency component in the spatial image.

$$F(u,v) = \frac{1}{MN}\sum_{x=0}^{M-1}\sum_{y=0}^{N-1} f(x,y)e^{-j2\pi\left(\frac{ux}{M}+\frac{vy}{N}\right)} \tag{3.1}$$

$$f(x,y) = \sum_{x=0}^{M-1}\sum_{y=0}^{N-1} F(u,v)e^{j2\pi\left(\frac{ux}{M}+\frac{vy}{N}\right)} \tag{3.2}$$

Features from the spatial image can be identified through the visual inspection of the frequency spectrum. The origin of the frequency spectrum is in the center as shown in Figure 3-1. The placement of the origin means that low frequency data, corresponding to slow changing pixels are plotted near the center of the spectrum, and higher frequency data corresponding to sharp edges is plotted further from the origin. An additional consideration is the implied periodicity of

the input signal that is made by the 2D-DFT. More information about this can be found in Appendix A.

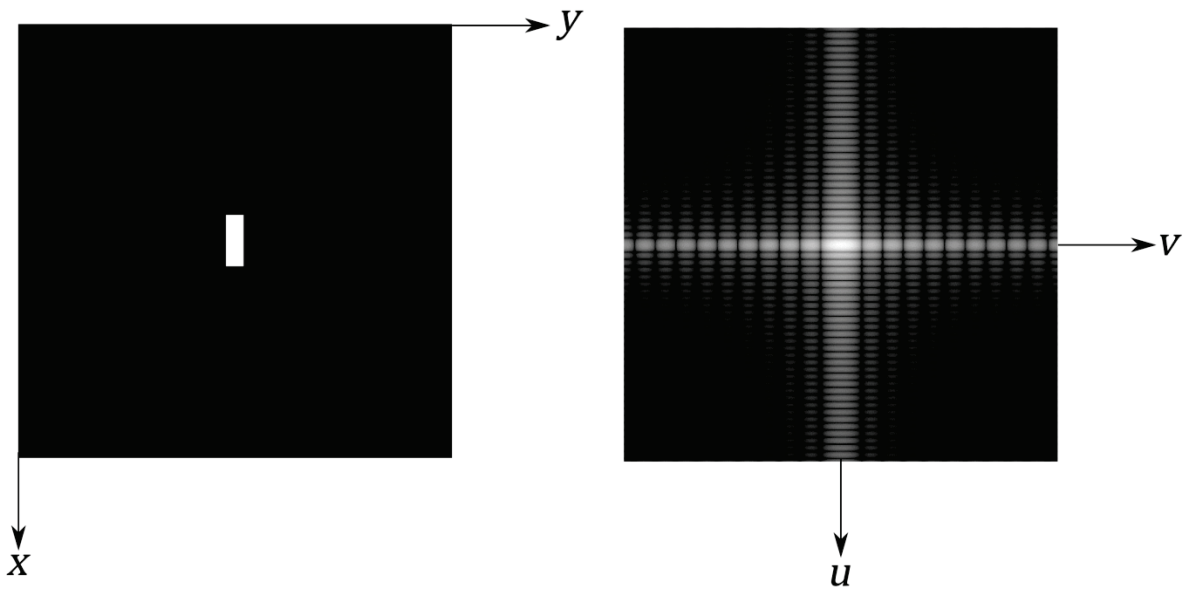

Figure 3-1: Spatial image (left) and frequency spectrum (right) showing respective coordinate systems (adapted from [50]).

3.2.2 Properties of 2D DFT

3.2.2.1 Symmetry of the power spectrum

The magnitude of the 2D DFT is two-fold rotationally symmetric which can be seen by visually inspecting the spectrum. For a real valued image, $f(x, y)$, the Fourier transform is conjugate symmetric, shown in Equation 3.3 [50]. This relationship can simplify to what is shown in Equation 3.4, which proves this symmetry.

$$F(u, v) = F^*(-u, -v) \tag{3.3}$$

$$|F(u, v)| = |F(-u, -v)| \tag{3.4}$$

3.2.2.2 Rotation invariance

An important characteristic of the 2D DFT is the rotation invariance described by the rotation theorem. This theorem states that a rotation or the image in the spatial domain corresponds to an identical rotation in the frequency domain [51]. This is proved by looking at the stretch theorem, shown in Equation 3.5, where *A* is a transformation matrix. A special case of this theorem is when the coordinate transform matrix, *A*, is defined as the rotation matrix, shown in Equation 3.6. The unique properties of the rotation matrix allow the general version of the stretch theorem to be simplified to the form shown in Equation 3.7 [52].

$$F\big(f(Ax)\big) = \frac{1}{detA} F(f(A^{-T}s)) \tag{3.5}$$

$$A = \begin{bmatrix} cos\theta & -sin\theta \\ sin\theta & cos\theta \end{bmatrix} \tag{3.6}$$

$$f(Ax) = F(As) \tag{3.7}$$

This theorem shows that a rotation in the spatial domain results in an equal rotation in the frequency domain. This property is very useful for optical measurement applications. The values of the transform do not change due to angular misalignments about the imaging axis between the sample and the camera plane, which can be seen in Figure 3-2. This adds to the robustness of the system and demonstrates the usefulness of this image processing method.

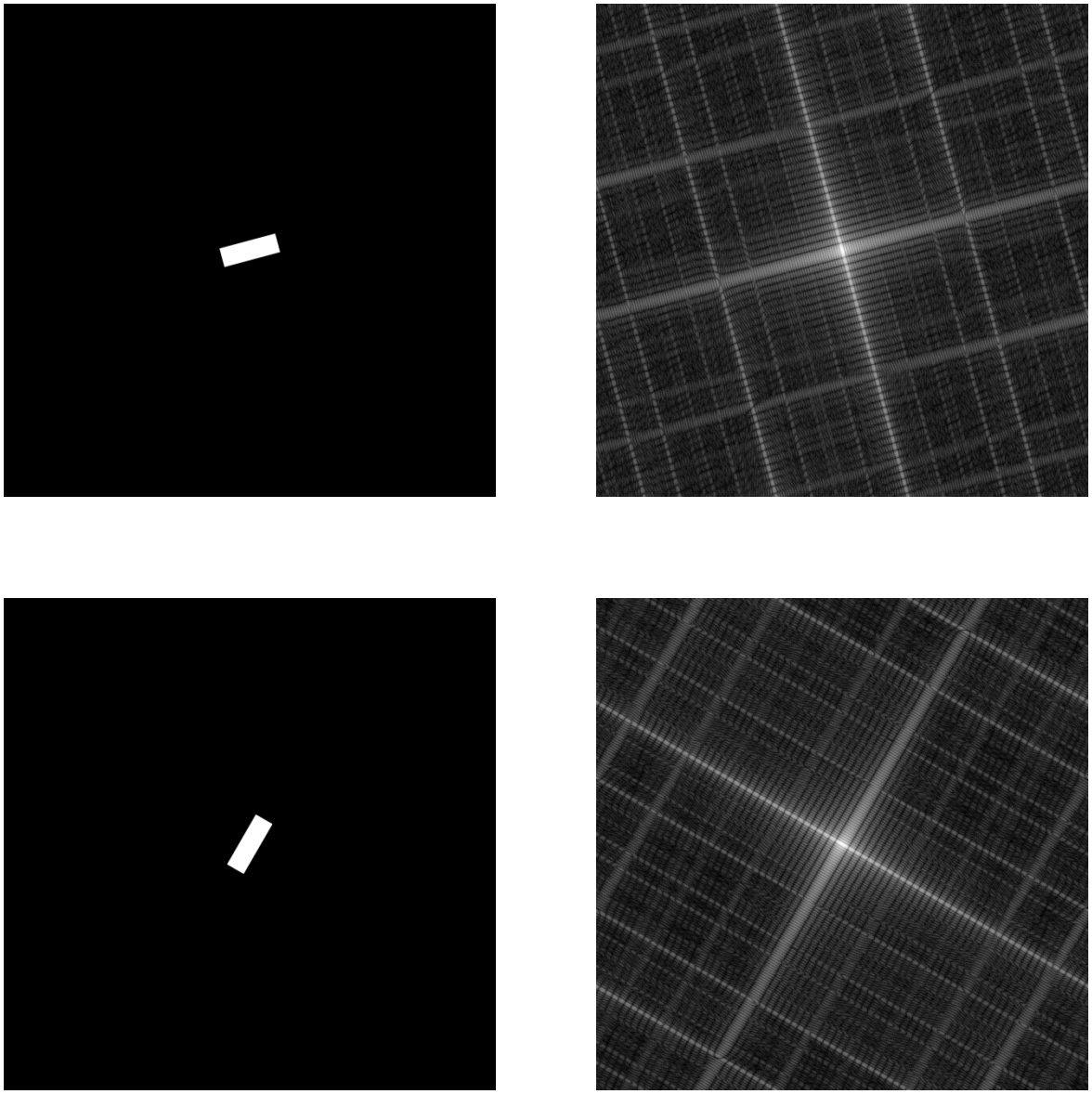

Figure 3-2: Frequency transform pair of computer generated images showing the rotation invariance property of the Fourier transform.

3.2.2.3 Linearity

The Fourier transform is a linear mathematical operation [53]. This means that the Fourier transform of the sum of multiple signals is equal to the sum of their transforms. For the application fiber orientation measurements, this means that two identical features will be superimposed in the frequency domain, producing a stronger frequency response as shown in Equation 3.8.

$$f_1(x,y) + f_2(x,y) = F_1(u,v) + F_2(u,v) \tag{3.8}$$

Scaling the input image by a constant value, *c*, results in an equal scaling in the frequency spectrum, shown in Equation 3.9. This shows that in the case of uniformly brightening the image, the magnitude of the features in the frequency spectrum will change by the same amount which will not create a different outcome.

$$c * f(x,y) = c * F(u,v) \tag{3.9}$$

3.2.2.4 Angular orientation preservation

The most important property of the frequency spectrum for this application is the angular preservation of features in the frequency spectrum [53]. As shown in Figure 3-3, the frequency response of features will be oriented at the same as the features in the spatial domain for square images [53]. By combining this property with the rotation invariance property, the relative orientation between features in the frequency spectrum will remain constant. A brief mathematical derivation of the relationship between the spatial orientation and the frequency components showing this property can be found in Appendix B.

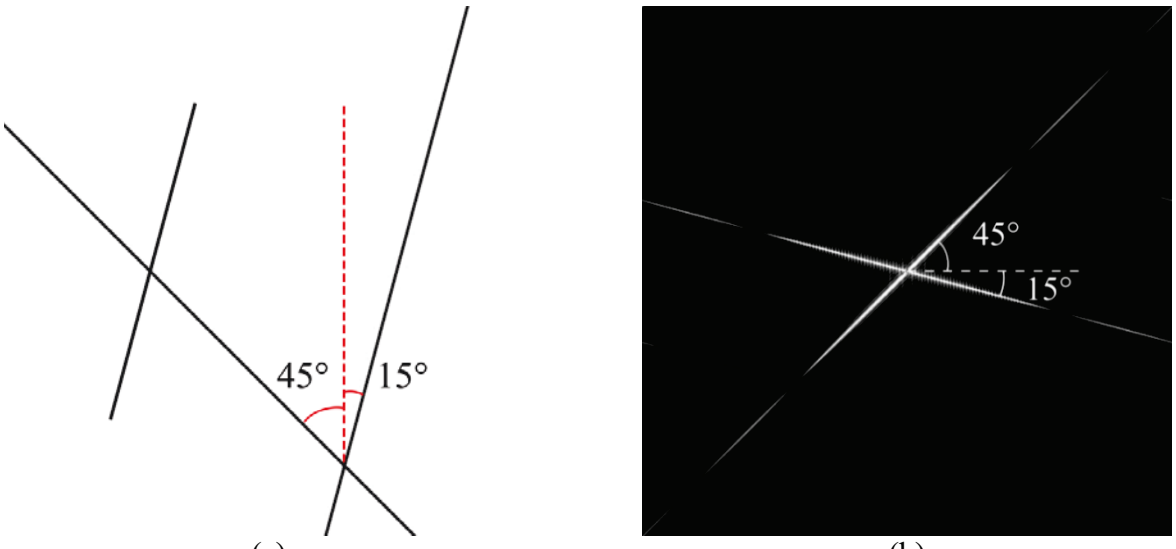

Figure 3-3: Demonstration of how the orientation of features is preserved with the 2D DFT. Annotated spatial image of lines (a), and the frequency spectrum (b) showing features with the same angular orientation

For this to be true, the frequency spectrum must be square. Thus, for images where $M \neq N$, the frequency spectrum must be scaled to a square. This is because a non-square frequency spectrum results in having different frequency discretizations in each direction. This affects the angle measurement due to axis scaling. This issue can be compensated for by rescaling the frequency spectrum [53]. Figure 3-4 shows a properly scaled frequency spectrum ($M = N$) and an improperly scaled frequency spectrum ($M \neq N$).

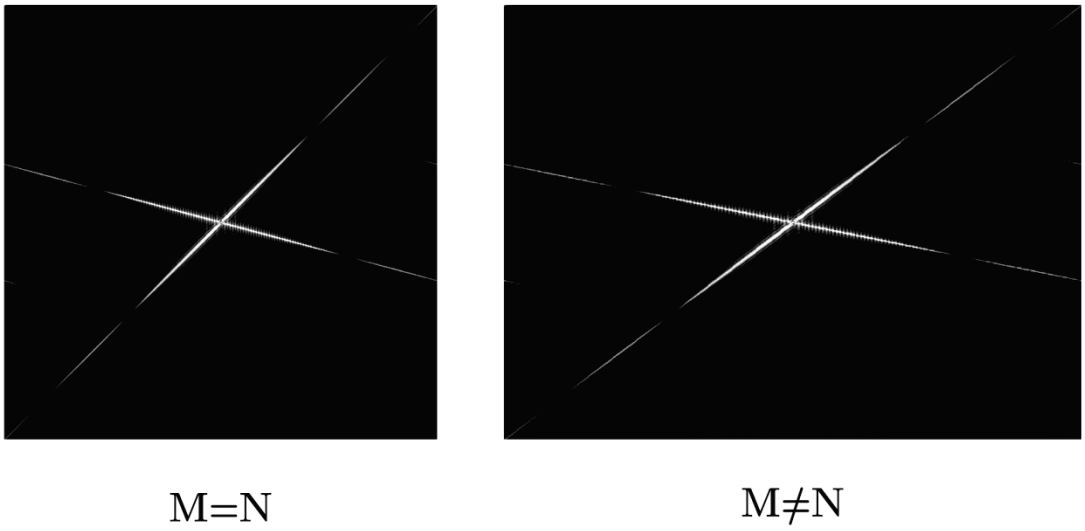

Figure 3-4: Square and rectangle frequency spectrum showing the effect that axis scaling has on the measured orientation of features in the frequency domain.

The last useful property of the two-dimensional Fourier transform is the removal of all spatial information in the frequency domain. As can be seen by again looking at Figure 3-3; the two lines inclined at 15° in the spatial domain are superimposed to produce a single line in the frequency spectrum. For a feature orientation measurement application, this is very useful for real-time applications as it removes the need to perform an exhaustive search for features in the spatial domain.

3.2.3 Image features

It was previously mentioned that certain spatial features can be identified in the frequency spectrum. To look at this relationship, image of a tubular braid preform and a filament wound sample can be seen in Figure 3-5. In each application, the fiber orientation will affect the material properties and must be measured. The features of interest stand out because the boundaries and edges of the braid yarns and filament wound fibers are sharp and in focus. This corresponds to a sharp change in pixel intensity, which is what the image processing technique will detect and measure from the images. An in-focus image is required to properly represent the imaged scene.

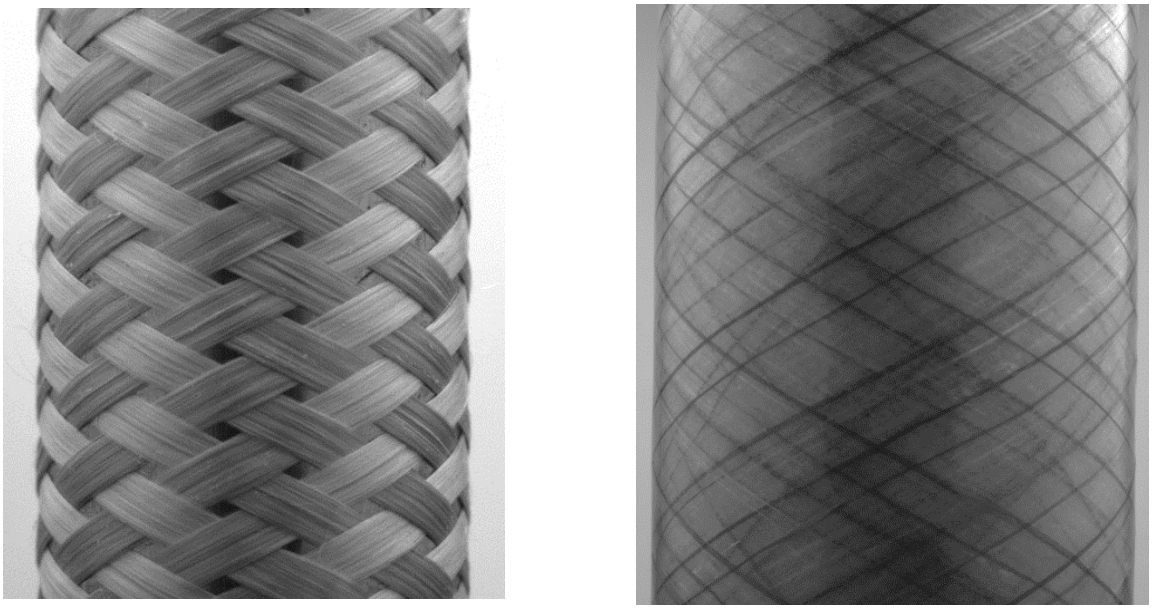

(a) (b)

Figure 3-5: Images of (a) braided fiber preforms, (b) filament wound pipes

In each image shown in Figure 3-5, there are two primary fiber directions relative to the longitudinal direction of the preform/part. Figure 3-6 shows the resulting frequency spectrums for the images in Figure 3-5. In each case, there are two features in the frequency spectrum

which correspond to the angular orientation of the fibers in the braid and the filament wound pipe.

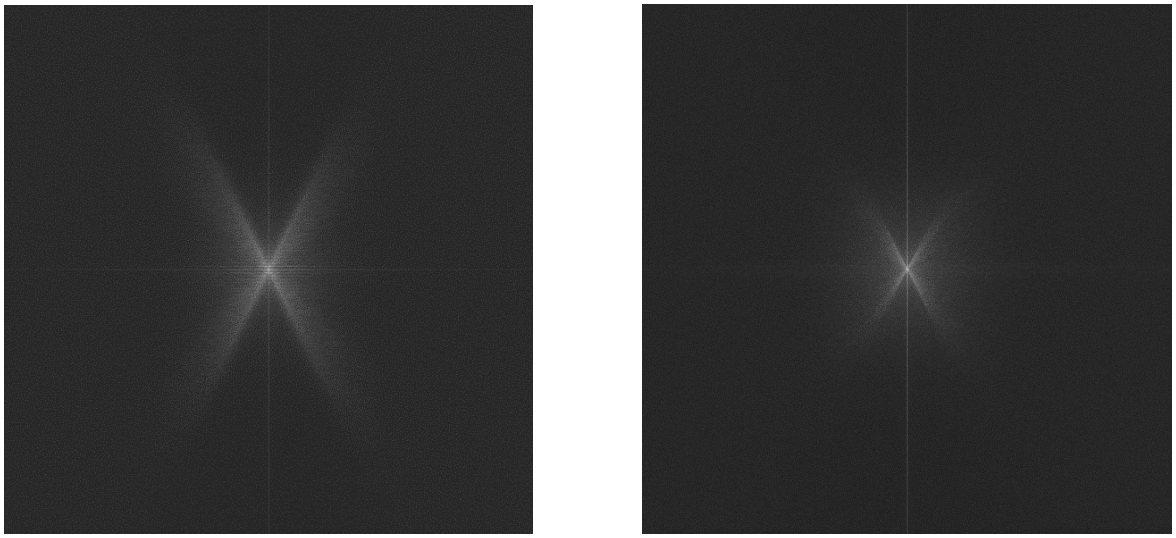

(a) (b)

Figure 3-6: Frequency spectrum of a tubular braided preform (a), and a filament wound pipe (b) showing the similarity of the of the results for different applications.

3.2.4 Analyzing the frequency spectrum

To measure the angle of the features in the image from the frequency spectrum, a scanning algorithm is used. This method takes advantage of the symmetry of the spectrum and the fact that all the features are symmetric about the (0,0) frequency component. An overview of the search algorithm is shown in Figure 3-7.

This process starts by discretizing a circle surrounding the center of the spectrum as well as a search vector. This search vector consists of a line connecting the center of the spectrum to the discretized circle. Both the discretization of the circle and lines were accomplished using Bresenham line and circle algorithms [54]. The orientation of the search vector which yields the highest mean pixel intensity is searched for by sweeping the vector around the semicircular path. The output of this process is the angular intensity of the frequency spectrum which plots the

mean pixel intensity of the pixels along the search vector in the frequency spectrum against the angular orientation of the search vector; an example is shown in Figure 3-8 for a braid preform with a braid angle of 63° and is referred to as the angular intensity distribution of the frequency spectrum.

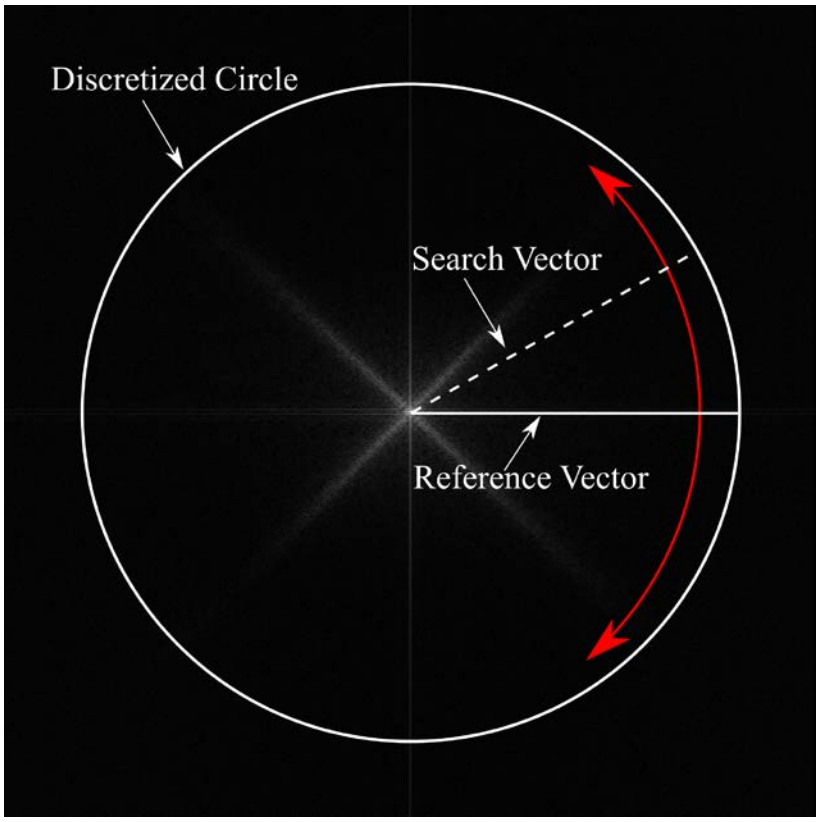

Figure 3-7: Annotated frequency spectrum showing the search routine used for angle measurement.

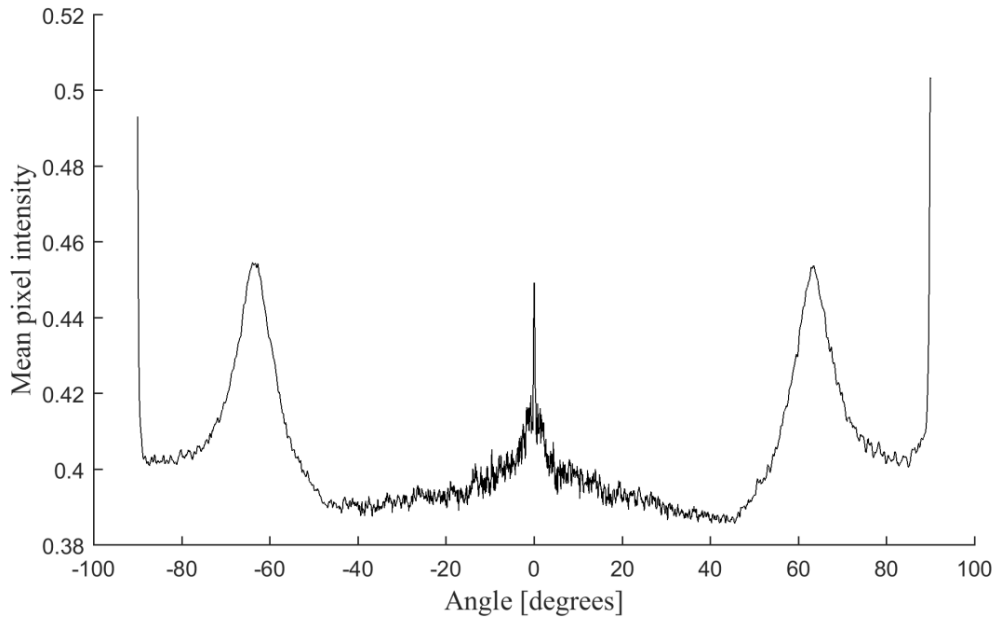

s

Figure 3-8: Angular intensity plot of the frequency spectrum which plots the mean pixel intensity against the angular orientation of the scan line.

Locating the significant features in the angular intensity distribution shown in Figure 3-8 is done using an exhaustive search routine which searches for the largest mean pixel intensity value within a predefined range of angles. The use of peak detection in future work can be used to improve this search algorithm.

The frequency spectrum and the angular intensity plot will differ depending on the features in the spatial image. Biaxial braids have yarns inclined at a positive and negative bias relative to the longitudinal mandrel direction. As a result, the angular intensity plot will show two maximums of interest at the positive and negative braid angle. In this plot, negative angles correspond to features inclined to the right of the vertical, and positive angles correspond to features inclined to the left of the vertical. The high mean pixel intensities located at 0° and ±90° are due to image borders associated with the implied periodicity of the Fourier transform [50, 52, 53]. Additional information regarding the periodicity of the Fourier transform can be found in Appendix A.

3.2.5 Sample production and data collection

The purpose of this test is to validate this technique as a suitable method for measuring the braid angle of 2D tubular braided preforms. Tubular braided preforms were produced on a 1" diameter mandrel with 1420 denier aramid yarns. A 36-carrier maypole braiding machine was set up in a 1/1 diamond unit cell configuration to produce the preforms. The machine speeds were set using Equation 3.10, which is the geometric braiding equation describing the steady state braid geometry for tubular mandrels [8, 12, 13, 55, 56]. The braiding process was given sufficient time to reach steady state prior to collecting the images to ensure that desired braid angle was produced. Braided fiber preforms with braid angles of 30°, 45° and 63° were produced and imaged to test the performance of the optical braid angle measurement technique for various fiber orientations.

$$tan\theta_{\infty} = \frac{\omega}{v} R_m \tag{3.10}$$

The imaging process was performed in-line with the braiding machine. Once the braid structure had reached steady state, the process was stopped and an image was captured. Four images were captured in different regions of interest along the steady state portion of the preform.

Images were captured using a scientific grade CCD camera with a 5 megapixel sensor [Basler Pilot piA1700-gm, Germany] with a fixed 35mm focal length lens [NMV-35, Navitar, New York, USA]. Image processing, camera control and image acquisition was done using custom written software in MatLab [Natick MA, USA].

3.2.6 Consideration of tubular shape of samples

The developed measurement system used image data from a single camera to measure the surface features on a tubular surface. The decision to use a single camera reduces the computational intensity of the image processing routine; however, it will also be responsible for perspective error in the image. Perspective error occurs when features on a three-dimensional surface are projected onto a two-dimensional imaging plane. This loss of depth information distorts image features that lie on the three-dimensional surface, which in this case is the direction of the braided fibers. This phenomenon can be seen in Figure 3-9 which demonstrates how the direction of a yarn wrapped in a helical fashion around a cylinder can become distorted when projected onto an imaging plane. From Figure 3-9, it is apparent that the perceived fiber orientation in the image depends on the distance from the centerline of the tubular sample. This causes a perceived fiber orientation distribution in the spatial image which is dependent on the distance from the centerline of the tubular mandrel.

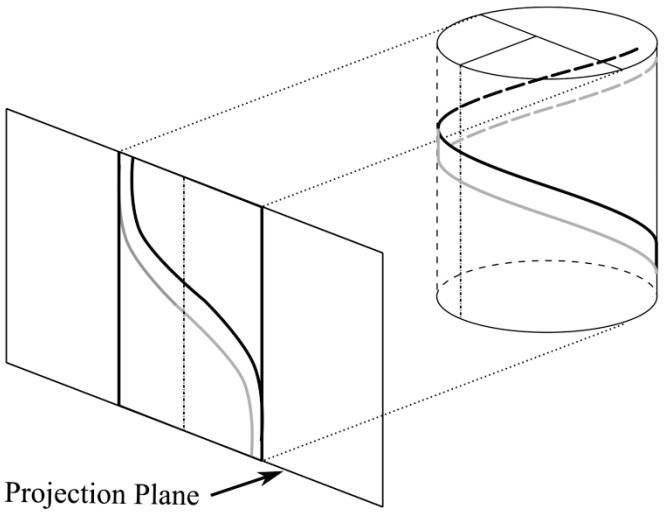

Figure 3-9: Projection of surface feature on a cylindrical surface onto a 2D plane.

3.2.6.1 Cropping braid images

The amount of distortion due to perspective error from the images is related to the changing distance between the surface and the imaging plane. This means that fibers further from the centerline of the tubular mandrel will appear more distorted than those that lie near the center of the mandrel. Thus to reduce the presence of error in the braid angle measurement, the distorted fibers can be removed with the use of a thresholding and cropping algorithm. Removing varying amounts of the braid image will allow the braid angle distribution due to perspective error to be controlled. Figure 3-10 shows three braid images which have been cropped to various extents, ranging from removing the background to a 50% reduction in width. The image is cropped by removing features from either side of the centerline. This is done to decrease the distribution of fiber angles in the image.

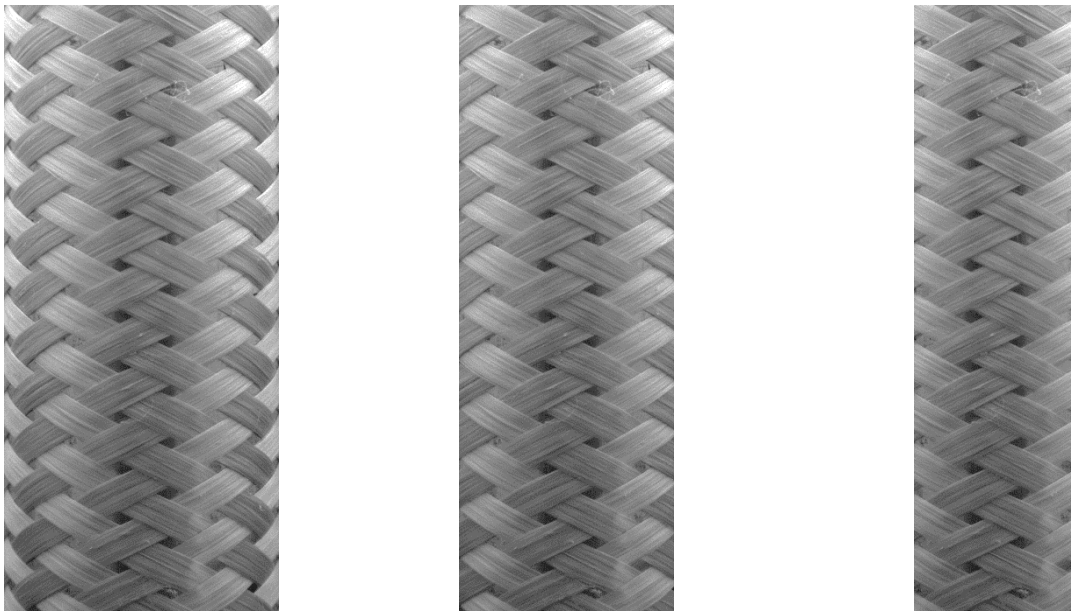

(a) (b) (c)

Figure 3-10: Cropped images obtained by (a) removing the background, (b) removing 20% width from each side, (c) removing 50% of the braid width from each side.

3.2.6.2 Perspective error model for tubular surfaces

To predict the braid angle distribution in an image, a geometric model of the projected yarn direction can be developed. Understanding the effect of perspective error on the perceived fiber orientation in images of tubular braided preforms will allow the techniques developed herein to be generalized for mandrels of different diameters. This modelling process requires consideration of two main geometries: the trajectory of the wrapped fibers on the tubular mandrel, and the projection of the tubular geometry onto a 2D plane.

Trajectory of fibers on a tubular surface

For a braiding machine operating at a constant linear take-up speed and a constant rotational speed, a single yarn will be wrapped in a helical fashion on the cylindrical mandrel. For this to be true, it is assumed that there are no inter-yarn forces which influence the yarn deposition. This assumption has been used in many geometric braiding models [11, 13, 18, 20, 57] and although this assumption causes discrepancies between predicted and measured results for complex mandrel geometries [18], the effects of inter-yarn forces are less significant for simple mandrels and braiding processes with a fewer number of yarns [13].

The deposition of a fiber during the 2D braiding process can be represented by wrapping a straight line, *u*, with a slope, c, onto a cylindrical surface, as shown in Figure 3-11. The act of wrapping this line onto a cylindrical surface will produce a helix with a constant inclination angle relative to the longitudinal direction of the cylinder.

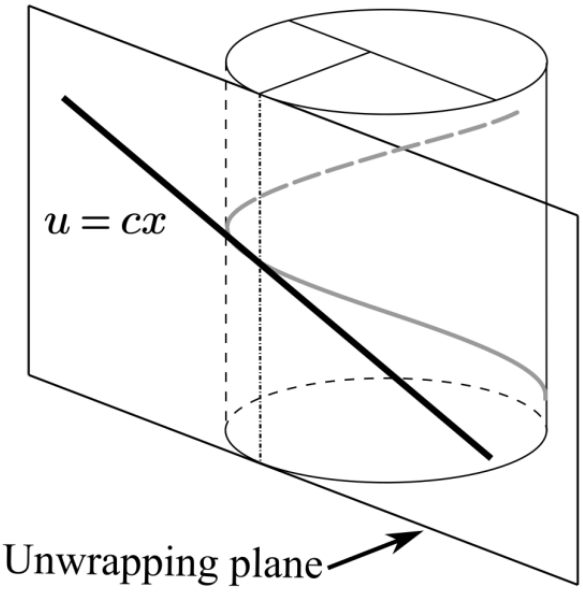

Figure 3-11: Straight line wrapped onto cylindrical surface

Projection of surface features onto a 2D plane

By wrapping a line with a constant slope onto a cylindrical surface, a helix was obtained. When imaged, this helical path is projected onto a 2D plane, which is the imaging plane. This is done by relating the tubular geometry, defined by the radius, r, and the polar angle θ, to the horizontal distance from the centerline of the tubular sample, t. A schematic showing this relationship is given in Figure 3-12.

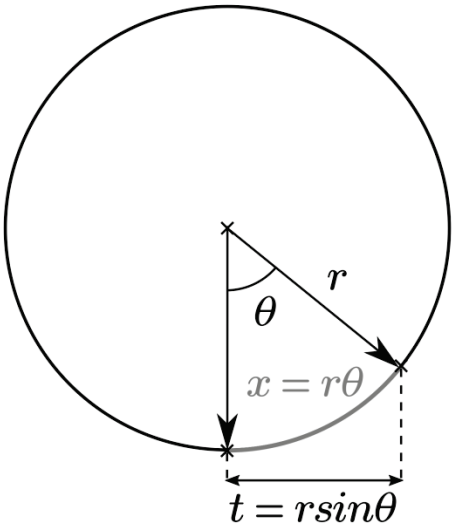

Figure 3-12: Cylinder projection schematic showing the relationship between the location on the tubular surface and the distance from the centerline of the tubular structure.

The projection of helical yarn path onto a 2D plane is described by the analytical function shown in Equation (3.11), where *c* is the slope of the line, *r* is the radius of the cylindrical surface, and *t* is the horizontal distance from the centerline of the cylinder [58]. By calculating the slope associated with a braid angle, Equation 3.11 produces the projected yarn path which would be seen in an image. Projected yarn paths for 30°, 45°, and 63° braid angles are shown in Figure 3-13.

$$p(t) = cr\arcsin\left(\frac{t}{r}\right) \tag{3.11}$$

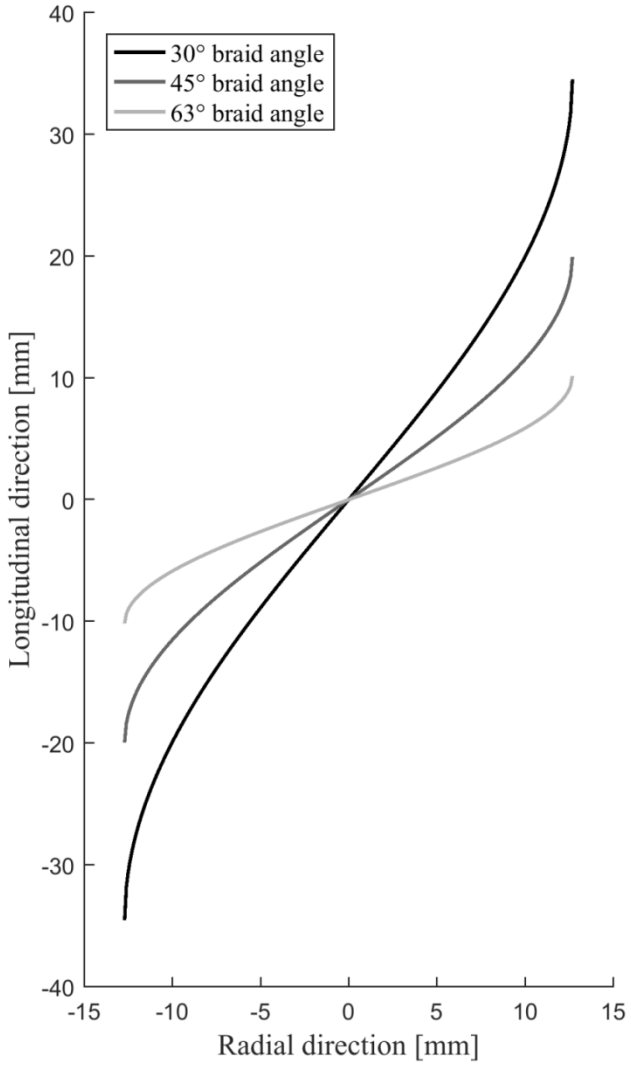

Figure 3-13: Projected yarn path as seen in an image. Lines oriented at 30°, 45°, and 63° relative to the longitudinal direction are compared.

Modelling braid angle distribution

To compare the projected yarn path to braid angles measured in the images, the slope of the yarn path, shown in Figure 3-13, is required. This is done by differentiating Equation 3.11 to obtain the slope of projected yarn path as a function of the horizontal distance from the centerline of the tubular braid. This is shown in Figure 3-14 for each of the yarn paths shown previously in

Figure 3-13. This plot shows the relationship between perspective error and the horizontal distance from the center of the tubular geometry. This result shows that the features along the centerline of the tubular mandrel (at a horizontal position of 0) will be inclined at the expected braid angle, however, as the distance from the centerline increase, as does the error due to perspective error.

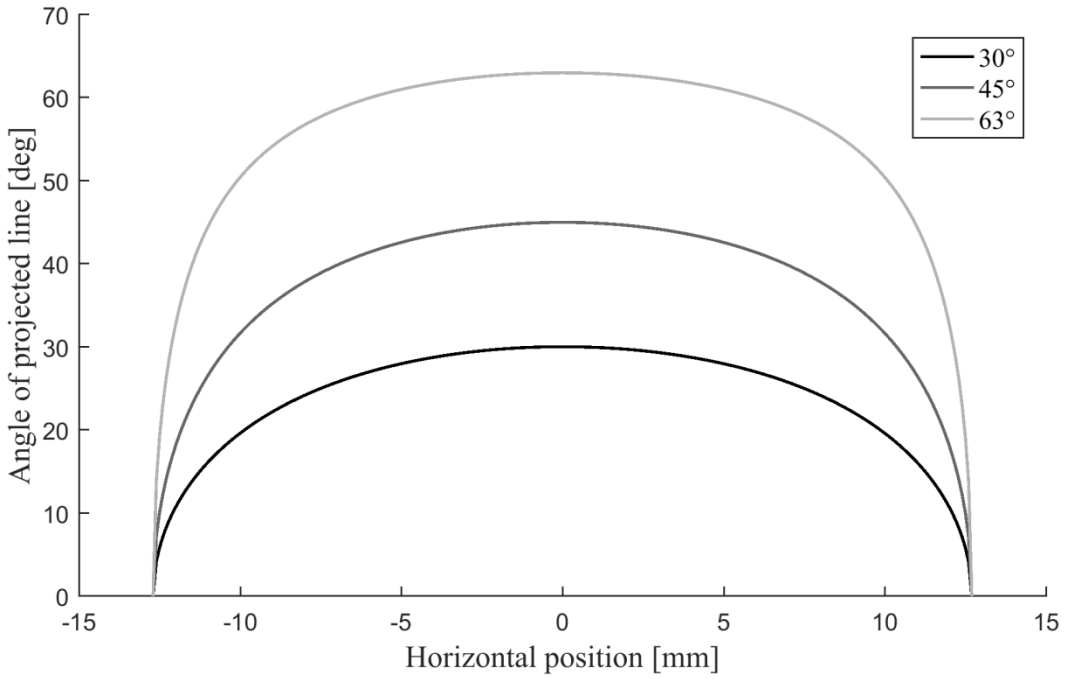

Figure 3-14: Angle of the projected yarn path with respect to the vertical direction as a function of horizontal positon from the centerline for a 1" diameter mandrel.

3.3 Results

3.3.1 Validation of predictive perspective error model

To validate the perspective error model, a series of braid angle measurements were taken at specific regions of an image of an image of a tubular braid. These locations were defined with the use of a rectangular grid, shown in Figure 3-15, which ensured that a series of measurements were taken at various horizontal distances from the centerline. A series of nine measurements were taking across the width of the braid at the top, middle and bottom of the image. A horizontal spacing of 100 pixels between measurements was chosen, which equates a spacing of 2.7 mm in the spatial domain. These measurements were made on braid preforms with a diameter of 1" with three different braid angles: 30, 45 and 63 degrees.

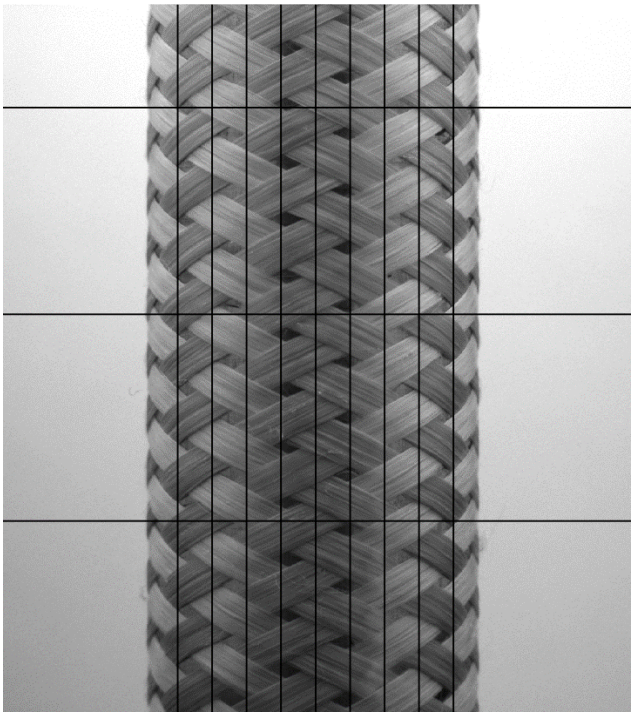

Figure 3-15: Rectangular grid traced overtop of a tubular braided preform with a 63-degree braid angle

At each point, the left and right braid angles were measured; this process is shown in Figure 3-16. The measurements were made in imageJ (ImageJ, Bethesda, Maryland, USA) by tracing vectors corresponding to the longitudinal direction and the fiber direction in an identical fashion to Figure 3-16. A protractor tool within the software automatically measured the angle between the defined vectors. This approach to measuring braid angle has been previously used in literature [20, 59] and gives the user more precision when making local angle measurements when compared to using a transparent protractor.

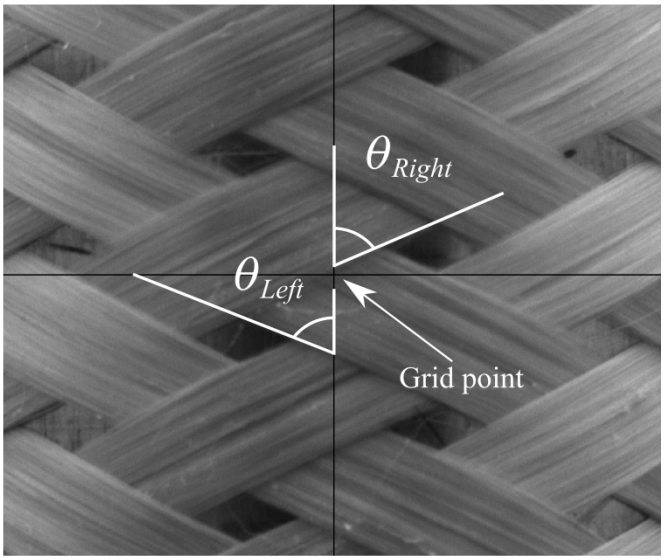

Figure 3-16: Close-up region of tubular braided preform showing grid point and sample measurements.

The results plotted in Figure 3-17 show the result of the manual measurements for each of the different braid preforms compared to the predicted plots from the perspective error model. Data points in Figure 3-17 were obtained by averaging all three measurements at each horizontal position.

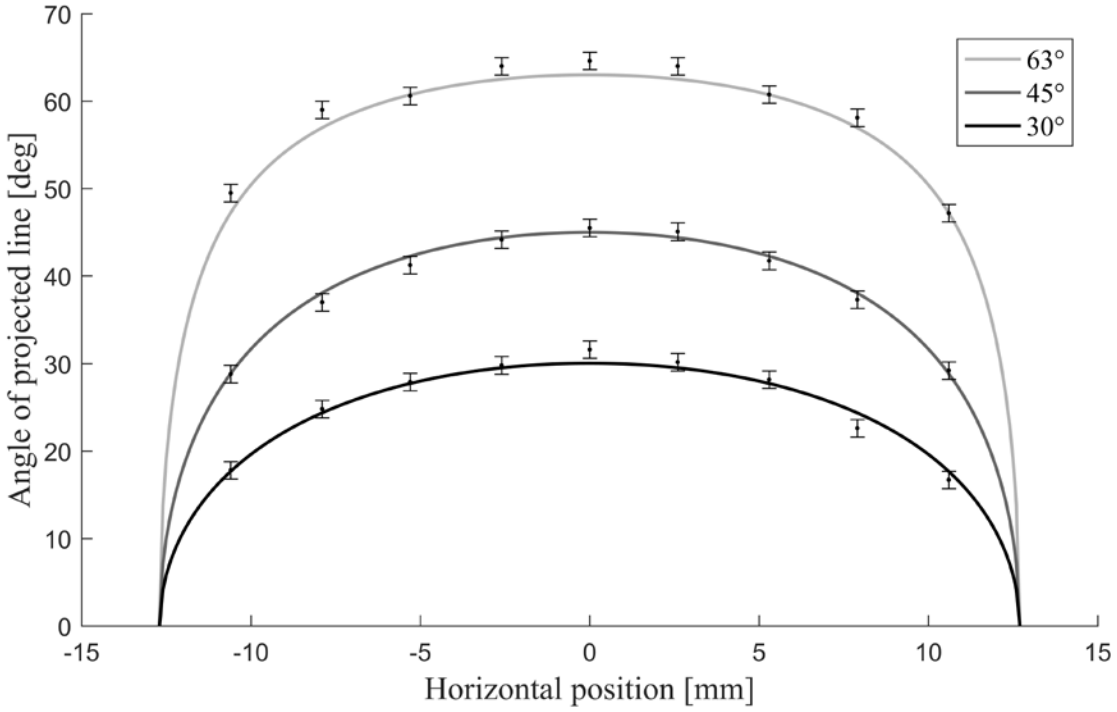

Figure 3-17: Comparison of model and manual measurements for 1" diameter braid preforms with 30°, 45° and 63° braid angles.

3.3.2 Braid angle distribution in spatial images

To predict the fiber angle distribution in the cropped images, the geometric yarn model can be used and by cropping regions of the braid image, as discussed in Section 3.2.6.1, this fiber angle distribution can be controlled. Figure 3-18 and Figure 3-19 show cropped braid images with 20% and 50% of the image cropped respectively. For each image, there is also the angle versus horizontal position plot from the perspective error model in Figure 3-18 (b) and Figure 3-19 (b). The bold line represents the portion of the braid image that remains after the cropping routine was performed.

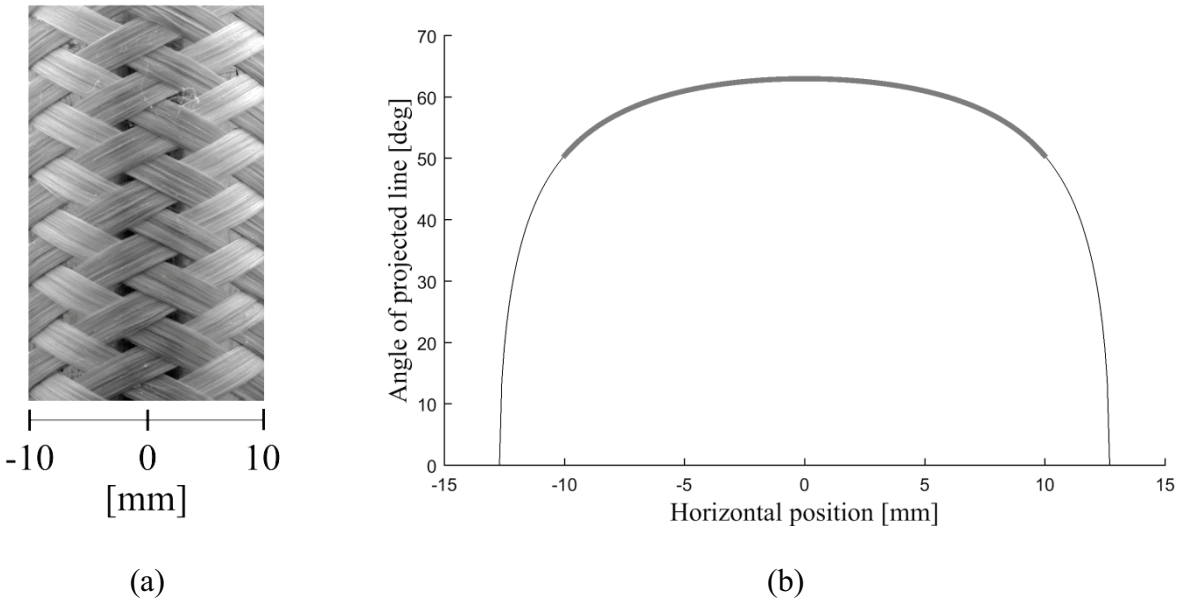

Figure 3-18: Cropped braid image with 20% of the width removed (a) and the predicted angular distribution plot obtained from the perspective error model (b). The thick gray line in (b) corresponds to the width of the cropped braid in (a).

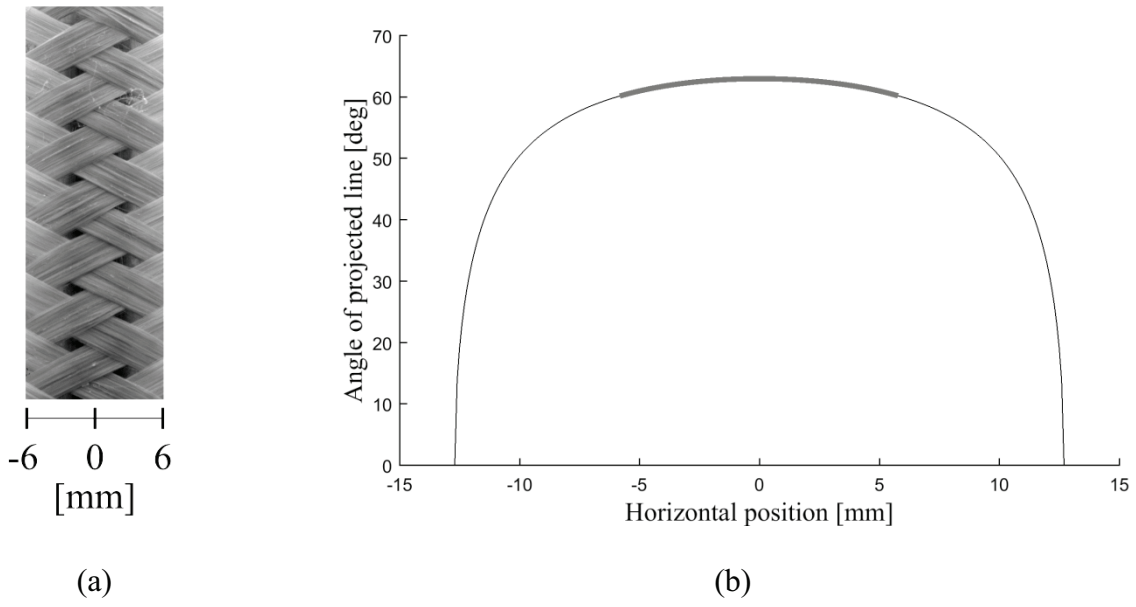

Figure 3-19: Cropped braid image with 50% of the width removed (a) and the predicted angular distribution plot obtained from the perspective error model (b). The thick gray line in (b) corresponds to the width of the cropped braid in (a).

Table 3-1 shows the predicted braid angle distributions for the cropped images. Since the braid angle is determined by measuring the angle of the fibers relative to the longitudinal direction of

the mandrel, the perspective error on the cylindrical surface creates a unidirectional distribution of braid angles that are less than the expected value. This is represented as a negative braid angle distribution in Table 3-1.

Table 3-1: Predicted distributions from geometric model for the cropped braid images in Figure 3-18 and Figure 3-19.

Width of cropped region	Nominal braid angle	Braid angle distribution
20%	63°	-13°
50%	63°	-3°

3.3.3 Braid angle distribution in the frequency spectrum

The frequency spectrum of the braid images provides directional information from the image. Using the measurement algorithm described in Section 3.2.4, pixel intensity versus angular orientation plots can be obtained which allow the visualization of the relative strength of features across ranging from -90 to 90 degrees relative to the longitudinal direction of the braid. Figure 3-20 shows the output from each of the two cropped images with 20% and 50% of the braid width removed. The images studied have an expected braid angle of 63°, and in each of the curves in Figure 3-20, there are peaks roughly centered at ±63°. The width of these peaks corresponds to the distribution of features within the image and as more of the braid image is removed, the width of the peaks is decreased. By removing the outer regions of the braid, fibers with a braid angle less than the expected value are removed from the image. In Figure 3-20, the outer-most sides of the peaks remain unchanged from the image cropping process which suggests that the features in the spatial image that are inclined at an angle greater than the fiber angle are not related to the fiber angle distribution in the image.

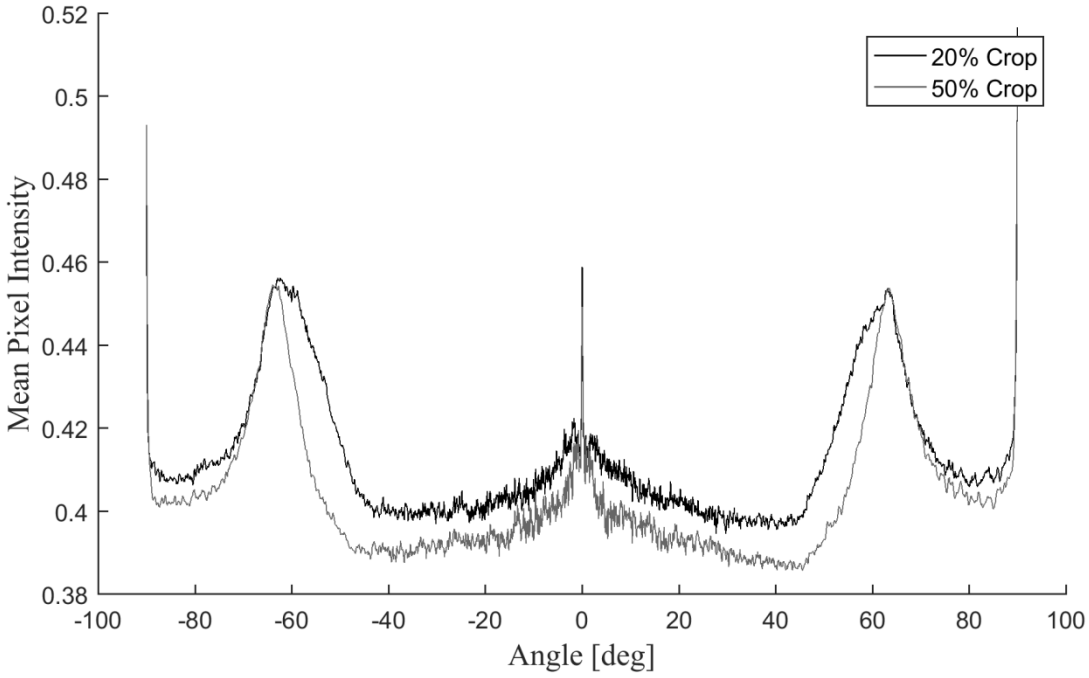

Figure 3-20: Mean pixel intensity vs. angle showing the effect of image cropping on the frequency spectrum

The ability to determine the fiber angle distribution from the angular intensity plot would be useful for further diagnosing the imaged sample and to do this, the width of the peaks in the angular intensity plot are compared to the expected braid angle distribution predicted by the yarn model. Lian et al. [45] propose that the distribution of angles in the image corresponds to the point at which the mean pixel intensity drops to 50% of its maximum value.

This technique was applied to each of the braid images in this study for each of the three braid angles. The average distribution for each sample and the expected angular distribution are shown in Table 2 and Table 3. These results show the underestimation of the angular distribution in the 20% cropped images and an overestimation of the distribution for the 50% cropped images. This shows that the 50% maximum intensity approach used by Lian et al. [45] does not agree with the predicted distributions from the geometric yarn model. This does however show that the width of the peaks in the angular intensity plot can be used as a

comparative measure of the angular distribution between different images, but the quantification of the fiber angle distribution from the angular intensity plot will not provide accurate results for quantifying the fiber angle due to perspective error.

Table 2: Braid angle distribution results for 50% cropped images.

Manufactured braid angle	Expected braid angle distribution	Measured distribution
30°	3°	5.5°
45°	3°	6.1°
63°	3°	5.8°

Table 3: Braid angle distribution results for 20% cropped images.

Manufactured braid angle	Expected braid angle distribution	Measured distribution
30°	13°	9.4°
45°	13°	11.7°
63°	13°	10.9°

3.3.4 Static braid angle measurements

The frequency domain measurement method and the cropping routine were used to test the accuracy of the measurement technique for different braid angles. However, defining the accuracy of this technique can become a challenge due to the uncertainty in the produced braid angle, as well as the uncertainty in manual measurements. The machine vision results were compared against the expected braid angle obtained from the steady state geometric braiding equation, shown in Equation 3.10. Past work has shown a distribution in braiding angles within a sample in flat [8, 10, 21] and tubular [31] braided composite samples. However, it is not known if this distribution is caused by inaccuracies in the geometric braiding model, or from displacement of the fibers during the impregnation and consolidation process. To mitigate the effects of manually displacing the fibers, the braided preform is not handled between the

production and imaging of the preform. Manual measurement techniques are influenced by human error [18, 22] and the curvature of the mandrel reduces the level of repeatability when using handheld tools such as protractors. Thus, the uncertainty of the machine vision measurement will be an important measure of success alongside the absolute measurement accuracy relative to the expected braid angle values.

3.3.4.1 Braid preforms with 1" diameter

The results in Table 3-4 show the average measurement for the four different regions of interest of the braided preform which shows a good agreement between the measured and expected braid angle. This was found to be true regardless of the amount of image that was cropped. To further study the effect of the image cropping procedure, the deviation between measurements, obtained from the standard deviation of the mean, can be studied, shown in Table 3-5. These results show that the lowest deviation between measurements occurred for the 50% cropped images.

Table 3-4: Average machine vision measurements showing the effect of image cropping on the measurement result.

Expected braid angle	Average measurement [deg]		
	Uncropped	20% removed	50% removed
30	29.37	29.30	29.48
45	44.93	44.57	44.93
63	63.14	63.33	63.64

Table 3-5: Measurement uncertainty showing the effect of image cropping on the variability between measurements.

Expected braid angle	Measurement uncertainty [±deg]		
	Uncropped	20% removed	50% removed
30	0.35	0.41	0.29
45	0.35	0.32	0.23
63	0.56	0.34	0.30

Although the cropping routine was not found to have a significant effect on the measurement result, this ensures that the frequency domain only contains contributions from non-distorted fiber directions. Thus, if the 50% cropped images are taken to be the most accurate, the percent error associated with this measurement technique is shown in Table 3-6.

Table 3-6: static braid angle measurement tests for 1" diameter tubular mandrel

Expected braid angle [deg]	Machine vision measurement [deg]	Percent Error (%)
30	29.40±0.20	2.0
45	44.93±0.23	0.2
63	63.64±0.30	1.0

Apart from image thresholding and cropping, other image preprocessing techniques such as edge detection and median filtering were tested to improve the measurement quality. These results were not successful. Results from these tests can be found in Appendix C.

3.4 Discussion

The objectives of this work were to develop and validate a method of measuring the braid angle of braided composite preforms in a way that is suitable for a machine vision application. Current measurement techniques used to measure the braid angle are time consuming and have shown error associated with repeatability due to human error. The error in manual measurement techniques can range from ±1° to ±2° [18, 22] By resolving these issues with an automated measurement technique, braid angle measurements can be made in-line with the braiding process. An optical technique using 2D imaging and the Fourier transform was developed and the accuracy of this technique was determined by modelling and evaluating the perspective error in the fiber directions in both the spatial and frequency domains.

3.4.1 Validation of predictive perspective error model

The agreement between the experimental and predicted data, shown in Figure 3-17, shows that the geometric perspective error model can predict the fiber orientation distortion due to perspective error for fibers on a tubular surface. Table 3-7 shows the maximum error in the data points plotted in Figure 3-17. For each sample, the point with the maximum error lies far from the centerline meaning that the error occurred when manually measuring highly distorted fiber directions. Tracing the vectors atop of these distorted fibers increases the variability between measurements making it difficult to collect consistent measurements in these regions of the braid. The significantly higher maximum error in the 30° sample is attributed to the larger unit cell size in the braided preforms with a 30° braid angle. With fewer unit cells in the field of view of the image, it was often not possible to measure the left and right angle measurements in the same location on the image.

Table 3-7: Maximum percent error in perspective error validation measurements.

Braid angle	Maximum percent error	Horizontal position of measurement [mm]
30°	7.1%	-7.9
45°	2.7%	-7.9
63°	4.8%	-10.6

The work done to model the effect that perspective error has on the fiber orientation in a two-dimensional image allows the error in this measurement technique to be quantified. A compromise that was made in this work was using the data collected with a two-dimensional imaging technique to measure features on a three-dimensional surface. By knowing the error associated with the loss of depth information, the accuracy of this frequency domain measurement technique can be put into perspective relative to other fiber orientation measurement techniques including digital image correlation [30, 31] and multi-image

photogrammetry [18] which are capable of taking the three-dimensional shape into account in their measurement at the expense of a real-time implementation.

3.4.2 Braid angle distribution in spatial images and in the frequency spectrum

The geometric yarn orientation model is used to predict the yarn orientation due to perspective error when imaging features on a cylindrical surface. These results are used to estimate the fiber angle distribution within specified portions of a braid sample image. The region of interest of the braid images can be controlled with the use of a thresholding and cropping algorithm, described in Section 3.2.6.1. To study the effect of image size on the measurement result, cropped images with 20% and 50% of the braid width removed are compared to the result obtained by processing the raw image. These image sizes were chosen to test the effect of the magnitude of the braid angle distribution on the measured braid angle. By cropping 50% of the width of the braid, the braid angle distribution from perspective error can be reduced from more than 13° for the uncropped image to 3°. Comparing the measurements obtained from the cropped images will test the measurement technique's ability to obtain an accurate result for images with a significant and non-significant braid angle distribution. A lower limit of 3° was chosen for the braid angle distribution because this was found to be within the range of current manufacturing limitations [60].

3.4.3 Braid angle measurement results

The measurement algorithm was applied to images collected of braided preforms with expected braid angles of 30°, 45° and 63°. Four images of non-overlapping regions were collected for each preform. The average measurement and the standard deviation of the mean of these measurements were used to determine the accuracy of the technique.

3.4.3.1 Effect of Cropping

Table 3-4 shows the effect of the cropped image sizes on the average braid angle measurement result compared to the expected braid angle calculated from the geometric braid angle equation shown in Equation 3.10. There is no consistent correlation between the size of the braid angle distribution in the image, and the accuracy of the average braid angle measurement when compared to the expected braid angle. For the case of the 63° preform, by increasing the amount of the image that is cropped, the reported braid angle increases. This trend, however, does not occur for the other braid geometries.

3.4.3.2 Comparison of Error

The error and uncertainty associated with current manual braid angle measurement techniques range from ±1° to ±2° due the manual alignment of measurement tools and the manual selection of image landmarks [18, 22]. The results shown in Table 3-6 show an improved uncertainty values for the developed measurement technique. The uncertainty values were obtained from the standard deviation of the mean measurement and show that the removal of human error produces fiber orientation measurements with a significantly reduced level of variation of between ±0.2 to ±0.3 degrees.

Another consideration is that manual measurement techniques consist of localized braid angle measurements. Due to the possibility of having significant variability across flat braided composite samples [8, 10, 21], manual braid angle measurement techniques are also affected by the chosen measurement location. This is not the case for the developed measurement technique as the frequency domain technique represents all the features in the image and obtains the measurement from the contribution of multiple unit cells. This property gives this measurement technique the ability to remain unaffected from local changes in braid angle which may not

accurately represent much of the fiber directions which plays a role in producing results with a low variability between measurements.

3.4.3.3 Optical measurement performance

The accuracy of the optical measurements of tubular braids were in good agreement with the expected braid angle, showing a maximum percent error of 2%. This level of accuracy in the fiber orientation measurements of tubular fiber preforms was found to be comparable to digital image correlation and photometric stereo techniques [30-32]. Digital image correlation techniques require the use of speckle patterns and image post processing; photometric stereo requires the capture of multiple frames under varying lighting condition. The developed measurement technique is advantageous due to the simplicity of the image acquisition and the fully automated nature of the measurement technique. This allows the frequency domain measurement technique to be used for real-time inspection processes.

3.4.4 Effect of image cropping for robust measurements

The previously discussed results showed the minimal effect that image cropping had on improving the accuracy of the measurement, as well as improving the measurement variability. The role of cropping the images of the tubular braided preforms is to remove the distorted fibers which decrease the angular distribution in the image. This was shown to significantly affect the frequency spectrum by narrowing the width of the peaks of the angular pixel intensity plot shown in Figure 3-20, but did not shift the location of the peaks, which would produce a different braid angle measurement. The benefit of the cropping process lies in having a more robust measurement system. The accurate results shown in Table 3-4 and Table 3-5 for the uncropped images show that the cropping process is not required for images with an ideal lighting setup consisting of even diffuse lighting. The reflective nature of the aramid fibers

means that reflections can occur very easily. For the proposed lighting setup used in this work, the light can easily get reflected off the distorted fibers. A comparison between an image collected with proper lighting, and one with reflections on the distorted fibers is shown in Figure 3-21.

The frequency domain measurement technique relies on image frequencies and changes in pixel intensity. When fibers are saturated in the image, they will produce a high frequency response in the frequency spectrum because of the higher than expected pixel value. This should be avoided as it is not representative of the features of the imaged sample. The frequency response from the reflections in the image can be greater than the response from the properly imaged fibers and when the reflections occur on the distorted fibers, the measurement will be skewed towards the orientation of the distorted fibers.

(a) (b)

Figure 3-21: Braid image without reflections and saturation (a), and braid image with saturation and reflections on the distorted fiber tows (b).

It was previously discussed that a single sharp peak for each fiber direction is expected in the angular pixel intensity plot of a good quality image. When the measurement algorithm is applied

to an improperly imaged braid preform with pixel saturation on the distorted tows, the angular pixel intensity plot, shown in Figure 3-22, is produced. This result is significantly different than what is expected. There are significant groups of features at angular orientations ranging from 10 to 45 degrees. The expected braid angle is 45°; yet, the plot also shows maximums at ±30°. These maximums correspond with the orientation of the saturated fibers; because of this saturation, these fibers produce a stronger frequency response than the central fibers which are oriented at the expected braid angle.

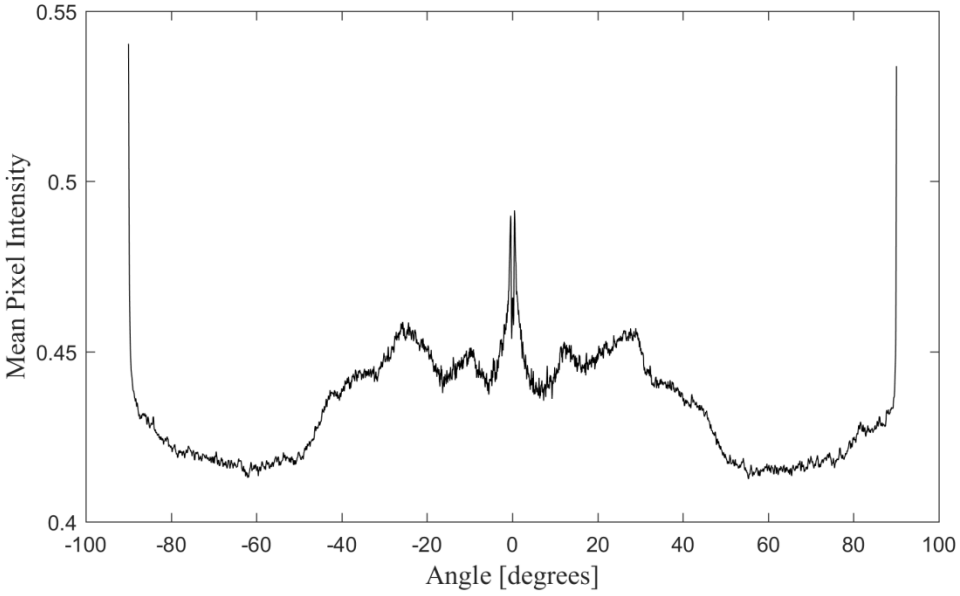

Figure 3-22: Mean pixel intensity versus angle plot for the braid image containing pixel saturation showing the spike leading to the incorrect measurement.

This false measurement can be corrected by using the previously described cropping procedure. By cropping the braided preform to 50% of the width, a much improved result can be obtained for the images containing saturation. The pixel intensity plot of the cropped image is shown in Figure 3-23; which now shows two peaks at ±45°. This plot shows the two symmetric peaks centered at the expected braid angle which signifies that the features in the image are inclined at two primary directions; which is what is expected for a biaxial braid. This shows that the

cropping routine is most useful for improving the robustness of this measurement technique. This process removes the distorted fibers which, under ideal imaging conditions, do not significantly affect the braid angle measured from the image. However, it is possible to have reflection from the distorted fibers which will affect the measurement quality. Hence, this routine will form an essential part in this measurement technique, especially when this method is used as a real-time technique where measurement stability will be essential.

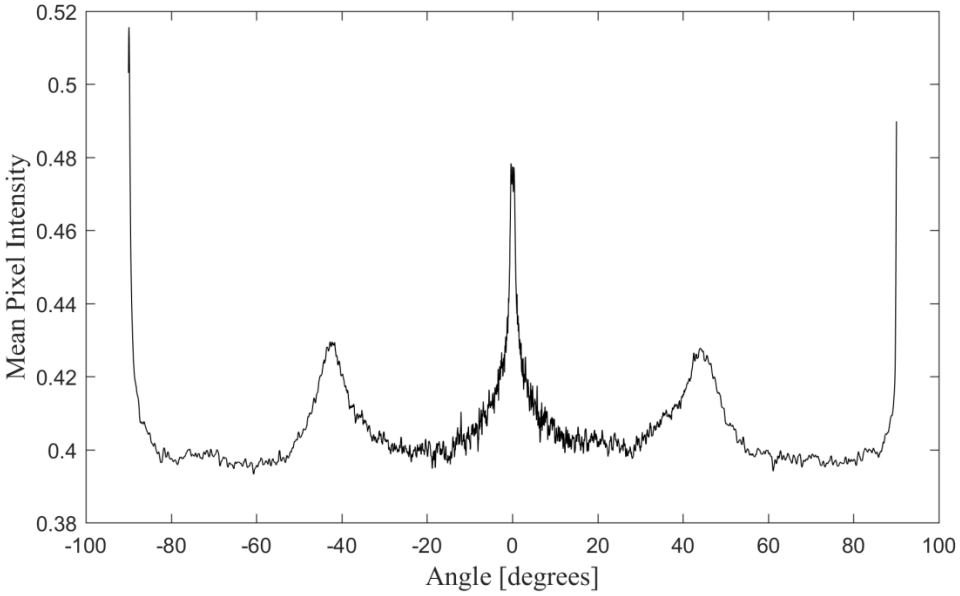

Figure 3-23: Mean pixel intensity versus angle plot for the braid image containing pixel saturation showing the effect cropping the saturated tows.

3.4.5 Alternative approaches for reducing effect of perspective error

The cropping routine described in Section 3.2.6 was shown to successfully reduce the presence of perspective error and decrease the braid angle distribution seen in the images. Due to the a priori knowledge of the tubular mandrel shape, orthographic projection techniques can be used to unwrap the tubular surface. This is done by determining the radius of the tubular braid from the image, and relating the distance from the centerline in the image to the corresponding unwrapped arc-length. This process, however, requires that intermediate values be interpolated, and the

amount of interpolated data will significantly increase for the outer regions of the braid. Another factor to consider is the radius at which the image is unwrapped. Previous work involving unwrapping micro CT scans of tubular braided composites showed that the unwrapping action depended on the thickness of the braided structure [61]. Because the 2D imaging approach would only be capable of detecting the outer radius of the structure, additional work would have to done to validate an orthographic projection approach.

3.5 Conclusions

Braiding manufacturing for braided composite applications has known challenges associated with the accurate deposition of fibers on the mandrel. The importance of fiber orientation on the resulting material properties of the braided composite part require the fiber orientation to be verified after the braiding process has been completed. The braid angle is the critical variable for determining the fiber orientation of braids, and current braid angle measurement techniques require manual interaction. By developing an optical, image based frequency domain measurement technique; braid angle measurements of tubular braids can be made in real-time in an automated fashion. The image processing measurement technique which is analyzes images based on their frequency content related to changes in pixel value.

The validity of this technique was determined for accurately measuring the fiber orientation atop of a three dimensional, tubular mandrel for single camera images. It is known that perspective error will distort the orientation of the fibers in the image and to predict the distribution of fiber directions within an image due to perspective error, a geometric model was developed and validated.

The accuracy of the measurement technique was determined by collecting a sample of images of tubular preforms with 30°, 45° and 63° degree braid angles. The use of a thresholding and cropping routine to remove the distorted fiber tows was shown to be beneficial to the measurement technique. For the images that were collected, the average braid angle measurement of the different regions of interest was not significantly affected by cropping the distorted regions of the image, however, doing so significantly minimized the variability between measurements. Additionally, the cropping routine can play a significant role in improving the robustness of the measurement technique in situations of poor lighting and reflections on the outer regions of the tubular braid.

This method is capable of making automated measurements of tubular braided preforms with a maximum percent error of 2%. This measurement technique does not require user interaction to select fiber boundaries or unit cells to make the fiber orientation measurement, which is an improvement over the other currently used measurement techniques. The low deviation between measurements which were found to be between 0.2° to 0.6° which is a significant improvement over the ±2° uncertainty associated with manually choosing landmarks. This method is also non-intrusive and automated, which means that this technique can be applied to real-time measurement applications.

3.6 References

[1] T. Schambron, A. Lowe and H.V. McGregor, "Effects of environmental ageing on the static and cyclic bending properties of braided carbon fibre/PEEK bone plates," Composites Part B: Engineering, vol. 39, pp. 1216-1220, 2008.

[2] A.D. Kelkar, J.S. Tate and R. Bolick, "Structural integrity of aerospace textile composites under fatigue loading," Materials Science and Engineering: B, vol. 132, pp. 79-84, 2006.

[3] M.A. Ivey, J.P.R. Carey and C. Ayranci, "Braid reinforced polymeric rebar production and characterization," in International SAMPE Technical Conference, 2014.

[4] C. Ayranci, D. Romanyk and J.P. Carey, "Elastic properties of large-open-mesh 2D braided composites: Model predictions and initial experimental findings," Polymer Composites, vol. 31, pp. 2017-2024, 2010.

[5] C. Ayranci and J.P. Carey, "Experimental validation of a regression-based predictive model for elastic constants of open mesh tubular diamond-braid composites," Polymer Composites, vol. 32, pp. 243-251, 2011.

[6] C. Ayranci and J.P. Carey, "Predicting the longitudinal elastic modulus of braided tubular composites using a curved unit-cell geometry," Composites Part B: Engineering, vol. 41, pp. 229-235, 2010.

[7] J. Carey, M. Munro and A. Fahim, "Longitudinal elastic modulus prediction of a 2-D braided fiber composite," J Reinf Plast Compos, vol. 22, pp. 813-831, 2003.

[8] K. Birkefeld, M. Röder, T. Von Reden, M. Bulat and K. Drechsler, "Characterization of biaxial and triaxial braids: Fiber architecture and mechanical properties," Appl Compos Mater, vol. 19, pp. 259-273, 2012.

[9] J.-. Byun, "The analytical characterization of 2-D braided textile composites," Composites Sci.Technol., vol. 60, pp. 705-716, 2000.

[10] J.S. Tate, A.D. Kelkar and J.D. Whitcomb, "Effect of braid angle on fatigue performance of biaxial braided composites," Int.J.Fatigue, vol. 28, pp. 1239-1247, 2006.

[11] G.W. Du and P. Popper, "Analysis of a circular braiding process for complex shapes," Journal of the Textile Institute, vol. 85, pp. 316-337, 1994.

[12] G. Guyader, A. Gabor and P. Hamelin, "Analysis of 2D and 3D circular braiding processes: Modeling the interaction between the process parameters and the pre-form architecture," Mechanism and Machine Theory, vol. 69, pp. 90-104, 2013.

[13] Q. Zhang, D. Beale and R.M. Broughton, "Analysis of circular braiding process, Part 1: theoretical investigation of kinematics of the circular braiding process," J.Manuf.Sci.Eng.Trans.ASME, vol. 121, pp. 345-350, 1999.

[14] H. Nishimoto, A. Ohtani, A. Nakai and H. Hamada, "Generation and prediction methods for circumferential distribution changes in the braiding angle on a cylindrical braided fabric," Proceedings of the Institution of Mechanical Engineers, Part L: Journal of Materials: Design and Applications, vol. 224, pp. 71-78, 2010.

[15] H. Nishimoto, A. Ohtani, A. Nakai and H. Hamada, "Generation for circumferential distribution of braiding angle on cylindrical tubular braided fabrics," in Proceedings of the 9th International Conference on Textile Composites - TEXCOMP9: Recent Advances in Textile Composites, pp. 471-480, 2008.

[16] J.H. Van Ravenhorst and R. Akkerman, "A yarn interaction model for circular braiding," Compos Part A Appl Sci Manuf, vol. 81, pp. 254-263, 2016.

[17] A. Pickett, A. Erber, T. Von Reden and K. Drechsler, "Comparison of analytical and finite element simulation of 2D braiding," Plast.Rubber Compos., vol. 38, pp. 387-395, 2009.

[18] J.H. Van Ravenhorst and R. Akkerman, "Circular braiding take-up speed generation using inverse kinematics," Compos Part A Appl Sci Manuf, vol. 64, pp. 147-158, 2014.

[19] J. Carey, G. Melenka, A. Hunt, C.M. Pastore and F.K. Ko, "Advanced testing of braided composites," in Handbook of Advances in 2D and 3D Braided Composite Materials, Woodhead Publishing, 2016, .

[20] A. Rawal, S. Gupta, H. Saraswat and A. Sibal, "Geometrical modeling of near-net shape braided preforms," Text.Res.J., vol. 85, pp. 1055-1064, 2015.

[21] S.V. Lomov, R.S. Parnas, S.B. Ghosh, I. Verpoest and A. Nakai, "Experimental and theoretical characterization of the geometry of two-dimensional braided fabrics," Text.Res.J., vol. 72, pp. 706-712, 2002.

[22] A.J. Hunt and J.P. Carey, "Geometry Measurement of Tubular Braided Composite Materials for Real-Time Applications," in CANCOM 2015 - Canadian International Conference on Composite Materials, 2015.

[23] L. Matela, "Real-time fault detection of braiding ropes using recognition methods," in Proceedings of SPIE - The International Society for Optical Engineering, pp. 253-261, 2004.

[24] C.J. Creighton, M.P.F. Sutcliffe and T.W. Clyne, "Multiple field image analysis procedure for characterization of fibre alignment in composites," Compos Part A Appl Sci Manuf, vol. 32, pp. 221-229, 2001.

[25] L. Shi and S. Wu, "Automatic Fiber Orientation Detection for Sewed Carbon Fibers," Tsinghua Sci.Tech., vol. 12, pp. 447-452, 2007.

[26] R. Schmitt, T. Pfeifer, C. Mersmann and A. Orth, "A method for the automated positioning and alignment of fibre-reinforced plastic structures based on machine vision," CIRP Ann.Manuf.Technol., vol. 57, pp. 501-504, 2008.

[27] R. Schmitt, C. Mersmann and A. Schoenberg, "Machine vision industrialising the textile-based frp production," in ISPA 2009 - Proceedings of the 6th International Symposium on Image and Signal Processing and Analysis, pp. 270-274, 2009.

[28] T. Aach, C. Mota, I. Stuke, M. Mühlich and E. Barth, "Analysis of superimposed oriented patterns," IEEE Trans.Image Process., vol. 15, pp. 3690-3700, 2006.

[29] T. Aach, I. Stuke, C. Mota and E. Barth, "Estimation of multiple local orientations in image signals," in ICASSP, IEEE International Conference on Acoustics, Speech and Signal Processing - Proceedings, pp. III556, 2004.

[30] C.K. Leung, G. Melenka, D.S. Nobes and J.P. Carey, "Validation of DIC as an Effective Tool for Composite Tubular Braid Characterization," in CSME International Congress, 2012.

[31] C. Leung, "Examination of Braided Composite Geometric Factors Using Three Dimensional Digial Image Correlation Measurement Techniques," MSc. Thesis, 2012.

[32] S. Zambal, W. Palfinger, M. Stger and C. Eitzinger, "Accurate fibre orientation measurement for carbon fibre surfaces," Pattern Recogn., vol. 48, pp. 3324-3332, 2015.

[33] B. Pourdeyhimi, R. Dent and H. Davis, "Measuring fiber orientation in nonwovens - Part III: Fourier transform," Text.Res.J., vol. 67, pp. 143-151, 1997.

[34] K.Y. Kang, K.Y. Lee, K.J. Jo and H.S. Kim, "Anisotropy in structure and mechanical properties of perpendicular-laid nonwovens," J.Mater.Sci., vol. 43, pp. 2754-2760, 2008.

[35] H.S. Kim, "Relationship between Fiber Orientation Distribution Function and mechanical anisotropy of thermally point-bonded nonwovens," Fibers Polym., vol. 5, pp. 177-181, 2004.

[36] M. Tunak, J. Antoch, J. Kula and J. Chvojka, "Estimation of fiber system orientation for nonwoven and nanofibrous layers: Local approach based on image analysis," Text.Res.J., vol. 84, pp. 989-1006, 2014.

[37] C. Redon, L. Chermant, J.-. Chermant and M. Coster, "Assessment of fibre orientation in reinforced concrete using Fourier image transform," J.Microsc., vol. 191, pp. 258-265, 1998.

[38] C.-. Chan, "Fabric defect detection by Fourier analysis," IEEE Trans.Ind.Appl., vol. 36, pp. 1267-1276, 2000.

[39] A.S. Malek, J.-. Drean, L. Bigue and J.-. Osselin, "Optimization of automated online fabric inspection by fast Fourier transform (FFT) and cross-correlation," Text.Res.J., vol. 83, pp. 256-268, 2013.

[40] D.-. Tsai and C.-. Hsieh, "Automated surface inspection for directional textures," Image Vision Comput., vol. 18, pp. 49-62, 1999.

[41] G.-. Hu, Q.-. Wang and G.-. Zhang, "Unsupervised defect detection in textiles based on Fourier analysis and wavelet shrinkage," Appl.Opt., vol. 54, pp. 2963-2980, 2015.

[42] J. Liu, B. Zhu, H. Jiang and W. Gao, "Image analysis measurement of cottonseed coat fragments in 100% cotton woven fabric," Fibers Polym., vol. 14, pp. 1208-1214, 2013.

[43] H. Sari-Sarraf and J.S. Goddard Jr., "Online optical measurement and monitoring of yarn density in woven fabrics," Proc SPIE Int Soc Opt Eng, vol. 2899, pp. 444-452, 1996.

[44] A. Kumar, "Computer-vision-based fabric defect detection: A survey," IEEE Trans.Ind.Electron., vol. 55, pp. 348-363, 2008.

[45] B. Lian, L. Jiang, J.J. McGrath and J. Jaranson, "Quantitative determination of morphological features of triaxially braided composites by the use of machine vision," Composites Sci.Technol., vol. 60, pp. 159-166, 2000.

[46] Z. Wan and J. Li, "Measurement Research of Parameter on Three-dimensional Braided Composite Material Preform Surface," J Compos Mater, vol. 38, pp. 435-448, 2004.

[47] Z. Wan and J. Li, "Braided angle measurement technique for three-dimensional braided composite material preform using mathematical morphology and image texture," Autex Res.J., vol. 6, pp. 30-39, 2006.

[48] E.R. Davies, Machine vision. Theory, algorithms, practicalities, San Diego: Academic Press, 1997, .

[49] E.J. Wood, "Applying Fourier and Associated Transforms to Pattern Characterization in Textiles," Text.Res.J., vol. 60, pp. 212-220, 1990.

[50] R. Gonzalez and R. Woods, Digital Image Processing, Prentice Hall, 2001, .

[51] R. Bracewell, Two-Dimensional Imaging, New Jersey, USA: Prentice-Hall, 1995, .

[52] B. Osgood, "Lecture Notes for EE 261 The Fourier Transform and its Applications ," .

[53] W. Burger and M. Burge, Digital Image Processing: An Algorithmic Introduction Using Java, New York, USA: Springer, 2008, .

[54] J.E. Bresenham, "Algorithm for computer control of a digital plotter," IBM Systems Journal, vol. 4, 1965.

[55] A.A. Head, F.K. Ko and C.M. Pastore, Handbook of Industrial Braiding, Atkins and Pearce, 1989, .

[56] H. Nishimoto, A. Ohtani and A. Nakai, "Prediction method for temporal change in fiber bundle orientation on cylindrical braided preforms," Sen'i Gakkaishi, vol. 68, pp. 27-32, 2012.

[57] P. Potluri, A. Rawal, M. Rivaldi and I. Porat, "Geometrical modelling and control of a triaxial braiding machine for producing 3D preforms," Composites Part A: Applied Science and Manufacturing, vol. 34, pp. 481-492, 2003.

[58] T.M. Apostol and M.A. Mnatsakanian, "Unwrapping curves from cylinders and cones," Am.Math.Mon., vol. 114, pp. 388-416, 2007.

[59] A. Rawal, A. Sibal and H. Saraswat, "Tensile behaviour of regular triaxial braided structures," Mech.Mater., vol. 91, pp. 277-289, 2015.

[60] J. Chen, T.M. McBride and S.B. Sanchez, "Sensitivity of Mechanical Properties to Braid Misalignment in Triaxial Braid Composite Panels," J.Compos.Technol.Res., vol. 20, pp. 13-17, 1998.

[61] G.W. Melenka, E. Lepp, B.K.O. Cheung and J.P. Carey, "Micro-computed tomography analysis of tubular braided composites," Compos.Struct., vol. 131, pp. 384-396, 2015.

Chapter 4 Real-time braid angle measurement of tubular braid preforms using machine vision

4.1 Introduction

The fiber orientation used to produce a tubular braided composite strongly affects its material properties. The braid angle is the most common measure of fiber orientation in braided structures and is one of the only geometrical fiber properties which can be measured after the production of the fiber structure. The braid angle is defined as the angle between the inclined fibers and the longitudinal direction of the mandrel [1, 2]. Verifying that the desired braid geometry has been produced is a crucial step in the braiding manufacturing process. This is because of the assumptions that have been made to derive the commonly used braiding models [3-5] (neglecting of inter-yarn friction and fiber slippage on the mandrel) have been shown to cause inaccuracies for certain braiding configurations. This is often measured manually, either through the use of protractors [6, 7] or by tracing vectors onto captured images [8-11], to determine if the desired fiber orientation has been obtained. The process of measuring the braid angle by hand is time consuming, error prone, and limits the automation of the braiding process. Additionally, manual braid angle assessment is a post-production process which prevents in-line quality control; which could be used to give the designer or operator feedback over the produced fiber geometry and be capable of detecting and correct undesirable braid geometry. Advanced measurement techniques involving computationally intensive image methods such as digital image correlation stereo imaging and multi-frame photogrammetry [11-13] have successfully been used to measure the fiber orientation of braided composites and preforms. However, the

sample preparation, data collection and image post-processing makes these techniques unsuitable for inline measurement applications of the fiber preform.

To address production quality control issues with the braiding process, a method to measure the braid angle is required which is non-contact, automated and provides measurements in real-time. An appropriate solution to this issue is the use of optical methods such as that developed in the previous chapter and machine vision. A machine vision system is a combination of real-time image collection, processing and analysis [14]. These systems can perform automated tasks to aid with manufacturing and production processes that suits the needs of the braiding process.

4.1.1 Applications of machine vision in textiles and textile composites

Machine vision systems have been used to automate quality control and fault detection tasks in the textiles and textile composite industries. The ability to automate visual inspection tasks allows for a significant reduction in missed faults and allows for the ability to compare patterns and measure features. Offline, manual visual inspection for textile fault detection has a maximum accuracy of 70-80% [15].

The current integration of machine vision systems in 2D braiding is limited. Branscomb and Beale [16] developed a low-cost fault detection system for rope. An area scan USB camera was used to track the motion of the braid point during braider operation and the presence of common braiding faults, such as a yarn tension imbalance and a jammed yarn carrier. The motion pattern of the braid point was analyzed to determine the feasibility of diagnosing braiding faults by monitoring the position of the braid point. Matela et al. [17] used a line scan camera to detect faults in braided ropes by correlating faults in braided ropes, such as a missing yarn, to fluctuations in pixel value along a scan line. Lastly, Mersmann [18] developed a Bayesian decision model to study the effect of integrating automated metrology techniques with the

production of carbon fiber reinforced plastics (CFRP). The models developed by Mersmann were applied to the specific application of automated CFRP braiding.

Mitchell et al. [19] used a texture segmentation approach to automatically locate the boundaries between various woven carbon fiber preforms. The algorithm achieved real-time performance by processing images in less than one second on standard computing hardware. Schmitt et al. [20] used an area scan camera to collect images of carbon fiber preforms. Their machine vision process was limited by the exposure time required by their camera, which illustrates the importance of the lighting system used for a machine vision system. Their work made use of a motorized lens capable of changing the focal point to allow for the successful imaging of samples with significantly varying thicknesses [21].

Fourier transform techniques

Several frequency domain inspection algorithms were developed for the inspection of periodic textiles patterns [15, 22-26]. These techniques were developed for use as machine vision algorithms, but were not tested in any in-line scenarios. A frequency domain technique was used in real-time, in-line with a textile loom to compute the yarn density of the fabric [26]. This work found that the sampling frequency of the line scan camera must be synchronized with the speed of the sample to obtain the desired image resolution.

4.1.2 Objectives

The importance of verifying the braid angle after the production of the braided fiber preform is a crucial step in the production process because of the strong relationship between the braid angle and the material properties. The braid angle is currently measured manually, which is a time consuming and error prone process. The objectives of the current work are to develop and assess

a real-time, in-line machine vision system to measure braid angle during the manufacturing process. A low-cost solution capable of running on standard computing equipment is desired to ensure that this system can be easily integrated into current braiding setups.

To be successful, the braid angle measurement system should provide immediate feedback regarding the orientation of the fibers on a tubular mandrel. The accuracy and uncertainty in the measurement should be within the neighborhood of other optical and manual measurement techniques which lie between ±1° and ±2° [11, 12]. The measurement system must obtain measurements without the need for constant user interaction. The goal of this system is to automate the quality assurance step in the production process and to reduce the effect of human error on the measurement process.

4.2 Methods

4.2.1 Machine vision system

Herein, the machine vision system will be described, which consists of two tasks: the data collection and the image processing routine. Data collection considers the physical components in the system, such as the camera and illumination. The image processing routine describes the tools used to obtain the braid angle from the collected images.

4.2.1.1 Data collection

Images of the braided preforms were captured using a single high resolution scientific grade area-scan camera [Basler Pilot pi2400-17gm, Germany] with a five-megapixel charged coupled device (CCD). A 35-mm fixed focal length lens was used to achieve the required magnification. The camera uses gigabit Ethernet communication to transfer the data to the computer.

Illumination significantly affects the results of a machine vision system. Due to the reflective nature of the yarns, care must be taken to avoid regions of pixel saturation or reflections because they produce features within the image which do not represent physical features on the sample. Early tests showed that direct lighting produced adverse effects on image quality; direct lighting from diffuse light sources also produced reflection issues. The optimal solution was the use of both a diffuse light dome [DL106, Advanced Illumination, Rochester, VT, USA] and matte white surfaces to further soften the light and reduce reflections on the sample. Figure 4-1 shows a schematic of the illumination setup. The effects of reducing the presence of reflections and the use of the proposed setup can be seen in Figure 4-2.

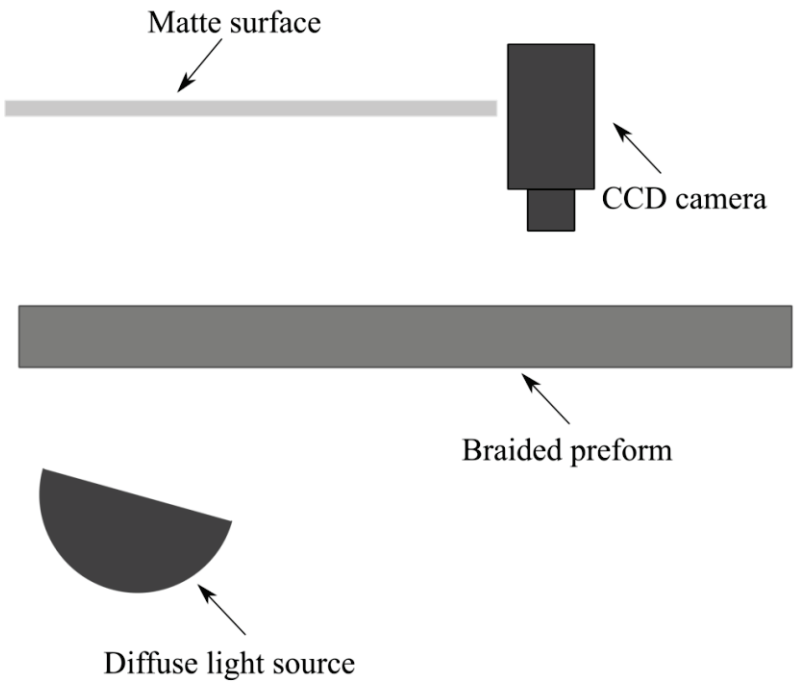

Figure 4-1: Illumination schematic

(a) (b)

Figure 4-2: Braid images showing the effects reflection. (a) shows a sample illuminated with direct light, (b) shows a sample illuminated with indirect light from the lightbox.

Images of the braided fiber preform are collected just downstream of the convergence ring. Doing so allows the region of interest to coincide with the braided fibers which are immediately deposited onto the mandrel. The placement of the camera and the light source can be seen in Figure 4-3.

Data collection and camera control operations were accomplished using custom written software in MatLab. Triggering was done electronically and the slower speeds associated with braid production allowed mandrel motion to be frozen without the use of specialized lighting, such as a stroboscope. Appropriately setting the lighting intensity and aperture size allows a sufficient amount of light to enter the sensor during the chosen exposure time used to freeze the sample motion.

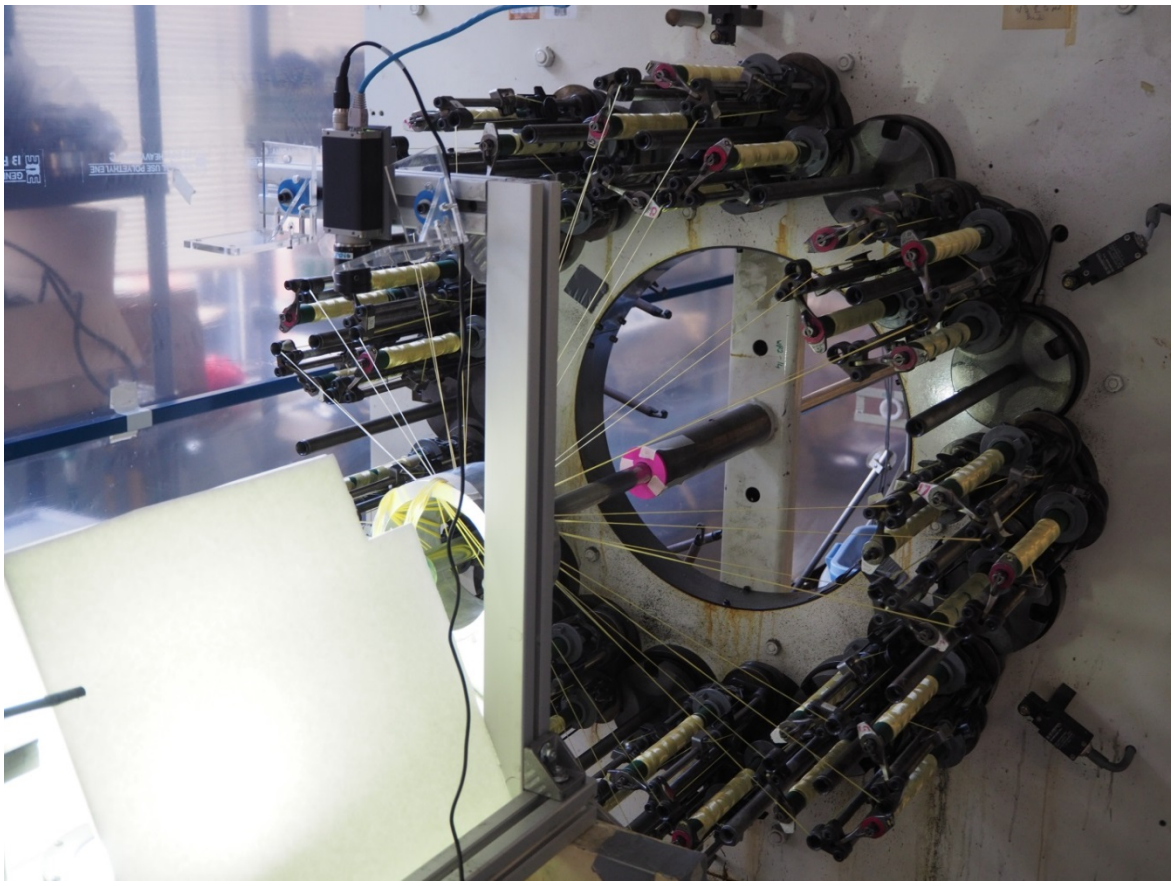

Figure 4-3: Image of the experimental setup showing the placement of the camera in-line with the maypole braiding machine.

4.2.1.2 Braid angle measurement algorithm

The images are analyzed in the frequency domain to measure the braid angle of the tubular braided preforms. The two-dimensional discrete Fourier transform (2D-DFT) is used as the primary image processing method to analyze the images. This technique suits the real-time application of this machine vision system through the implementation of the fast Fourier transform (FFT) algorithm. Computation of the 2D-DFT using a FFT algorithm reduces the computational intensity from $O(N^2)$ for a standard discrete Fourier transform to $O(NlogN)$ [14].

The 2D-DFT, shown in Equation 4.1, of an image produces the frequency spectrum *F(u,v),* of size MxN. Where *x* and *y* are the spatial coordinates of the image and *u* and *v* are the frequency

variables in the x and y directions respectively [27]. The produced frequency spectrum represents the two dimensional frequency components in the input image, *f(x,y)* with a size MxN. The frequency spectrum is a two dimensional array of values where each pixel value represents a two dimensional frequency component, with the magnitude of the pixel value representing the significance of the specific frequency component in the spatial image [27, 28].

$$F(u,v) = \frac{1}{MN}\sum_{x=0}^{M-1}\sum_{y=0}^{N-1} f(x,y)e^{-j2\pi\left(\frac{ux}{M}+\frac{vy}{N}\right)} \tag{4.1}$$

The image pair shown in Figure 4-4 show the coordinate systems for the spatial image and frequency spectrum of a braided preform image. By placing the origin of the frequency spectrum in the center of the image, features from the spatial image can be identified by visually inspecting the frequency spectrum. Low frequency data is plotted in the center of the spectrum and high frequency data is plotted further form the origin.

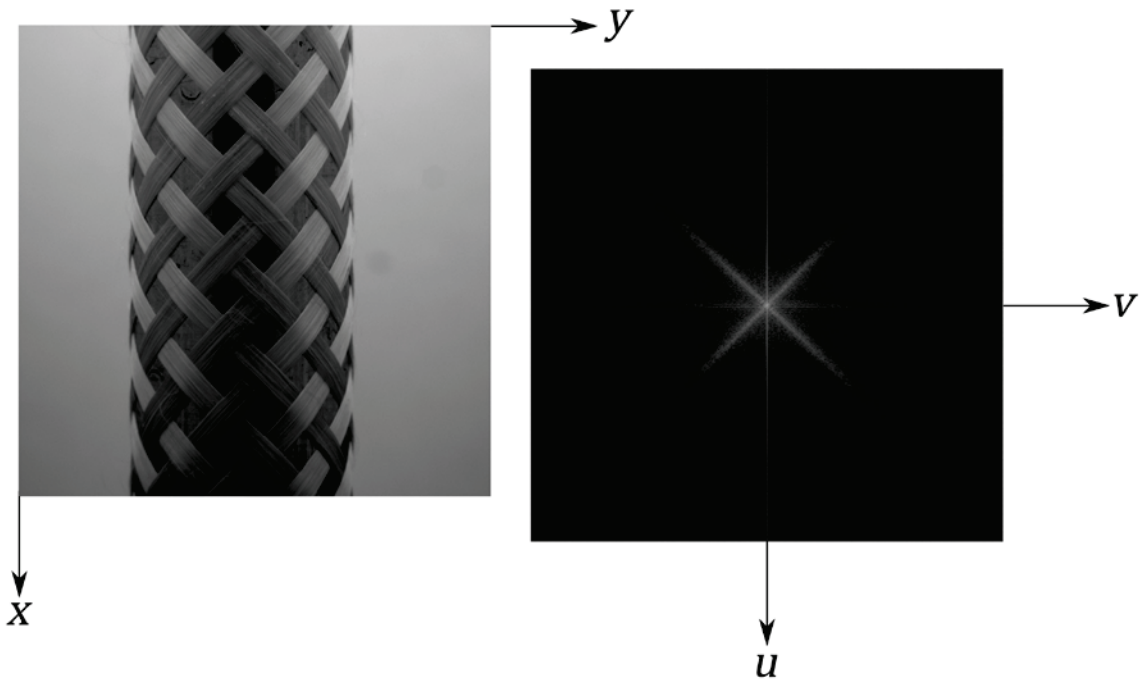

Figure 4-4: Spatial image (left) and frequency spectrum (right) showing respective coordinate systems of the spatial and frequency domains.

The high frequency data in the frequency spectrum corresponds with the sharp transitions in pixel value in the image. When applied to images of braided preforms, the majority of the high frequency data corresponds with the boundaries of the braided fibers. Unique properties of the Fourier transform, such as rotation invariance, symmetry, linearity and the preservation of angular orientation [27-29] allow the braid angle to be measured from the frequency spectrum. The most useful property of frequency domain image processing as it pertains to fiber orientation measurements is the relationship between the edges in the image and their corresponding image frequencies. In the spatial image, the viewer can observe the individual features in each image due to the contrast and the boundaries of the various features. The frequency spectrum allows the strength and directionality of all pixel changes in the image to be visualized. By outputting a properly scaled frequency spectrum, the angular orientation of features in the frequency spectrum will be perpendicular to those in the spatial image [28]. The relationship between the braid angle of a braided preform and the angle between the features in the frequency spectrum can be seen in Figure 4-5.

Figure 4-5: Annotated image of braided preform and frequency spectrum showing relationship between features in the spatial and frequency domains.

A search routine is used to locate the angular orientation of the features in the frequency spectrum, similar to those shown in Figure 4-5, which correspond to the fiber directions. This is done by searching for the angular direction in the frequency domain corresponding to the highest average pixel intensity in the frequency spectrum. A circle is discretized around the center of the spectrum and for each discrete direction; a scan line is drawn outwards from the center of the spectrum to the discretized circle to consider both low and high frequency data for each discretized direction. This process is shown in Figure 4-6 and the result of this process, the angular intensity plot, is shown in Figure 4-7. This plot shows the average pixel intensity of the pixels along the scan line as a function of the orientation of this line.

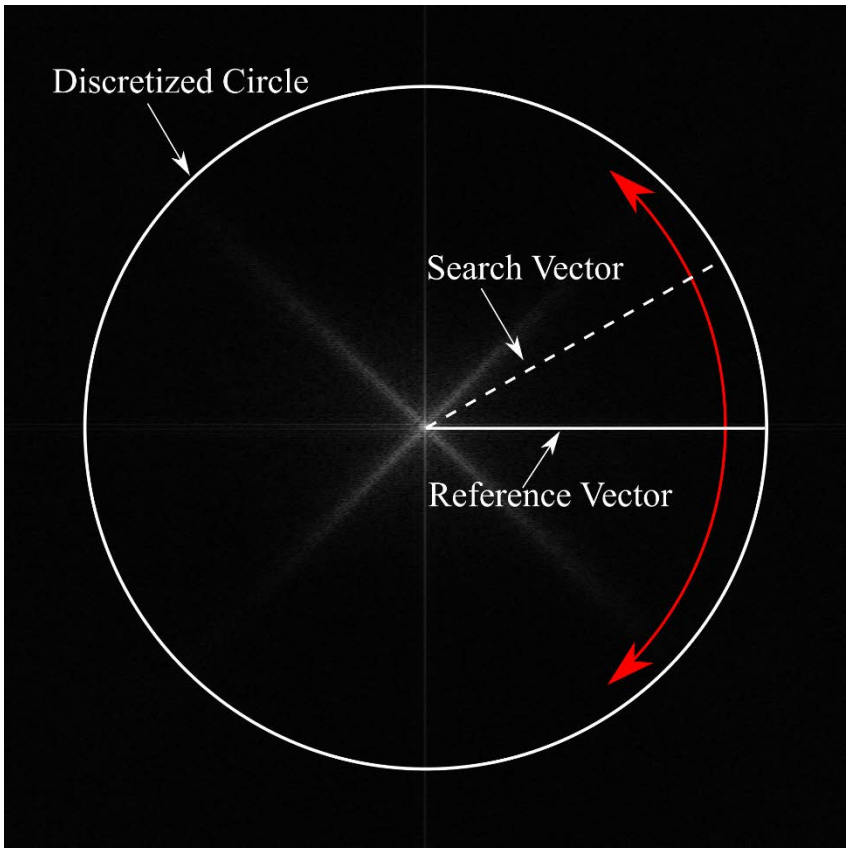

Figure 4-6: Annotated frequency spectrum showing search routine for analysis

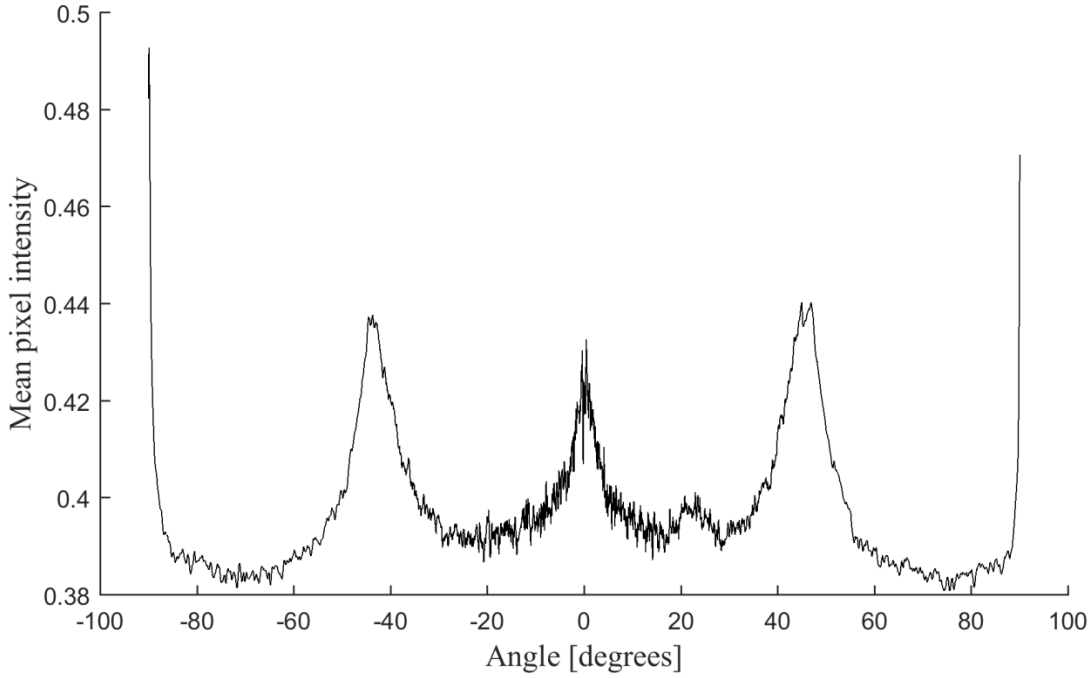

Figure 4-7: The angular intensity plot of the frequency spectrum. This is obtained by plotting the mean pixel intensity vs. angle of scan line.

4.2.2 Operation of maypole braiding machine

Control over the fiber orientation of the braided preforms is achieved by modifying the rotational speed of the yarn carriers and the linear speed of the mandrel. These processes are powered by electric motors which are controlled through user written software written in LabView [National Instruments, Texas, USA]. The braiding machine and the puller can be seen in Figure 4-8 and Figure 4-9 respectively. The speed of each device can be set in volts, ranging from 0-10 VDC. Determining the conversion factor from input voltage to linear of rotational speeds for the puller and braider respectively, a speed calculation was performed. Details regarding the calibration process are described in Appendix C.

Figure 4-8: Annotated image of the 36-carrier braiding machine used to produce the tubular braid preforms.

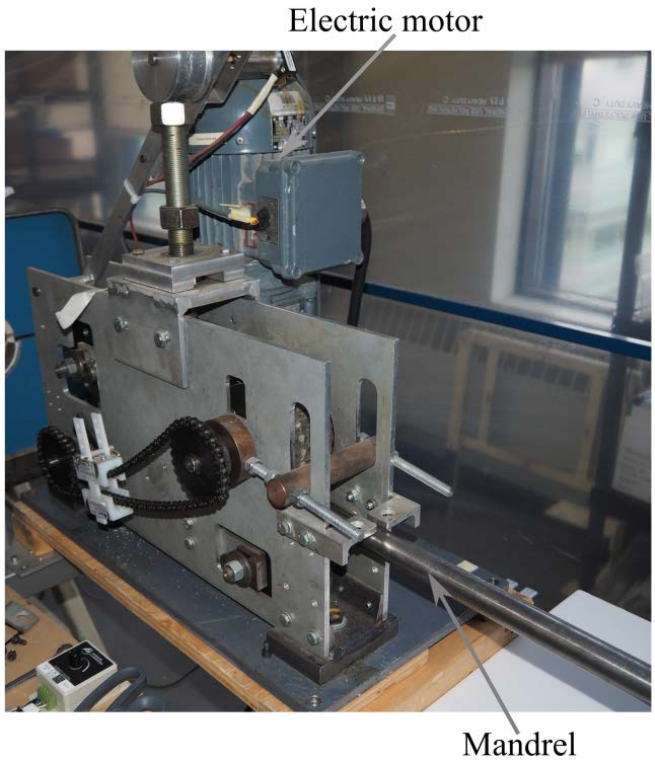

Figure 4-9: Annotated image of the puller used to advance the mandrel.

4.2.2.1 Production of constant braid angle preforms

The production of braided preforms with a constant braid angle was done with the use of Equation 4.2, which is the geometric braiding equation which relates the rotational speed of the carriers, ω, linear velocity of the mandrel v and the radius of the mandrel R_m to the steady state braid angleθ_∞ [3, 5, 30-32]. The braid angle will converge on the steady state value calculated with Equation 4.2; sufficient time must be given to ensure that the braid angle has reached steady state.

$$tan\theta_\infty = \frac{\omega}{v} R_m \tag{4.2}$$

4.2.2.2 Production of transient braid angle preforms

A transient braid pattern can be obtained by changing the braiding machine speeds and allowing the braid geometry to converge to a new steady state geometry. Du and Popper [3] derived differential equations to model this transient process. This is done by using the following three equations. A key geometric factor is the ratio of the mandrel radius R_m and the track plate radius, R_g, given by λ, shown in Equation 4.3.

$$\lambda = \frac{R_m}{R_g} \tag{4.3}$$

To observe the transient relationship between the braiding machine speeds and the braid angle, Equations 4.4 and 4.5 are used. Equation 4.4 calculates the location of the convergence plane, *h(t)*, as a function of time. The convergence length is related to the braid angle, θ, by using Equation 4.5. These two equations are used to predict how the braid angle changes with a

change in braiding speeds and will be used in experiments discussed in later sections of this chapter.

$$h(t) = \frac{v}{\omega}\frac{\sqrt{1-\lambda^2}}{\lambda} + \left[h_0 - \frac{v}{\omega}\frac{\sqrt{1-\lambda^2}}{\lambda}\right] e^{\frac{\lambda}{\sqrt{1-\lambda^2}}\omega t} \tag{4.4}$$

$$tan\theta(z) = \frac{R_g}{h(t)}\sqrt{1-\lambda^2} \tag{4.5}$$

Applying the machine vision system to a transient braiding process accomplishes two tasks. It allows the performance of this measurement technique to be determined for a non-constant braid angle and it allows the accuracy of the Du and Popper's transient braid model [3] to be determined for the braiding setup used in this work. Their model is currently being used and adapted due to its simplicity and because of the possibility of solving an inverse solution [33], which is valuable for automated braiding. Du and Popper [3] have reported that this model under-predicts the braid angle by approximately 5° degrees. Although there is the possibility for significant error, the accuracy of a braid model has not previously been verified in real-time and the comparison of the machine vision results to the predicted model results will have value.

4.2.3 Experimental procedure

To assess the developed frequency domain measurement technique as a suitable real-time machine vision algorithm, tubular braided preforms will be imaged under dynamic conditions during the braiding process. Aramid fibers [DuPont, Canada] with a 1420 denier are braided atop a tubular mandrel with a diameter of 1". Images are collected and processed during the production of the braided preforms to obtain the braid angle measurement in real-time. Software

used to control the cameras and process the images was done using custom written software in Matlab [Natick MA, USA]. All samples were imaged at a constant frame rate of 1 frame per second.

The first set of testing involves measuring the steady state braiding process in real-time. This will allow the accuracy of measuring a constant braid angle to be determined. Preforms were produced with braid angles of 30°, 45° and 55°. Images were collected along preform lengths ranging from 0.5 to 1.0 meters depending on the time required before reaching steady state. For each braid geometry two samples were imaged and measured. Each data set consists of a series of images and braid angle measurements which correspond to the different locations along the mandrel. The linear and rotational speeds of the mandrel and yarn carriers used to produce the constant braid angle preforms are shown in Table 4-1.

Table 4-1: Braiding production parameters for steady state braiding tests

Steady state braid angle	30°	45°	55°
Mandrel speed [mm/min]	280	280	280
Carrier speed [RPM]	2.64	3.54	4.98

The second test involves imaging a transient braid pattern which will determine the ability of this measurement technique to track a changing braid angle. A transient braid angle will occur each time the braiding speeds are altered, which makes this a common scenario in which the braid angle must be measured. This was done by imaging the transient change in braid angle which is seen during the transition between two steady state braid angles; 30° and 55° were chosen as the steady state braid angles. A stepwise change in yarn carrier speeds according to the speeds shown in Table 4-2 was used to initiate the transient braid pattern. Two preforms were produced for both increasing and decreasing braid angles. The comparison of these results to Du and

Popper's model [3] was done by comparing the measured braid angles to expected results which were calculated with Equations 4.3 to 4.5.

Table 4-2: Braiding production parameters for the transient braid angle tests

Steady state braid angle	30°	55°
Mandrel speed [mm/min]	280	280
Carrier speed [RPM]	2.64	4.98

4.3 Results

4.3.1 Constant braid angle tests

The results of the braid angle measurement tests are shown in Table 4-3. This table shows the average and standard deviation of all the collected images. The average measurements are in close agreement with the predicted braid angle, as well as in close agreement between two repeat tests. The magnitude of the measurement standard deviation is comparable to what has been reported for the static braid angle measurements discussed in Chapter 3. The standard deviation of the static braid angle measurements ranged between 0.2° and 0.3°. These values lie within the range of standard deviation values in Table 4-3 which shows that the accuracy and uncertainty in measuring a constant braid angle in real-time is comparable to static braid measurement tests. Two braided preforms were produced and measured for each braid geometry. The results in Table 4-3 show a very good repeatability between the repeated tests; the average and standard deviation differ by a maximum of 0.4°.

Plots of the measured braid angle as a function of mandrel position for the 30°, 45 ° and 55° preforms are shown in Figure 4-10, Figure 4-11 and Figure 4-12, respectively. Dashed lines are plotted alongside the experimental data to show the effectiveness of this measurement technique. The dashed lines correspond to a ±1° band surrounding the mean measurement. This band is a

measure of the uncertainty associated with the conventional manual measurement techniques that this automated method aims to replace.

Table 4-3: Steady state real-time braid angle measurement results for each of the three braid geometries. Mean and standard deviation values are given in degrees.

	30°		45°		55°	
	Mean [deg]	St. dev [deg]	Mean [deg]	St. dev [deg]	Mean [deg]	St. dev [deg]
Sample 1	29.7	0.33	44	0.38	54.5	0.21
Sample 2	29.8	0.37	44.1	0.37	54.6	0.25

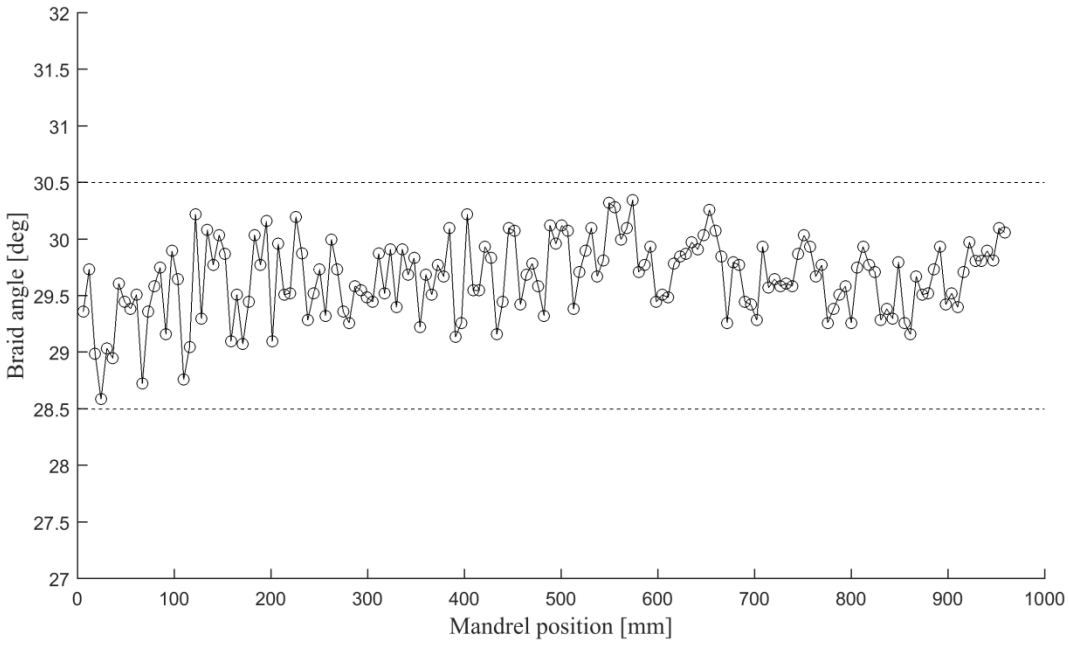

Figure 4-10: Braid angle plot for braided preform with 30 braid angle. The dashed lines indicate ±1° band surrounding the mean associated with the uncertainty of past measurement methods.

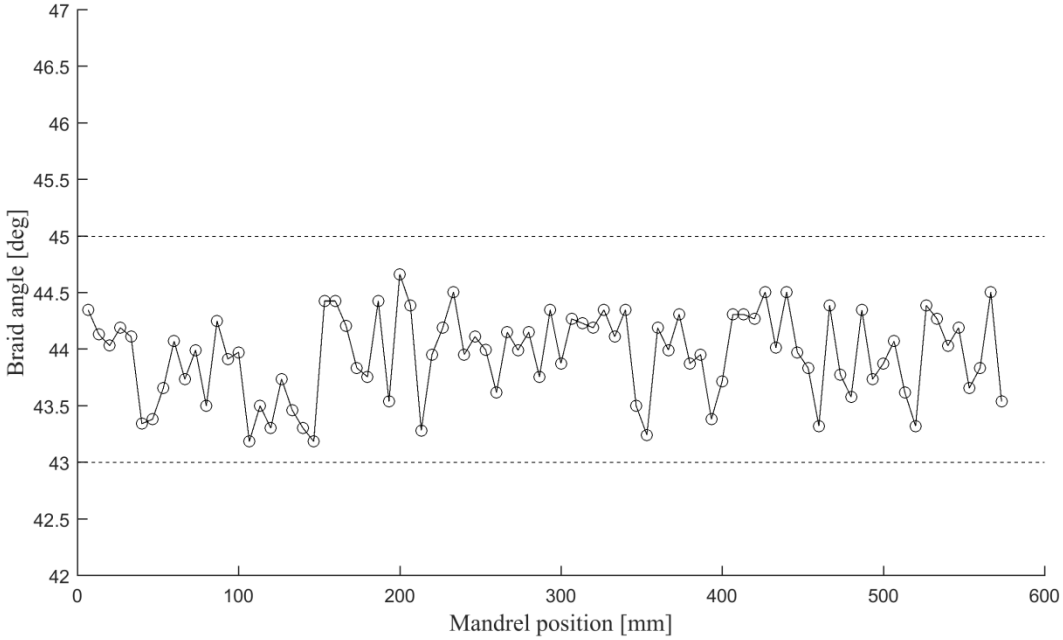

Figure 4-11: Braid angle plot for braided preform with 45° braid angle. The dashed lines indicate ±1° band surrounding the mean associated with the uncertainty of past measurement methods.

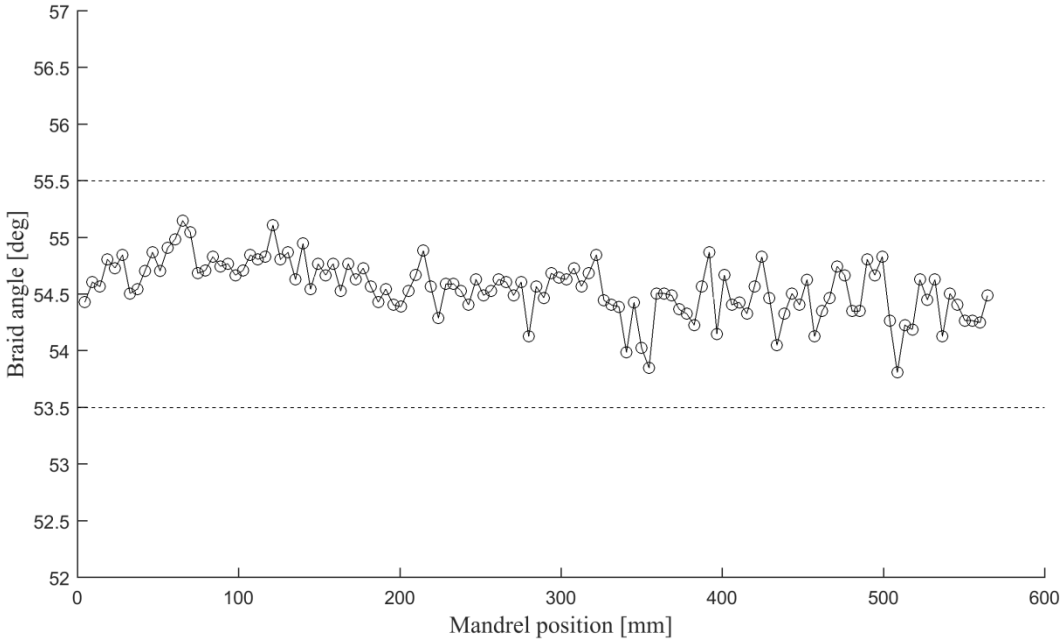

Figure 4-12: Braid angle plot for braided preform with 55° braid angle. The dashed lines indicate ±1° band surrounding the mean associated with the uncertainty of past measurement methods.

Images were collected at a fixed frame rate of 1 frame per second. As a result, the number of images between tests varied depending on the braiding speed and the time taken for the braid pattern to converge to the steady state braid angle. For each constant braid angle data set, the transient region is removed by visual inspection. The transient braid angle region can be clearly seen in the machine vision measurements, as shown by the region of increasing braid angle plotted in Figure 4-13.

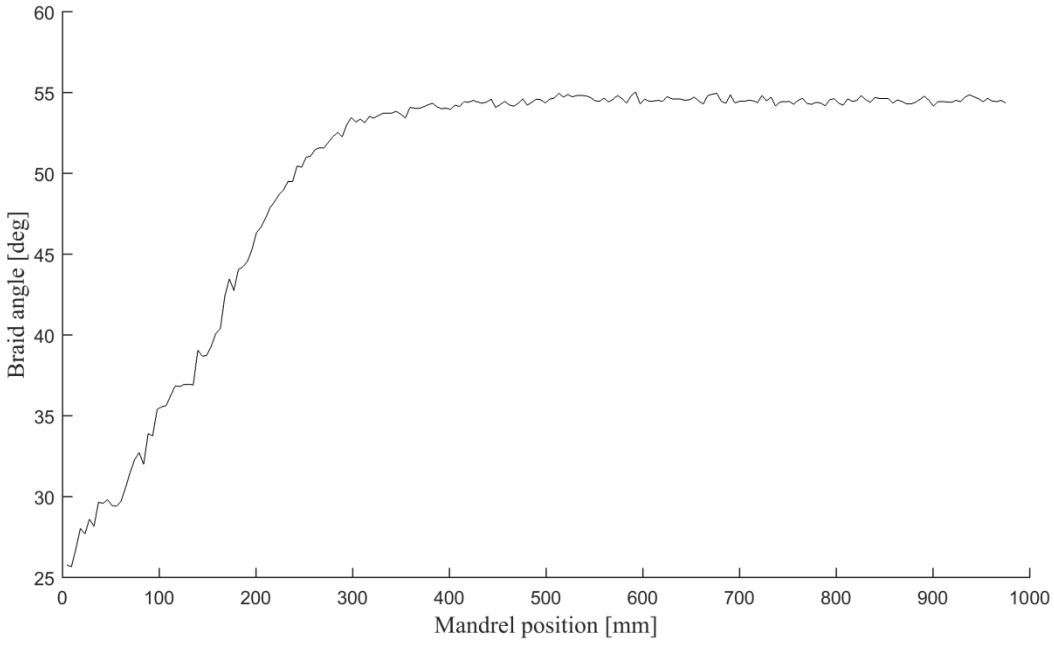

Figure 4-13: The complete braid angle plot for a braided preform with a 55° braid angle showing the initial convergence zone prior to the region of steady state braid angle.

4.3.2 Transient braid tests

The developed measurement technique has been shown to make accurate braid angle measurements on stationary braided preforms (Chapter 3) and dynamic samples with a constant braid angle (Section 4.3.1). For validation, the braid angle results up this point were compared against manual measurements and expected braid angle values using the steady state braiding equations developed by Du and Popper [3]. Good results indicate that the measurement

technique accurately represents the orientation of the fibers on the mandrel so for the upcoming test, the measured braid angle will not be compared to a specific braid angle, but to a transient braid angle curve.

One of the advantages of using braided composite materials is the ability to control the material properties by varying the braid angle of the fibers along the length of the mandrel. To test the performance of this measurement technique at measuring a transient braid angle, braiding speeds are changed in a stepwise fashion from one steady state braid angle to another. Tests are done to track an increasing and decreasing transition in braid angle between steady state braid angles of 30° and 55°. The process parameters used to produce these braid geometries are shown in Table 4-4. The measured transient braid angle is compared to the kinematic braiding equations, given in Equations 4.3-4.5, which were developed by Du and Popper [3]. The results of the increasing and decreasing braid angle transition are shown in Figure 4-14 and Figure 4-15. The experimental results are in good agreement with the predicted curve from the Du and Popper model [3].

Table 4-4: Braiding machine process parameters for the transient braiding test

Steady state braid angle	30°	55°
Mandrel speed [mm/min]	280	280
Carrier speed [RPM]	2.09	4.98

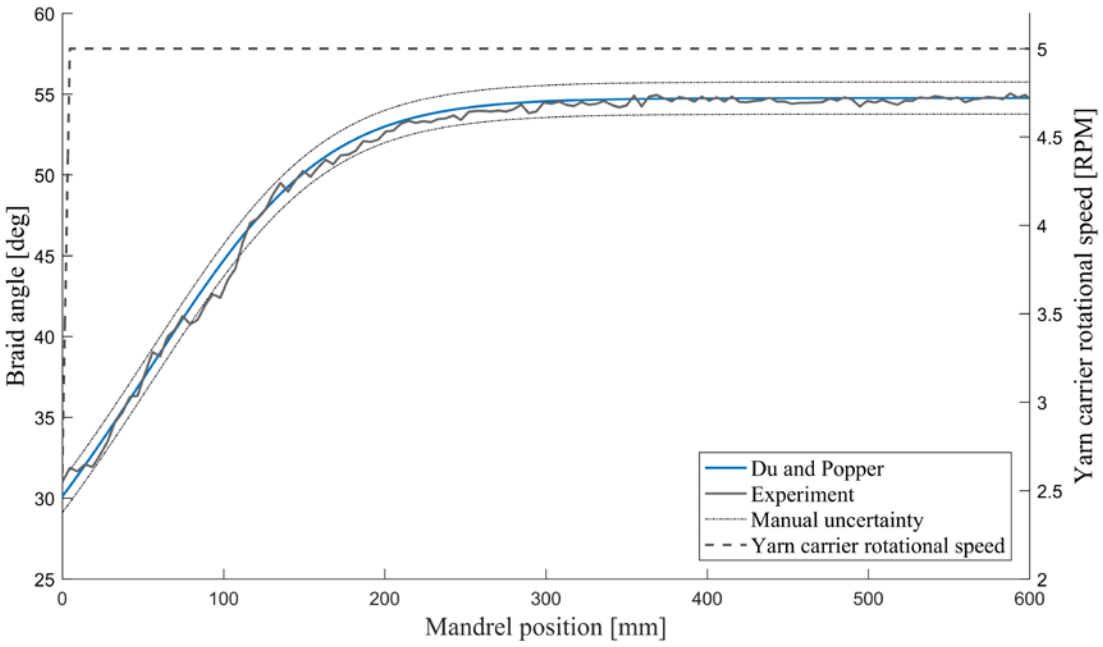

Figure 4-14: Braid angle measurement results for stepwise change in braiding speeds resulting in an increase in braid angle from 30° to 55°. The dotted lines indicate ±1° band surrounding the mean associated with the uncertainty of past measurement methods. The dashed line shows the stepwise change in rotational speed.

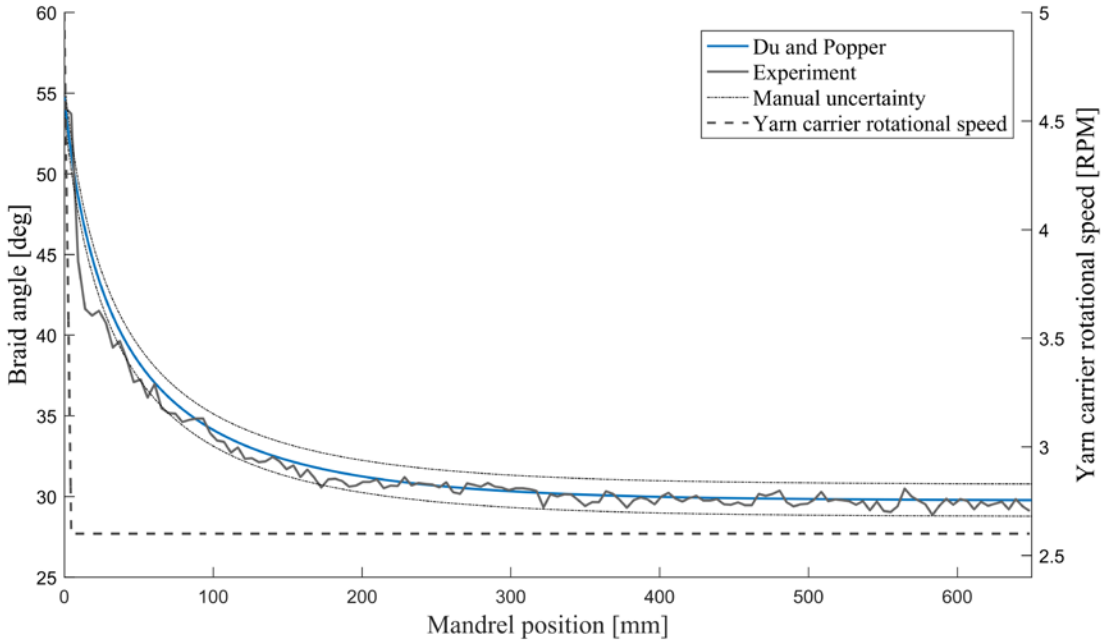

Figure 4-15: Braid angle measurement results for stepwise change in braiding speeds resulting in a decrease in braid angle from 55° to 30°. The dotted lines indicate ±1° band surrounding the mean associated with the uncertainty of past measurement methods. The dashed line shows the stepwise change in rotational speed.

4.4 Discussion

The objectives of this work were to assess the performance of a frequency domain measurement technique as a suitable automated and real-time braid angle measurement technique. Such a system allows the braid angle to be measured in-line with the braiding process. This system benefits the braiding process by eliminating the need to manually measure the braid angle after the braiding process and eliminates human error from the measurement process which ranges from ±1° to ±2° [7, 11]. Imaging and measuring tubular braided preforms with a braid angle with constant and transient braid angles allows the performance of the Fourier transform measurement technique to be assessed for the real-time measurement of braided composite materials.

4.4.1 Accuracy of the braid angle measurement

The braid angle results shown in Section 4.3 showed an unexpected fluctuation between adjacent measurements. This was thought to be due to the potential measurement instability of the image processing techniques. To determine if this is true, a series of 15 images were taken at one frame per second of a stationary braided preform to determine the repeatability of the braid angle measurement. In each image, the region of interest of the camera was kept the same. The measurements from this process resulted in measurement fluctuation, as shown in Figure 4-16. The fluctuations are small compared to the band of uncertainty which is associated with manual measurement techniques, shown by the hatched lines. By analyzing the collected images, it was found that the image pixels varied slightly between collected frames. An average difference in pixel value between consequent frames was found to be 1.69 by subtracting the 8-bit images. The change in pixel value suggests that the measurement inconsistency is partly due to the data collection process. The results show that the frequency domain technique is sensitive to these small changes in pixel value which can be a result of sensor noise and subtle changes in lighting. These results showed a standard deviation of 0.11°. Although these fluctuations are small in comparison to the uncertainty of ±1° associated with manual measurement techniques, it shows the sensitivity of this measurement technique to subtle changes in pixel value.

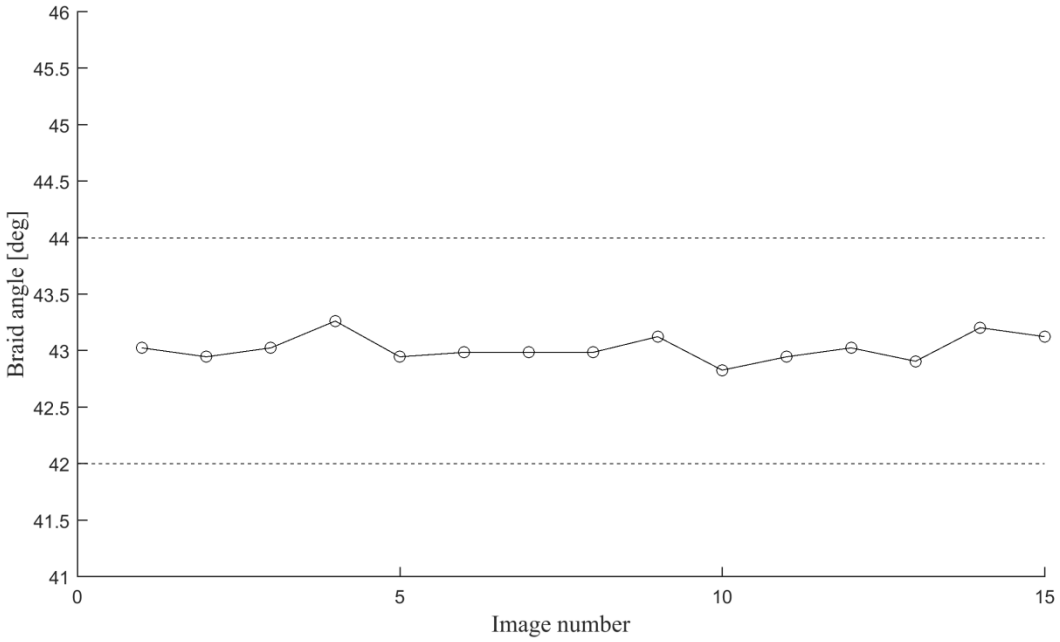

Figure 4-16: Braid angle measurement for repeat images of the same region of interest. The dashed lines indicate ±1° band surrounding the mean associated with the uncertainty of past measurement methods.

4.4.2 Constant braid angle measurements

Figure 4-10 to Figure 4-12 shows plots of the braid angle as a function of mandrel position for the 30°, 45° and 55° braid angle preforms. These results show the fluctuation of the machine vision measurement. Although the measurement result fluctuates between consequent images, the spread of this data is within ±1°, which is the uncertainty associated with measuring the braid angle through manual techniques. The average of the real-time measurements was in good agreement with the expected braid angle results with a maximum percent error of 2% for the 45° braid angle test. The standard deviation of the measurements was comparable to the uncertainties from the static braid angle tests, which ranged from 0.23° to 0.3° as discussed in Chapter 3 which shows that imaging a dynamic braid preform does not change the measurement results.

The measurement error due to the data collection process was found to be ±0.11° from the findings the previous section. The fluctuations in the results shown in Figure 4-10 to Figure 4-12 are larger than the measurement repeatability associated with a stationary region of interest. To investigate these fluctuations, the images captured during operation of the machine vision system can be studied. Figure 4-17 shows two consecutive cropped images of the 45-degree braid preform. The fixed frame rate used for the image acquisition results in a significant region of overlap between the two images. This results in a significant portion of spatial features to remain the same between the two images.

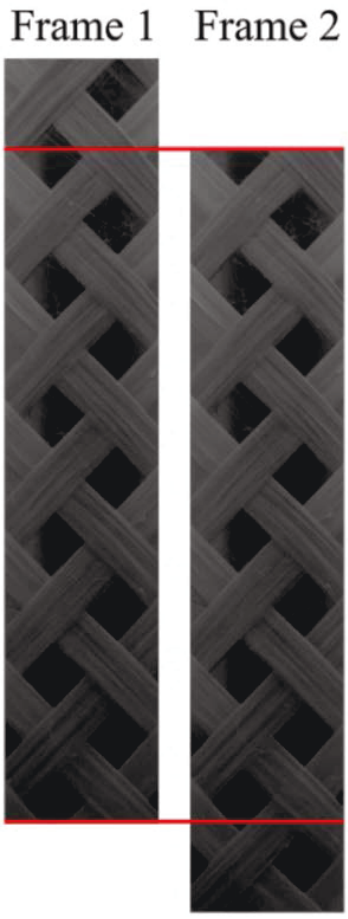

Figure 4-17: Schematic showing the overlapping region of interest between images

The overlapping region of interest and the area scan data collection affect the presented measurement results in several ways. The first is that for each image, a single braid angle measurement is made from the consideration of the multiple unit cells in each region of interest. In this technique, the braid angle is obtained determining the orientation of the most dominant image frequencies, as opposed to locally measuring the angle of two intersecting fibers for the case of manual braid angle measurement techniques. This is beneficial as it eliminates the need to perform a series of localized measurements to characterize the fiber orientation as was done in [8, 31]. Secondly, the overlapping area scan images means that a single unit cell on the surface of the braid preform will influence multiple consecutive braid angle measurements for a dynamic sample. Knowing that the braid angle measurement is dependent on features used in past measurements allows certain conclusions to be made. One of which is the impossibility of a sharp and abrupt change in braid angle for a constant cross section mandrel moving at a constant linear velocity. This increases confidence in an error handling process to remove a measurement which is significantly larger that all surrounding braid angle measurements due to the physics behind the braiding kinematic models and the repeat contributions from unit cells.

4.4.3 Transient braid tests

Having the ability to modify the fiber orientation along the length of the mandrel enables the production of braided composites with varying material properties along the length. The angular speed of the yarn carriers was changed in a stepwise fashion to produce the transient braid pattern used in these tests. The results, shown in Figure 4-14 and Figure 4-15 compare the machine vision braid angle measurements to the predicted curve from Du and Popper [3]. Increasing and decreasing braid angles were tested.

The transient braiding equations developed by Du and Popper [3] are valuable due to their simplicity and the ability to provide analytical equations describing the resulting braid geometry. Because of these merits, their work is still the focus of attention for automated braiding applications [33] even though they report a 5° error in predicting the braid angle [3]. The plots shown in Figure 4-14 and Figure 4-15 comparing the experimental data to Du and Popper's transient braid model show a good agreement between the measured and predicted braid angles. The reported error of 5° was not seen in these results. Experiments done by Du and Popper [3] also found that their model was capable of accurately predicting the convergence zone length of the braided preforms. Their ability to predict the convergence zone length but not the resulting braid angle suggests that the inter-yarn forces created by the yarn interactions at the interlacing points in the convergence zone invalidate the straight yarn assumption and affect the orientation at which the fibers rest on the mandrel. Increasing the number of braid yarns increases the number of interlacing points and inter-yarn friction [6, 30] which is critical to consider in this comparison. Du and Popper [3] used a 72 carrier braider whereas the braiding machine used in this work had 36. This decrease in the number of braid yarns significantly affects the amount of inter-yarn friction that could affect the geometric braiding models and suggests that these models have limited applicability to certain fiber types and braider geometries. The dependence of model accuracy on yarn type and yarn tension was explored by Zhang et al [6], however, no similar verification of transient braid models were done.

Guyader et al. [5], and Ravenhorst and Akkerman [11] also reported error of 3° in predicting the braid angle in tubular and non-tapered mandrels. Each of their predictive models relied on neglecting yarn interactions similar to Du and Popper [3, 4]. Guyader et al. [5] used a 64-carrier and Ravenhorst and Akkerman [11] used a large scale radial braiding machine. In each case, the

number of interlacing points in greater that the experiments performed in this work. Similar to the comparison between the experimental results and the Du and Popper model, this reported error and large number of braiding yarns suggests that there is limit to which the frictionless and straight yarn assumptions are valid.

Through inspection of these plots, the errors in regions of rapidly changing braid angle are greater than those of regions with a constant braid angle. This results in some measurements which fall outside of the ±1° uncertainty band that was used in all other tests in this work. The method in which data is collected and processed may contribute to the increased error in regions of rapidly changing braid angle. As was previously discussed, 2D images are collected and processed to obtain a braid angle measurement which considers the frequency component of all the image features in the frequency domain. This means that a single measurement is made from the information of multiple braid unit cells. The region of interest in the longitudinal direction measures a 60 mm long portion of the preform; and in regions where the braid angle is changing rapidly with mandrel position; it is possible that there is a non-constant braid angle in the field of view of the camera. This is shown in Figure 4-18 where, found through manual measurements, there is approximately 6° difference between the fibers at the top and bottom of the image.

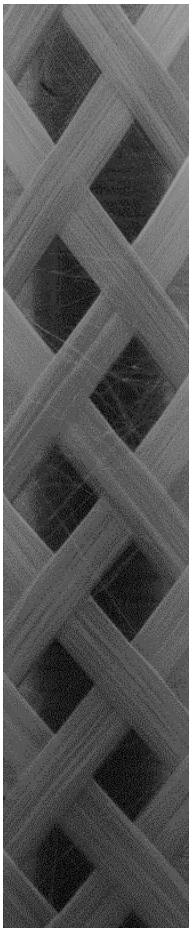

Figure 4-18: Cropped braided preform image captured during the transient braiding process showing the difference in braid angle in the longitudinal direction of the image.

This will lead to a distribution of fiber angles in the frequency spectrum which affects the angular intensity plot in a similarly to the braid angle distribution caused by perspective error which was discussed in Chapter 3. The angular intensity plots shown in Figure 4-19 and Figure 4-20 show the effect that this has on the frequency spectrum. The image containing the changing braid angle as a function of mandrel position contains a larger braid angle distribution, seen as wider peaks in the plot shown in Figure 4-19. For comparison, an image of the braid preform captured during the steady state braider operation produces the plot shown in Figure 4-20, which shows much sharper peaks due to the constant braid angle of the fibers in the image.

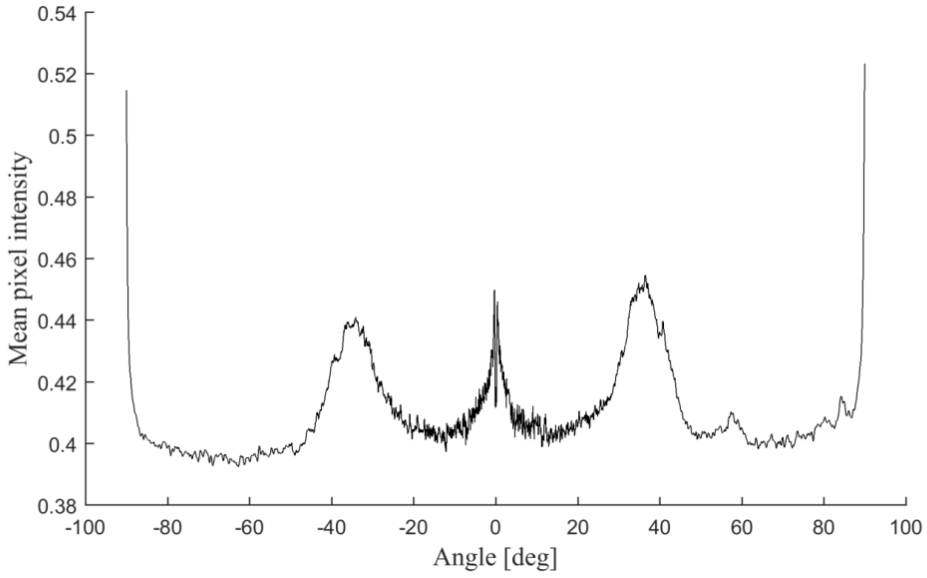

Figure 4-19: Angular intensity plot of the image shown in Figure 4-18. The wide peaks suggest a significant braid angle distribution within the images.

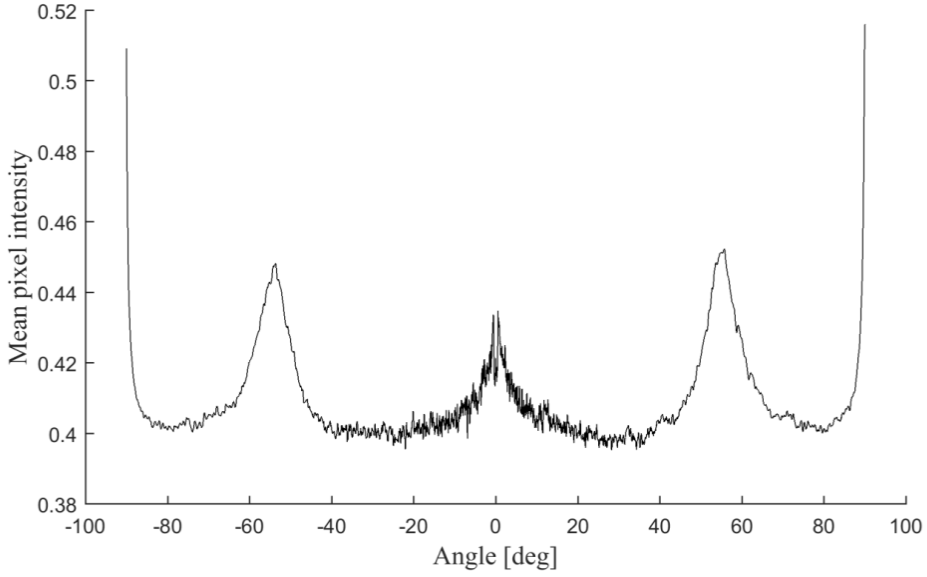

Figure 4-20: Angular intensity plot of an image captured during the steady state braid angle region showing sharper peaks which indicate a smaller distribution of yarn directions in the image.

The wider peaks in Figure 4-19 mean that there is a distribution of features in the spatial image whose frequency components have a similar magnitude in the frequency spectrum. Because of the sensitivity of the Fourier transform measurement to small changes in pixel value, there is a

greater chance that one of these angles in this distribution is identified as the maximum value for a given image, increasing the possibility for fluctuations between measurements.

The ability to track the transient braid angle is important. The only other real-time system capable of accomplishing this task is the cone angle measurement device developed by Mazzawi [34]. However, the machine vision system has notable advantages over the mechanical implement developed by Mazzawi; which required that the braid angle be inferred from the convergence length. Several geometric models have struggled to accurately calculate the convergence length including what was developed by Mazzawi [34] and Guyader [5]. Directly imaging the braided structure is a much better source of data and eliminates the need to infer the braid structure from other geometric factors.

4.4.4 Filtering braid angle measurements

It was aforementioned that the high frequency fluctuations in the real-time braid angle measurements may be due to the sensitivity of the measurement to subtle changes in image data. Because of the fact that these measurement fluctuations are due to the limitations of the imaging process and not the fluctuation off fiber angle, it would be beneficial for these fluctuations to be removed for future applications, which could include using this measurement system for feedback control.

The high frequency fluctuations in the real-time braid angle measurements can be removed by a standard low-pass, moving average filter. Design of the filter is done by considering the amount of overlap in the collected images. For the image acquisition rate of 1 frame per second and the chosen mandrel speeds, a single unit cell will be in 8 consecutive images. Thus by choosing an 8-term moving average filter, the current measurement will be influenced by the previous 7 past braid angle measurements. The result of this process is shown in Figure 4-21 and it shows that

by using a window size of 8, significant measurement fluctuation can be removed. However, this is done at the expense of introducing a time delay in the filtered signal. This delay affects the tracking of a transient braid angle and the effect of this delay should be further explored for feedback control applications.

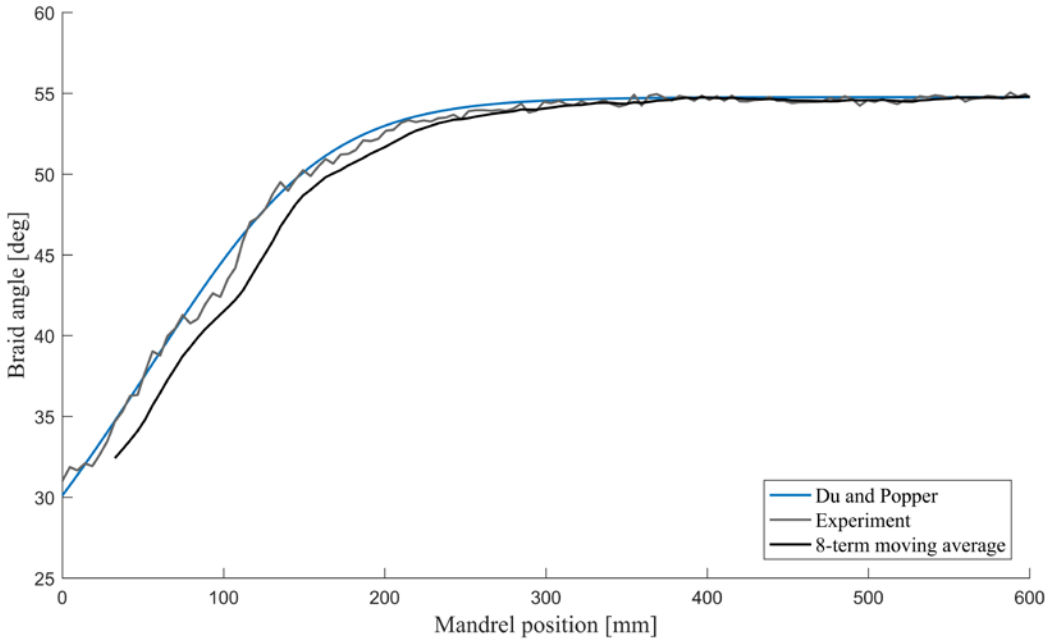

Figure 4-21: Increasing transient braid angle plot showing the smoothed 8-term moving average curve.

The time delay can be compensated for by adjusting the data by the appropriate number of samples. For the moving average filter, this delay is given by half of the size of the filter window. This produces the plot shown in Figure 4-22. The 8-term window removes the unexpected measurement fluctuations and produces a braid angle plot which closely matches the kinematic relationship derived in Figure 4-22. This result simultaneously validates the kinematic equations, as well as the braid angle measurement method which is the first system to be used to validate kinematic braiding equations in-line with the braiding process.

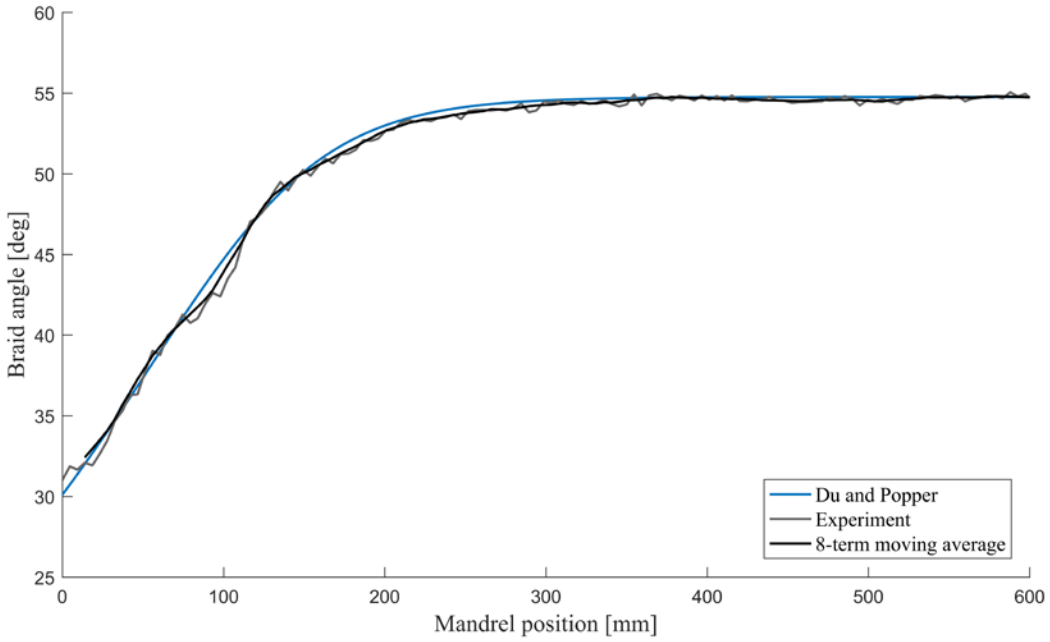

Figure 4-22: Plot showing the delay compensated 8-term moving average curve.

4.4.5 Braided sample limitations

The machine vision system was developed to further automate the braiding production process. However, fiber production is only the first step in producing braided composite materials. In-line resin impregnation techniques have been used in braided composite applications [35] and future application of this measurement technique to wet fiber braided structures will be beneficial. The success of the proposed measurement technique relies on having high frequency components in the image which correspond to the primary fiber directions. If this image property is preserved, then the developed technique will work as a braid angle measurement technique, however, this has yet to be verified. Additional to this, the wet fibers may have different reflectance properties than the dry fiber braids. Thus, a new illumination setup may have to be developed to capture images of the impregnated fibers.

4.5 Conclusions

The production of 2D braided composite materials is limited by the multi-step manufacturing process required to go from yarns to rigid composite part. To further automate the production of the fiber structure, a machine vision system was developed to measure the braid angle of tubular braided preforms. The ability to make automated braid angle measurements addresses two shortcomings in the braiding process. Real-time feedback of the braid geometry can be used to ensure that the desired braid geometry is produced with the chosen braiding speeds. This also eliminates the need to manually characterize the braid geometry with manual measurement techniques. These measurements are affected by human error, are time consuming and are not suitable for the large-scale production of braided preforms.

The developed machine vision system was found to be successful for measuring constant and transient braid angle preforms in real-time, with lower uncertainty compared with manual measurement techniques. The results showed that measuring the braid angle of tubular braided preforms in-line with the braiding process produced similar levels or error to static braid angle measurements. By comparing the transient braid angle pattern obtained from a stepwise change in machine speeds to Du and Popper's transient braid equations, good agreement was obtained, suggesting that braider size and configuration affect the validity of assumptions made in the derivation of geometric braiding models. Although the machine vision technique was applied to tubular samples, directly measuring the braid angle with imaging allows this technique to be applied to various mandrel geometries, as well as other braiding setups, such as radial braiders and 3D braiders by simply mounting a camera in-line with the braiding process.

These results also show that the fiber deposition process can be accurately monitored in real-time with a low cost machine vision system. The fully automated machine vision system can

eliminate the need to perform manual quality assurance measurements of the braid angle and has shown to be more accurate than some multi-frame techniques due to the removal of human error associated with landmark selection.

4.6 References

[1] D. Brunschweiler, "Braids and Braiding," Journal of the Textile Institute Proceedings, vol. 44, pp. 666-686, 1953.

[2] C. Ayranci and J. Carey, "2D braided composites: A review for stiffness critical applications," Composite Structures, vol. 85, pp. 43-58, 2008.

[3] G.W. Du and P. Popper, "Analysis of a circular braiding process for complex shapes," Journal of the Textile Institute, vol. 85, pp. 316-337, 1994.

[4] G.W. Du, P. Popper and T.W. Chou, "Process Model of Circular Braiding for Complex Shaped Preform Manufacturing," in Proc. Symp. on Processing of Polymers and Polymeric Composites, 1990.

[5] G. Guyader, A. Gabor and P. Hamelin, "Analysis of 2D and 3D circular braiding processes: Modeling the interaction between the process parameters and the pre-form architecture," Mechanism and Machine Theory, vol. 69, pp. 90-104, 2013.

[6] Q. Zhang, D. Beale, R.M. Broughton and S. Adanur, "Analysis of circular braiding process, part 2: Mechanics analysis of the circular braiding process and experiment," J.Manuf.Sci.Eng.Trans.ASME, vol. 121, pp. 351-357, 1999.

[7] A.J. Hunt and J.P. Carey, "Geometry Measurement of Tubular Braided Composite Materials for Real-Time Applications," in CANCOM 2015 - Canadian International Conference on Composite Materials, 2015.

[8] S.V. Lomov, R.S. Parnas, S.B. Ghosh, I. Verpoest and A. Nakai, "Experimental and theoretical characterization of the geometry of two-dimensional braided fabrics," Text.Res.J., vol. 72, pp. 706-712, 2002.

[9] A. Rawal, S. Gupta, H. Saraswat and A. Sibal, "Geometrical modeling of near-net shape braided preforms," Text.Res.J., vol. 85, pp. 1055-1064, 2015.

[10] A. Rawal, P. Potluri and C. Steele, "Geometrical modeling of the yarn paths in three-dimensional braided structures," Journal of Industrial Textiles, vol. 35, pp. 115-135, 2005.

[11] J.H. Van Ravenhorst and R. Akkerman, "Circular braiding take-up speed generation using inverse kinematics," Compos Part A Appl Sci Manuf, vol. 64, pp. 147-158, 2014.

[12] C. Leung, "Examination of Braided Composite Geometric Factors Using Three Dimensional Digial Image Correlation Measurement Techniques," MSc. Thesis, 2012.

[13] C.K. Leung, G. Melenka, D.S. Nobes and J.P. Carey, "Validation of DIC as an Effective Tool for Composite Tubular Braid Characterization," in CSME International Congress, 2012.

[14] E.R. Davies, Machine vision. Theory, algorithms, practicalities, San Diego: Academic Press, 1997, .

[15] A.S. Malek, J.-. Drean, L. Bigue and J.-. Osselin, "Optimization of automated online fabric inspection by fast Fourier transform (FFT) and cross-correlation," Text.Res.J., vol. 83, pp. 256-268, 2013.

[16] D. Branscomb and D.G. Beale, "Fault detection in braiding utilizing low-cost USB machine vision," Journal of the Textile Institute, vol. 102, pp. 568-581, 2011.

[17] L. Matela, "Real-time fault detection of braiding ropes using recognition methods," in Proceedings of SPIE - The International Society for Optical Engineering, pp. 253-261, 2004.

[18] C. Mersmann, "Industrializing metrology - Machine vision integration in composites production," CIRP Ann.Manuf.Technol., vol. 60, pp. 511-514, 2011.

[19] T.A. Mitchell, R. Bowden and M. Sarhadi, "Automated visual inspection of dry carbon-fibre reinforced composite preforms," Proc.Inst.Mech.Eng.Part G J.Aerosp.Eng., vol. 213, pp. 377-386, 1999.

[20] R. Schmitt, A. Orth and C. Niggemann, "A method for edge detection of textile preforms using a light-section sensor for the automated manufacturing of fibre-reinforced plastics," in Proceedings of SPIE - The International Society for Optical Engineering, 2007.

[21] R. Schmitt, T. Pfeifer, C. Mersmann and A. Orth, "A method for the automated positioning and alignment of fibre-reinforced plastic structures based on machine vision," CIRP Ann.Manuf.Technol., vol. 57, pp. 501-504, 2008.

[22] C.-. Chan, "Fabric defect detection by Fourier analysis," IEEE Trans.Ind.Appl., vol. 36, pp. 1267-1276, 2000.

[23] D.-. Tsai and C.-. Hsieh, "Automated surface inspection for directional textures," Image Vision Comput., vol. 18, pp. 49-62, 1999.

[24] G.-. Hu, Q.-. Wang and G.-. Zhang, "Unsupervised defect detection in textiles based on Fourier analysis and wavelet shrinkage," Appl.Opt., vol. 54, pp. 2963-2980, 2015.

[25] J. Liu, B. Zhu, H. Jiang and W. Gao, "Image analysis measurement of cottonseed coat fragments in 100% cotton woven fabric," Fibers Polym., vol. 14, pp. 1208-1214, 2013.

[26] H. Sari-Sarraf and J.S. Goddard Jr., "Online optical measurement and monitoring of yarn density in woven fabrics," Proc SPIE Int Soc Opt Eng, vol. 2899, pp. 444-452, 1996.

[27] R. Gonzalez and R. Woods, Digital Image Processing, Prentice Hall, 2001, .

[28] W. Burger and M. Burge, Digital Image Processing: An Algorithmic Introduction Using Java, New York, USA: Springer, 2008, .

[29] R. Bracewell, Two-Dimensional Imaging, New Jersey, USA: Prentice-Hall, 1995, .

[30] Q. Zhang, D. Beale and R.M. Broughton, "Analysis of circular braiding process, Part 1: theoretical investigation of kinematics of the circular braiding process," J.Manuf.Sci.Eng.Trans.ASME, vol. 121, pp. 345-350, 1999.

[31] K. Birkefeld, M. Röder, T. Von Reden, M. Bulat and K. Drechsler, "Characterization of biaxial and triaxial braids: Fiber architecture and mechanical properties," Appl Compos Mater, vol. 19, pp. 259-273, 2012.

[32] A.A. Head, F.K. Ko and C.M. Pastore, Handbook of Industrial Braiding, Atkins and Pearce, 1989, .

[33] P. Monnot, J. Lvesque, O. Vermeersch and L.L. Lebel, "Automated braiding of dry preforms for aerospace structural components," in International SAMPE Technical Conference, 2016.

[34] A. Mazzawi, "The Steady State and Transient Behaviour of 2D Braiding, PhD Thesis," Ottawa-Carleton Institute for Mechanical and Aerospace Engineering, University of Ottawa, 2001.

[35] M.A. Ivey, J.P.R. Carey and C. Ayranci, "Braid reinforced polymeric rebar production and characterization," in International SAMPE Technical Conference, 2014.

Chapter 5 Conclusions and future work

5.1 Conclusions

Two-dimensional braiding is a high fiber deposition rate process capable of producing near-net shape fiber preforms. To improve the production process of 2D braided materials, the 36 carrier Steeger braiding machine at the Multipurpose Composites Group at the University of Alberta was used to develop an automated quality assurance system.

The goal of this project was to develop and validate an optical measurement technique, suitable for machine vision applications, capable of measuring the braid angle of tubular braided preforms in an automated and real-time fashion. This was done by first developing a Fourier transform measurement scheme and validating it with images of static tubular braided samples. The measurement technique was used to measure the braid angle during the braiding process in real-time. This work addresses shortcomings of 2D braided composite production. Due to the strong relationship between the fiber orientation and material properties, the braid angle is measured for quality assurance purposes. Current measurement methods are error prone and are not suitable for automation.

This system provides real-time feedback of the fiber orientation during the braiding process, which has not been previously accomplished through optical means. This system works to accomplish two specific issues regarding the production of the fiber structure. The first is that it gives the manufacturer the ability to ensure that the desired braid pattern is being produced from the selected braiding machine process parameters. This was previously an issue due to the inaccuracies associated with the commonly used kinematic braiding models. Secondly, it removes the need for manual quality assurance. This system allows the braid angle to be made

in-line with the production process and the braiding process will no longer have to stop to allow for manual braid angle measurements to be made. Instead, the braided preform can be impregnated in-line with the braiding process to improve throughput of the manufacturing process.

In this work, a single camera machine vision system was developed for making fiber orientation measurements of 2D tubular braided preforms. A single camera system was chosen in the interest of developing a low cost and real-time system at the expense of measurement accuracy. This decision meant that the fiber direction atop the tubular mandrel would be affected by perspective error. By modelling the deposition of a fiber onto the mandrel as the wrapping of an inclined line around a cylinder, a perspective error model predicting the fiber distortion in the image was developed. This model allowed the distribution of fiber angle to be predicted in images of tubular braids and allowed the effectiveness of image cropping to be determined. Cropping portions of the braid image allow the highly distorted fibers to be removed and decreases the braid angle distribution in the image.

The braid angle measurement method was tested on both stationary and translating braided preforms at various braid angles ranging from 30° to 63° and the measurement results were shown to have uncertainties which are less than manual measurement techniques and image based techniques which require user landmark selection. Braid angle measurements made using the Fourier transform were shown to have comparable accuracy when compared to DIC and photometric stereo methods. This was true for both static and dynamic measurements of braids with a constant braid angle. The machine vision system also successfully tracked the transient braid angle caused by a stepwise change in braiding speeds. These results showed that the transient braiding equations derived by Du and Popper are accurate in predicting the transient

braid angle the 36 carrier braiding setup that was used in the experiments. Kinematic braiding models have not previously been validated in real-time in-line with the braiding process.

The developed machine vision system was successful in making real-time, automated braid angle measurements with uncertainties of less than half that of currently used manual measurement techniques. The simplicity of the machine vision system makes this simple to integrate into braiding setups. The current state of braiding processes have not widely adopted machine vision and automated visual inspection technologies, and this work makes steps towards accomplishing this goal.

5.2 Limitations/recommendations

The machine vision system developed for measuring the braid angle of tubular preforms has shown to be successful for the tested braid geometry and braider configuration. The following recommendations will assist in improving this measurement technique and help to apply this technique to more braider configurations.

The optical setup had a relatively shallow depth of field. It was large enough to capture all of the necessary features on the tubular mandrel; however, it was possible that the mandrel displaces slightly and falls out of focus. The robustness of the measurement system would benefit from a wider depth of field. This can be accomplished by increasing the f-number of the optics, which requires a greater lighting intensity while still avoiding reflections from the braided fibers.

To improve camera stability and alignment, the optical equipment can be mounted with optical grade rails, sliders and mounts. The current system was assembled using 3D printed parts and basic aluminium rails. To improve the setup, it is suggested that optical rails be used if this system is desired to be used for long term applications.

The data collection was accomplished using an area scan camera. This did not have negative effects on the measurement results, however, the overlapping region of interest which occurs when capturing 2D images increases the total amount of data to be processed and stored. The use of a line scan camera may help to reduce the amount of data that must be stored for higher speed applications.

5.3 Future work

The development of this braid angle measurement system is the first automated visual inspection system for monitoring the production of braided fiber preforms. As a result, there are numerous aspects of braiding that can be monitored in real-time, or applications of this work that can be expanded upon. The project met all of its initial goals.

This measurement method has successfully been applied to the measurement of aramid fibers. No testing has been done on other common fibers used for fiber reinforced composites, such as carbon or glass fibers. However, the principles behind this measurement technique may suggest that this will work for properly imaged samples. The sample illumination plays the largest role in image collection and it may be necessary to modify the illumination setup to compensate for reflection or contrast issues that were not apparent during the imaging of aramid fibers.

The application of this work was limited to a tubular mandrel with a constant cross section. This was done to evaluate the feasibility of this real-time braid angle measurement system, however, not all braided composite parts will be tubular or have a constant cross section. For applications where the mandrel has a changing cross section, a variable focal length lens will be required to keep the sample within the focal plane. The image pre-processing used in this work was tailored to improving the measurement quality of fibers on tubular surfaces. It is possible that these steps

are insufficient, or not required for other mandrel geometries. It is not guaranteed that the exact approach outlined in this work will produce accurate fiber orientation measurements, the unique aspects of the mandrel geometry must be considered.

It is known that mandrel eccentricity causes a circumferential braid angle distribution. To detect this phenomenon, multiple cameras can be mounted to image the preform in different circumferential locations. Comparison of these measurements can be made to diagnose mandrel eccentricity.

A machine vision system for measuring the braid angle forms a portion of what is required to establish a closed loop feedback system to control a 2D braiding machine. By comparing the machine vision measurements to the desired, used defined braid geometry, braiding speeds can be automatically adjusted to obtain the desired braid structure. In order to accomplish this, a PID control scheme must be implemented to properly adjust the speeds. Additionally, a proper filtering scheme must be developed which removes the fluctuations in the braid angle measurement. The presence of these fluctuations could create instabilities in control scheme.

The dry fiber preform must be impregnated in resin in order to become a braided composite material. Due to the possibility that the fiber orientation can become changed after the fiber wetting process, this inline measurement technique should be tested on wet fibers as inline impregnation is an essential step in developing an automated manufacturing process.

References

[1] B. Schmitt, "The Making of the Lexus LFA Supercar. An inside report, chapter 2, The Clean Room," .

[2] M.A. Ivey, J.P.R. Carey and C. Ayranci, "Braid reinforced polymeric rebar production and characterization," in International SAMPE Technical Conference, 2014.

[3] A.D. Kelkar, J.S. Tate and R. Bolick, "Structural integrity of aerospace textile composites under fatigue loading," Materials Science and Engineering: B, vol. 132, pp. 79-84, 2006.

[4] C. Ayranci, "Predicting the Elastic Properties of Two Dimensionally Braided Tubular Composite Structures Towards the Design of Braid-Reinforced Polymer Medical Catheters," ProQuest Dissertations and Theses, 2010.

[5] A.J. Hunt and J.P. Carey, "Geometry Measurement of Tubular Braided Composite Materials for Real-Time Applications," in CANCOM 2015 - Canadian International Conference on Composite Materials, 2015.

[6] J.H. Van Ravenhorst and R. Akkerman, "Circular braiding take-up speed generation using inverse kinematics," Compos Part A Appl Sci Manuf, vol. 64, pp. 147-158, 2014.

[7] W. Michaeli, U. Rosenbaum and M. Jehrke, "Processing strategy for braiding of complex-shaped parts based on a mathematical process description," Composites Manuf., vol. 1, pp. 243-251, 1990.

[8] G.W. Du and P. Popper, "Analysis of a circular braiding process for complex shapes," Journal of the Textile Institute, vol. 85, pp. 316-337, 1994.

[9] J.-. Byun, "The analytical characterization of 2-D braided textile composites," Composites Sci.Technol., vol. 60, pp. 705-716, 2000.

[10] G. Guyader, A. Gabor and P. Hamelin, "Analysis of 2D and 3D circular braiding processes: Modeling the interaction between the process parameters and the pre-form architecture," Mechanism and Machine Theory, vol. 69, pp. 90-104, 2013.

[11] A.A. Head, F.K. Ko and C.M. Pastore, Handbook of Industrial Braiding, Atkins and Pearce, 1989, .

[12] Q. Zhang, D. Beale and R.M. Broughton, "Analysis of circular braiding process, Part 1: theoretical investigation of kinematics of the circular braiding process," J.Manuf.Sci.Eng.Trans.ASME, vol. 121, pp. 345-350, 1999.

[13] A. Rawal, S. Gupta, H. Saraswat and A. Sibal, "Geometrical modeling of near-net shape braided preforms," Text.Res.J., vol. 85, pp. 1055-1064, 2015.

[14] C. Ayranci, D. Romanyk and J.P. Carey, "Elastic properties of large-open-mesh 2D braided composites: Model predictions and initial experimental findings," Polymer Composites, vol. 31, pp. 2017-2024, 2010.

[15] G.W. Melenka, D.S. Nobes and J.P. Carey, "3D DIC Measurement of Tubular Braided Composites," in 19th International Conference on Composite Materials, 2013.

[16] C. Ayranci and J.P. Carey, "Experimental validation of a regression-based predictive model for elastic constants of open mesh tubular diamond-braid composites," Polymer Composites, vol. 32, pp. 243-251, 2011.

[17] J. Carey, M. Munro and A. Fahim, "Regression-based model for elastic constants of 2D braided/woven open mesh angle-ply composites," Polymer Composites, vol. 26, pp. 152-164, 2005.

[18] J.S. Tate and A.D. Kelkar, "Stiffness degradation model for biaxial braided composites under fatigue loading," Composites Part B: Engineering, vol. 39, pp. 548-555, 2008.

[19] A. Kelkar and J.D. Whitcomb, "Characterization and Structural Behavior of Braided Composites," U.S. Department of Transportation., Tech. Rep. DOT/FAA/AR-08/52, 2009.

[20] T. Liao and S. Adanur, "3D structural simulation of tubular braided fabrics for net-shape composites," Text.Res.J., vol. 70, pp. 297-303, 2000.

[21] J.S. Tate, A.D. Kelkar and J.D. Whitcomb, "Effect of braid angle on fatigue performance of biaxial braided composites," Int.J.Fatigue, vol. 28, pp. 1239-1247, 2006.

[22] S. Nasu, A. Ohtani, A. Nakai and H. Hamada, "Deformation behavior and mechanical properties of braided rectangular pipes," Composite Structures, vol. 92, pp. 752-756, 2010.

[23] K. Birkefeld, M. Röder, T. Von Reden, M. Bulat and K. Drechsler, "Characterization of biaxial and triaxial braids: Fiber architecture and mechanical properties," Appl Compos Mater, vol. 19, pp. 259-273, 2012.

[24] S.V. Lomov, R.S. Parnas, S.B. Ghosh, I. Verpoest and A. Nakai, "Experimental and theoretical characterization of the geometry of two-dimensional braided fabrics," Text.Res.J., vol. 72, pp. 706-712, 2002.

[25] C. Leung, "Examination of Braided Composite Geometric Factors Using Three Dimensional Digial Image Correlation Measurement Techniques," MSc. Thesis, 2012.

[26] J. Chen, T.M. McBride and S.B. Sanchez, "Sensitivity of Mechanical Properties to Braid Misalignment in Triaxial Braid Composite Panels," J.Compos.Technol.Res., vol. 20, pp. 13-17, 1998.

[27] G.W. Melenka, E. Lepp, B.K.O. Cheung and J.P. Carey, "Micro-computed tomography analysis of tubular braided composites," Compos.Struct., vol. 131, pp. 384-396, 2015.

[28] A.E. Scott, I. Sinclair, S.M. Spearing, M.N. Mavrogordato and W. Hepples, "Influence of voids on damage mechanisms in carbon/epoxy composites determined via high resolution computed tomography," Compos.Sci.Technol., vol. 90, pp. 147-153, 2014.

[29] D. Brunschweiler, "Braids and Braiding," Journal of the Textile Institute Proceedings, vol. 44, pp. 666-686, 1953.

[30] A. Mazzawi, "The Steady State and Transient Behaviour of 2D Braiding, PhD Thesis," Ottawa-Carleton Institute for Mechanical and Aerospace Engineering, University of Ottawa, 2001.

[31] ISO 10122:2014, "ISO 10122:2014 Reinforcement Materials - Tubular Braided Sleeves - Basis for Specification
," 2014.

[32] G.W. Du, P. Popper and T.W. Chou, "Process Model of Circular Braiding for Complex Shaped Preform Manufacturing," in Proc. Symp. on Processing of Polymers and Polymeric Composites, 1990.

[33] H. Nishimoto, A. Ohtani, A. Nakai and H. Hamada, "Generation for circumferential distribution of braiding angle on cylindrical tubular braided fabrics," in Proceedings of the 9th International Conference on Textile Composites - TEXCOMP9: Recent Advances in Textile Composites, pp. 471-480, 2008.

[34] H. Nishimoto, A. Ohtani and A. Nakai, "Prediction method for temporal change in fiber bundle orientation on cylindrical braided preforms," Sen'i Gakkaishi, vol. 68, pp. 27-32, 2012.

[35] F.K. Ko, "Braiding," in Engineered Materials Handbook, Metals Park, OH: ASM International, 1987, pp. 519-528.

[36] H. Nishimoto, A. Ohtani, A. Nakai and H. Hamada, "Generation and prediction methods for circumferential distribution changes in the braiding angle on a cylindrical braided fabric," Proc.Inst.Mech.Eng.Part L J.Mat.Des.Appl., vol. 224, pp. 71-78, 2010.

[37] A. Rawal, P. Potluri and C. Steele, "Geometrical modeling of the yarn paths in three-dimensional braided structures," Journal of Industrial Textiles, vol. 35, pp. 115-135, 2005.

[38] H. Nishimoto, A. Ohtani, A. Nakai and H. Hamada, "Prediction method for temporal change in fiber orientation on cylindrical braided preforms," Text.Res.J., vol. 80, pp. 814-821, 2010.

[39] A. Rawal, A. Sibal and H. Saraswat, "Tensile behaviour of regular triaxial braided structures," Mech.Mater., vol. 91, pp. 277-289, 2015.

[40] J.H. Van Ravenhorst and R. Akkerman, "A yarn interaction model for circular braiding," Compos Part A Appl Sci Manuf, vol. 81, pp. 254-263, 2016.

[41] Q. Zhang, D. Beale, R.M. Broughton and S. Adanur, "Analysis of circular braiding process, part 2: Mechanics analysis of the circular braiding process and experiment," J.Manuf.Sci.Eng.Trans.ASME, vol. 121, pp. 351-357, 1999.

[42] A.K. Pickett, J. Sirtautas and A. Erber, "Braiding simulation and prediction of mechanical properties," Applied Composite Materials, vol. 16, pp. 345-364, 2009.

[43] A. Pickett, A. Erber, T. Von Reden and K. Drechsler, "Comparison of analytical and finite element simulation of 2D braiding," Plast.Rubber Compos., vol. 38, pp. 387-395, 2009.

[44] P. Monnot, J. Lvesque, O. Vermeersch and L.L. Lebel, "Automated braiding of dry preforms for aerospace structural components," in International SAMPE Technical Conference, 2016.

[45] A. Rawal, A. Sibal, H. Saraswat and V. Kumar, "Geometrically controlled tensile response of braided sutures," Mater.Sci.Eng.C, vol. 48, pp. 453-456, 2015.

[46] C.K. Leung, G. Melenka, D.S. Nobes and J.P. Carey, "Validation of DIC as an Effective Tool for Composite Tubular Braid Characterization," in CSME International Congress, 2012.

[47] S. Thumfart, W. Palfinger, M. Stöger and C. Eitzinger, "Accurate fibre orientation measurement for carbon fibre surfaces," Lecture Notes in Computer Science (Including

Subseries Lecture Notes in Artificial Intelligence and Lecture Notes in Bioinformatics), vol. 8048 LNCS, 2013.

[48] S. Zambal, W. Palfinger, M. Stger and C. Eitzinger, "Accurate fibre orientation measurement for carbon fibre surfaces," Pattern Recogn., vol. 48, pp. 3324-3332, 2015.

[49] B. Jahne, H. Haussecker and P. Grissler, "Reflectance-Based Shape Recovery," in Handbook of Computer Vision and Applications, San Diego, CA: Academic Press, 1999, pp. 532-590.

[50] T. Schambron, A. Lowe and H.V. McGregor, "Effects of environmental ageing on the static and cyclic bending properties of braided carbon fibre/PEEK bone plates," Composites Part B: Engineering, vol. 39, pp. 1216-1220, 2008.

[51] C. Ayranci and J.P. Carey, "Predicting the longitudinal elastic modulus of braided tubular composites using a curved unit-cell geometry," Composites Part B: Engineering, vol. 41, pp. 229-235, 2010.

[52] J. Carey, M. Munro and A. Fahim, "Longitudinal elastic modulus prediction of a 2-D braided fiber composite," J Reinf Plast Compos, vol. 22, pp. 813-831, 2003.

[53] H. Nishimoto, A. Ohtani, A. Nakai and H. Hamada, "Generation and prediction methods for circumferential distribution changes in the braiding angle on a cylindrical braided fabric," Proceedings of the Institution of Mechanical Engineers, Part L: Journal of Materials: Design and Applications, vol. 224, pp. 71-78, 2010.

[54] J. Carey, G. Melenka, A. Hunt, C.M. Pastore and F.K. Ko, "Advanced testing of braided composites," in Handbook of Advances in 2D and 3D Braided Composite Materials, Woodhead Publishing, 2016, .

[55] L. Matela, "Real-time fault detection of braiding ropes using recognition methods," in Proceedings of SPIE - The International Society for Optical Engineering, pp. 253-261, 2004.

[56] C.J. Creighton, M.P.F. Sutcliffe and T.W. Clyne, "Multiple field image analysis procedure for characterization of fibre alignment in composites," Compos Part A Appl Sci Manuf, vol. 32, pp. 221-229, 2001.

[57] L. Shi and S. Wu, "Automatic Fiber Orientation Detection for Sewed Carbon Fibers," Tsinghua Sci.Tech., vol. 12, pp. 447-452, 2007.

[58] R. Schmitt, T. Pfeifer, C. Mersmann and A. Orth, "A method for the automated positioning and alignment of fibre-reinforced plastic structures based on machine vision," CIRP Ann.Manuf.Technol., vol. 57, pp. 501-504, 2008.

[59] R. Schmitt, C. Mersmann and A. Schoenberg, "Machine vision industrialising the textile-based frp production," in ISPA 2009 - Proceedings of the 6th International Symposium on Image and Signal Processing and Analysis, pp. 270-274, 2009.

[60] T. Aach, C. Mota, I. Stuke, M. Mühlich and E. Barth, "Analysis of superimposed oriented patterns," IEEE Trans.Image Process., vol. 15, pp. 3690-3700, 2006.

[61] T. Aach, I. Stuke, C. Mota and E. Barth, "Estimation of multiple local orientations in image signals," in ICASSP, IEEE International Conference on Acoustics, Speech and Signal Processing - Proceedings, pp. III556, 2004.

[62] B. Pourdeyhimi, R. Dent and H. Davis, "Measuring fiber orientation in nonwovens - Part III: Fourier transform," Text.Res.J., vol. 67, pp. 143-151, 1997.

[63] K.Y. Kang, K.Y. Lee, K.J. Jo and H.S. Kim, "Anisotropy in structure and mechanical properties of perpendicular-laid nonwovens," J.Mater.Sci., vol. 43, pp. 2754-2760, 2008.

[64] H.S. Kim, "Relationship between Fiber Orientation Distribution Function and mechanical anisotropy of thermally point-bonded nonwovens," Fibers Polym., vol. 5, pp. 177-181, 2004.

[65] M. Tunak, J. Antoch, J. Kula and J. Chvojka, "Estimation of fiber system orientation for nonwoven and nanofibrous layers: Local approach based on image analysis," Text.Res.J., vol. 84, pp. 989-1006, 2014.

[66] C. Redon, L. Chermant, J.-. Chermant and M. Coster, "Assessment of fibre orientation in reinforced concrete using Fourier image transform," J.Microsc., vol. 191, pp. 258-265, 1998.

[67] C.-. Chan, "Fabric defect detection by Fourier analysis," IEEE Trans.Ind.Appl., vol. 36, pp. 1267-1276, 2000.

[68] A.S. Malek, J.-. Drean, L. Bigue and J.-. Osselin, "Optimization of automated online fabric inspection by fast Fourier transform (FFT) and cross-correlation," Text.Res.J., vol. 83, pp. 256-268, 2013.

[69] D.-. Tsai and C.-. Hsieh, "Automated surface inspection for directional textures," Image Vision Comput., vol. 18, pp. 49-62, 1999.

[70] G.-. Hu, Q.-. Wang and G.-. Zhang, "Unsupervised defect detection in textiles based on Fourier analysis and wavelet shrinkage," Appl.Opt., vol. 54, pp. 2963-2980, 2015.

[71] J. Liu, B. Zhu, H. Jiang and W. Gao, "Image analysis measurement of cottonseed coat fragments in 100% cotton woven fabric," Fibers Polym., vol. 14, pp. 1208-1214, 2013.

[72] H. Sari-Sarraf and J.S. Goddard Jr., "Online optical measurement and monitoring of yarn density in woven fabrics," Proc SPIE Int Soc Opt Eng, vol. 2899, pp. 444-452, 1996.

[73] A. Kumar, "Computer-vision-based fabric defect detection: A survey," IEEE Trans.Ind.Electron., vol. 55, pp. 348-363, 2008.

[74] B. Lian, L. Jiang, J.J. McGrath and J. Jaranson, "Quantitative determination of morphological features of triaxially braided composites by the use of machine vision," Composites Sci.Technol., vol. 60, pp. 159-166, 2000.

[75] Z. Wan and J. Li, "Measurement Research of Parameter on Three-dimensional Braided Composite Material Preform Surface," J Compos Mater, vol. 38, pp. 435-448, 2004.

[76] Z. Wan and J. Li, "Braided angle measurement technique for three-dimensional braided composite material preform using mathematical morphology and image texture," Autex Res.J., vol. 6, pp. 30-39, 2006.

[77] E.R. Davies, Machine vision. Theory, algorithms, practicalities, San Diego: Academic Press, 1997, .

[78] E.J. Wood, "Applying Fourier and Associated Transforms to Pattern Characterization in Textiles," Text.Res.J., vol. 60, pp. 212-220, 1990.

[79] R. Gonzalez and R. Woods, Digital Image Processing, Prentice Hall, 2001, .

[80] R. Bracewell, Two-Dimensional Imaging, New Jersey, USA: Prentice-Hall, 1995, .

[81] B. Osgood, "Lecture Notes for EE 261 The Fourier Transform and its Applications" .

[82] W. Burger and M. Burge, Digital Image Processing: An Algorithmic Introduction Using Java, New York, USA: Springer, 2008, .

[83] J.E. Bresenham, "Algorithm for computer control of a digital plotter," IBM Systems Journal, vol. 4, 1965.

[84] P. Potluri, A. Rawal, M. Rivaldi and I. Porat, "Geometrical modelling and control of a triaxial braiding machine for producing 3D preforms," Composites Part A: Applied Science and Manufacturing, vol. 34, pp. 481-492, 2003.

[85] T.M. Apostol and M.A. Mnatsakanian, "Unwrapping curves from cylinders and cones," Am.Math.Mon., vol. 114, pp. 388-416, 2007.

[86] C. Ayranci and J. Carey, "2D braided composites: A review for stiffness critical applications," Composite Structures, vol. 85, pp. 43-58, 2008.

[87] D. Branscomb and D.G. Beale, "Fault detection in braiding utilizing low-cost USB machine vision," Journal of the Textile Institute, vol. 102, pp. 568-581, 2011.

[88] C. Mersmann, "Industrializing metrology - Machine vision integration in composites production," CIRP Ann.Manuf.Technol., vol. 60, pp. 511-514, 2011.

[89] T.A. Mitchell, R. Bowden and M. Sarhadi, "Automated visual inspection of dry carbon-fibre reinforced composite preforms," Proc.Inst.Mech.Eng.Part G J.Aerosp.Eng., vol. 213, pp. 377-386, 1999.

[90] R. Schmitt, A. Orth and C. Niggemann, "A method for edge detection of textile preforms using a light-section sensor for the automated manufacturing of fibre-reinforced plastics," in Proceedings of SPIE - The International Society for Optical Engineering, 2007.

Appendix A The discrete Fourier transform

A.1 Periodicity of the 2D discrete Fourier transform

The use of the 2D discrete Fourier transform (2D-DFT) assumes that the input signal is periodic in every dimension [1, 2]. This means that in addition to the spatial features in the image, the discontinuities between images are also brought into the frequency spectrum. This means that rather than a single image, a mosaic of MxN images, as shown in Figure A-1, is implied by the 2D-DFT. The discontinuities can also be seen in Figure A-1 at the image border. In the frequency spectrum, this would appear as a high vertical frequency which is not representative of any spatial features in the braid image.

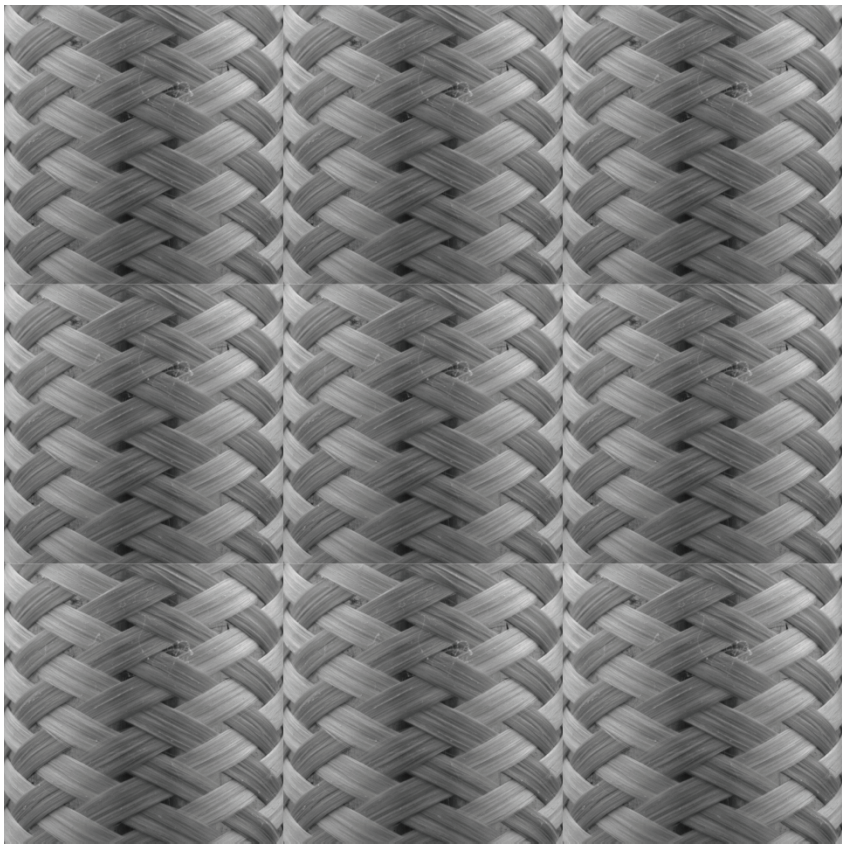

Figure A-1: Image of braided preform showing the discontinuities at the image boundaries associated with the implied periodicity of the 2D-DFT

A.2 Spatial windowing

To eliminate discontinuities between images resulting from the implied periodicity of the input signal, spatial windowing can be used. This is where the original image, $g(x, y)$ can be multiplied by a windowing function, $w(x, y)$ prior to the frequency domain transformation. The role of the windowing function is to attenuate the pixel values at the image borders, which at the expense of adding new low frequency data, removes the discontinuities at the image borders. One example of such a window is the circular Hanning window, as shown in Equation A.1, which attenuates pixels based on their distance from the center of the image, $r(x, y)$. The effect that this has on the spatial image and spectrum is shown in Figure A-2.

$$w(x, y) = 0.5 - 0.5 \cos\left(\pi * \left(1 - \frac{r(x, y)}{r_{max}}\right)\right) \tag{A.1}$$

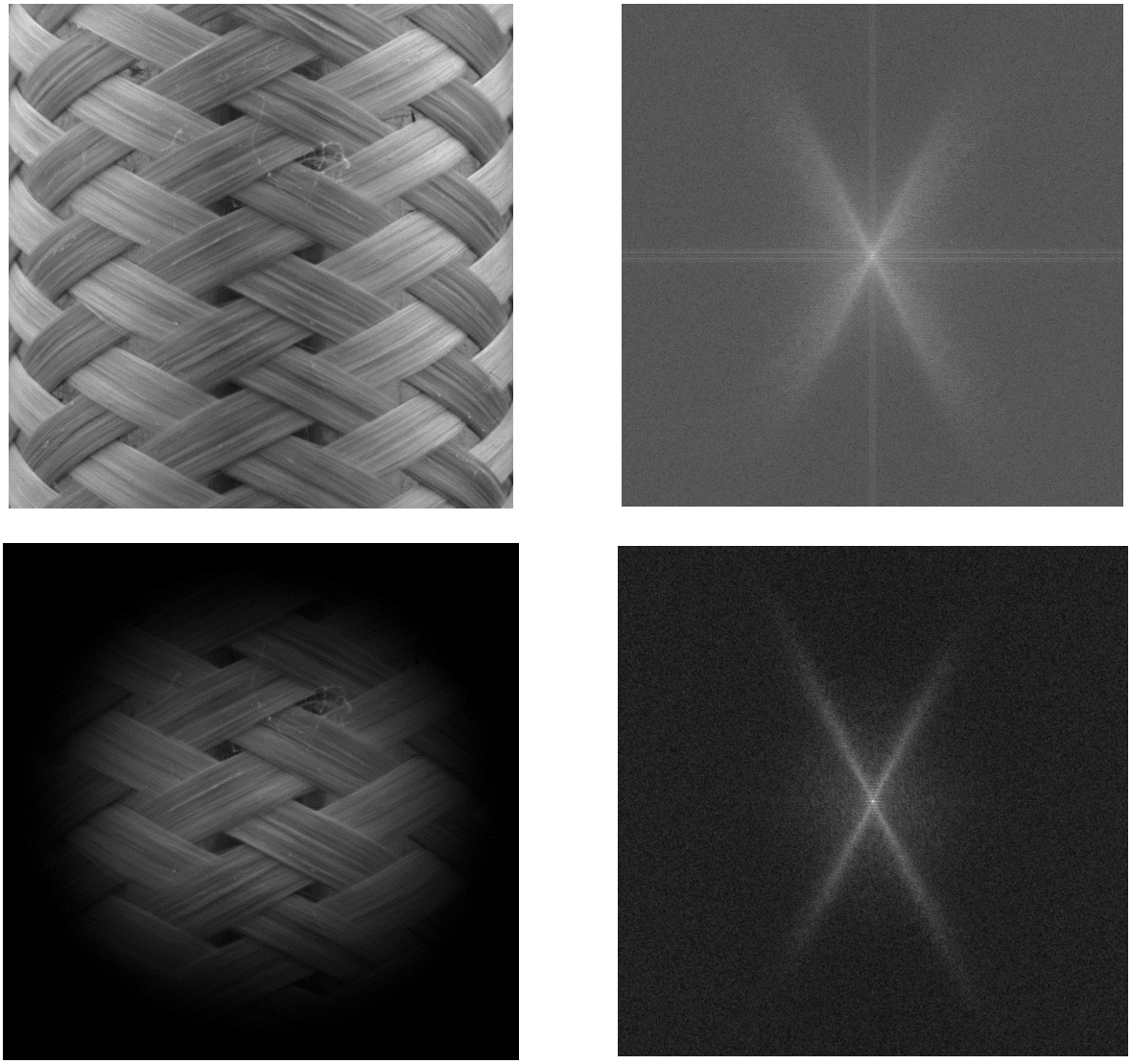

Figure A-2: Spatial image and frequency pairs of the original image (top) and the windowed image (bottom) showing the removal of the high vertical and horizontal frequencies

Spatial windowing was found to not be a necessary step for determining the braid angle of biaxial braids. Early work found that spatial windowing successfully attenuated the distorted fibers in the image; however, the development of the image cropping routine produced better results by cropping the distorted fibers as opposed to attenuating these portions of the image with a windowing function. The cropping method also offered the advantage of not attenuating data

in the image. Combining windowing and cropping was not used because of the aspect ratio of the image, which causes a significant loss of information, shown in Figure A-3.

The effect that these horizontal and vertical frequencies in the frequency spectrum have on the braid angle measurement is negligible. These are shown as high frequency spikes at 0° and ±90° degrees in the angular intensity plot, shown in Figure A-4. These frequencies are ignored during the search routine and do not affect the braid angle measurement. If this measurement technique is to be applied to triaxial braids, the concept of spatial windowing may have to be used. The longitudinal fibers will contribute to horizontal frequency components which will be important for characterizing braid geometry and may not be ignored as was previously done.

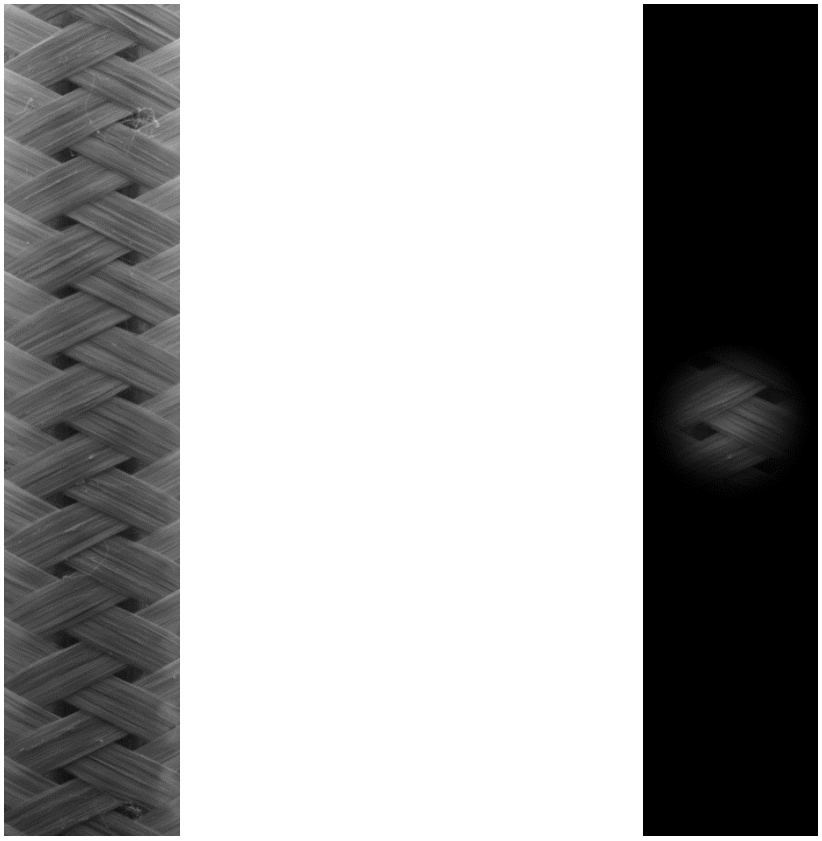

Figure A-3: Application of a circular windowing function to cropped images showing a significant removal of spatial information

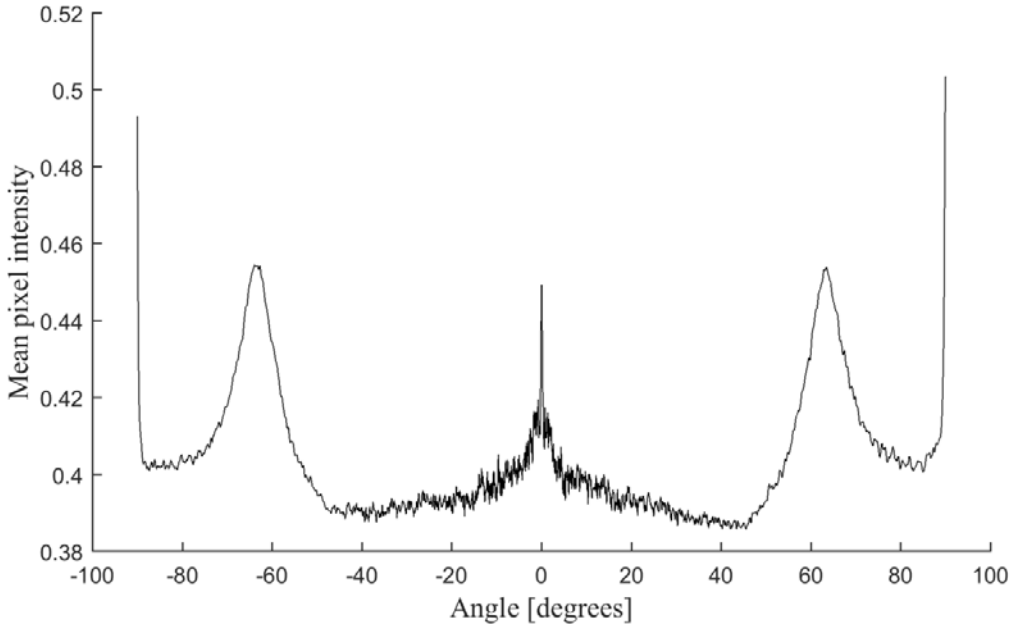

Figure A-4: Angular intensity plot of a 63° braided preform showing the high frequency components at 0° and ±90°.

A.3 References

[1] W. Burger and M. Burge, Digital Image Processing: An Algorithmic Introduction Using Java, New York, USA: Springer, 2008, .

[2] R. Gonzalez and R. Woods, Digital Image Processing, Prentice Hall, 2001, .

Appendix B Mathematical validation of the preservation of angular features in the frequency domain

This appendix uses the Fourier transform of the impulse pair to demonstrate that the angular orientation of features in the spatial domain, and the orientation of the frequencies remains the same for a square frequency spectrum. This is done by looking at the derivation of the Fourier transform of a symmetric impulse pair. This derivation shows that the position of the impulses relative to the center of the spatial image is the same as the horizontal and vertical frequencies of the resulting two-dimensional sinusoid in the frequency domain.

B.1 Fourier transform of an impulse pair

Consider an impulse pair which is symmetric about the (0,0) coordinate in the spatial domain. The impulses are located at (*a*,*b*) and (-*a*,-*b*).

$$0.5\delta^2(x+a,y+b)+0.5\delta^2(x-a,y-b) \tag{B.1}$$

The two dimensional delta function, δ^2, is given by Equation B.2

$$\delta^2(x+a,y+b)=\delta(x+a)\delta(y+b) \tag{B.2}$$

Taking the 2D Fourier transform of the impulse pair:

$$\int_{-\infty}^{\infty}\int_{-\infty}^{\infty}[0.5\delta^2(x+a,y+b)+0.5\delta^2(x-a,y-b)]e^{-i2\pi(ux+vy)}dxdy \tag{B.3}$$

By expanding the two dimensional delta functions in Equation B.3 with the relationship given in Equation B.2:

$$\int_{-\infty}^{\infty}\int_{-\infty}^{\infty}[0.5\delta(x+a)\delta(y+b)+0.5\delta(x-a)\delta(y-b)]e^{-i2\pi(ux+vy)}dxdy \tag{B.4}$$

Equation B.4 can be simplified with the application of the sifting property, which is an important property of the delta function [1]. The 2D sifting property for an arbitrary function $f(x,y)$ is given by:

$$\int_{-\infty}^{\infty}\int_{-\infty}^{\infty}f(x,y)\delta(x-a)\delta(y-b)dxdy = f(a,b) \tag{B.5}$$

Applying the sifting property shown in Equation B.5 to Equation B.4, it becomes equation:

$$\int_{-\infty}^{\infty}\int_{-\infty}^{\infty}[0.5\delta(x+a)\delta(y+b)]e^{-i2\pi(ux+vy)}dxdy + \int_{-\infty}^{\infty}\int_{-\infty}^{\infty}[0.5\delta(x-a)\delta(y-b)]e^{-i2\pi(ux+vy)}dxdy \tag{B.6}$$

Evaluating each term at (–a,-b) and (a,b) respectively:

$$0.5e^{-i2\pi(u(-a)+v(-b))} + 0.5e^{-i2\pi(u(a)+v(b))} \tag{B.7}$$

Expanding this using Euler's equation:

$$0.5\left[\cos\left(2\pi(ua+vb)\right)+isin\left(2\pi(ua+vb)\right)\right] + 0.5\left[\cos\left(2\pi(ua+vb)\right)-isin\left(2\pi(ua+vb)\right)\right] \tag{B.8}$$

Simplifying:

$$\cos(2\pi(ua+vb)) \tag{B.9}$$

This result shows that the location of the spatial features directly affects the orientation of features in the frequency spectrum. The derivation process of going from an impulse pair in the spatial domain, to a sinusoid in the frequency domain shown in Figure B-1, was done due to simplicity of the derivation. However, because these two functions are a Fourier transform pair,

the inverse relationship is true; namely, taking the 2D Fourier transform of a 2D sinusoid will produce an impulse pair.

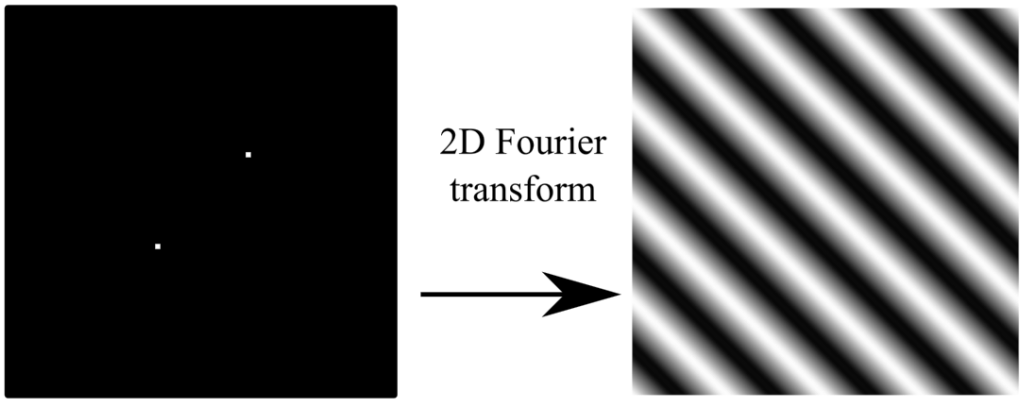

Figure B-1: Schematic showing the Fourier transform pair that is derived in this Appendix showing the rotational similarity between the spatial impulse pair and the sinusoid in the frequency domain

The process of applying the Fourier transform to a 2D image can be thought of as follows. The lines and features in the spatial image are all represented by a series of 2D sinusoids of varying frequencies and amplitudes. The 2D Fourier transform of each of these sinusoids produces an impulse pair which is symmetric about the origin of the frequency spectrum. Due to the relationship between the orientation of the sinusoids and the impulse pairs that was previously derived, the angle of spatial features can be measured from their orientation in the frequency spectrum.

B.2 References

[1] R. Bracewell, Two-Dimensional Imaging, New Jersey, USA: Prentice-Hall, 1995, .

Appendix C Effect of image preprocessing on braid angle measurement results

Several image pre-processing techniques were used in an attempt to improve the measurement quality. Measuring the braid angle involves measuring the direction of the yarn boundaries, hence, image processing techniques were selected by their ability to either accentuate these features of interest or removes unnecessary image data. Early work involving image processing techniques tested the effect of edge detection and median filtering.

C.1 Edge detection

Edges are boundaries which are marked by changes in grayscale intensity which separate regions in an image [1]. An ideal edge consists of an instantaneous change in pixel value; however, due to factors including optical aberrations, discrete sampling and image spatial resolution, a digital edge model is used [1]. The difference between these two can be seen in grayscale representations, as well as a grayscale profiles. Figure C-1 (b) also shows the first derivative of the grayscale profile, which results in a step function. The location and size of these steps show how common gradient based edge detection schemes work.

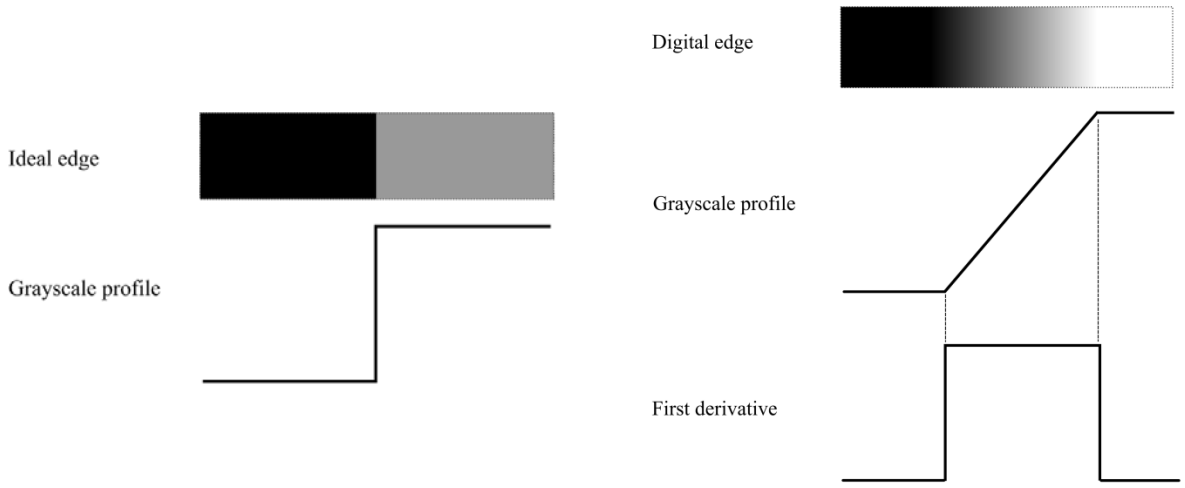

Figure C-1: Schematic of the ideal (a) and digital edge models (b). In each image, a representation of the grayscale image and profile of the edges can be seen.

Gradient based edge detection use convolution kernels to approximate the first order derivative in the image. Convolving the image with convolution kernel allows the image gradients to be determined. The Prewitt edge detection kernel is a simple 3x3 edge detection kernel which approximates the first derivative; the horizontal and vertical kernels are shown in Equations C.1 and C.2 respectively.

$$\begin{matrix} -1 & 0 & 1 \\ -1 & 0 & 1 \\ -1 & 0 & 1 \end{matrix} \tag{C.1}$$

$$\begin{matrix} -1 & -1 & -1 \\ 0 & 0 & 0 \\ 1 & 1 & 1 \end{matrix} \tag{C.2}$$

The Canny edge detection algorithm uses these principles to detect image gradients, and to improve performance, the process combines Gaussian noise removal filtering and edge tracking routines to combine broken contours [1, 2].

The application of an edge detection routine produces a binary image with edges marked with 1's. This process removes low frequency data and weak boundary features. The effect of applying the Canny edge detection algorithm to a braid image is shown in Figure C-2

(a) (b)

Figure C-2: Raw braid image (a), and Canny edge detection applied to the braid image (b).

C.2 Median filtering

Median filtering is a common, non-linear noise removal filter. Which modifies image pixels by replacing the current pixel with the medial of all neighboring pixel values in a given window size [1, 2]. One of the adverse effects of median filtering is that it affects all pixels in the image. The goal of the median filter was to remove the un-necessary fiber orientation within each yarn. The braid angle is a measure of the yarn directions and in an attempt to isolate these directions, this filtering process was tested. The effect of median filtering on the braid images can be seen in

Figure C-3. Through visual inspection, the application of the median filter appears to smooth the individual fibers at the expense of also blurring the fiber boundaries.

(a) (b)

Figure C-3: Raw braid image (a), braid image processed with a 13x13 median filter (b).

C.3 Combining edge detection and median filtering

The edge detection image shown in Figure C-2successfully produces a binary image showing all significant contours in the raw image. This process means the contours from the fibers are given an identical weighting the frequency domain due to the binary nature of the image. This is undesirable as the braid angle is measured by the direction of the braid yarns, not the individual fibers. By blurring the raw image with a median filter prior to detecting edges with the Canny algorithm, the images shown in Figure C-4 show that by increasing the size of the median filter, which increases the amount of blurring, edges are removed.

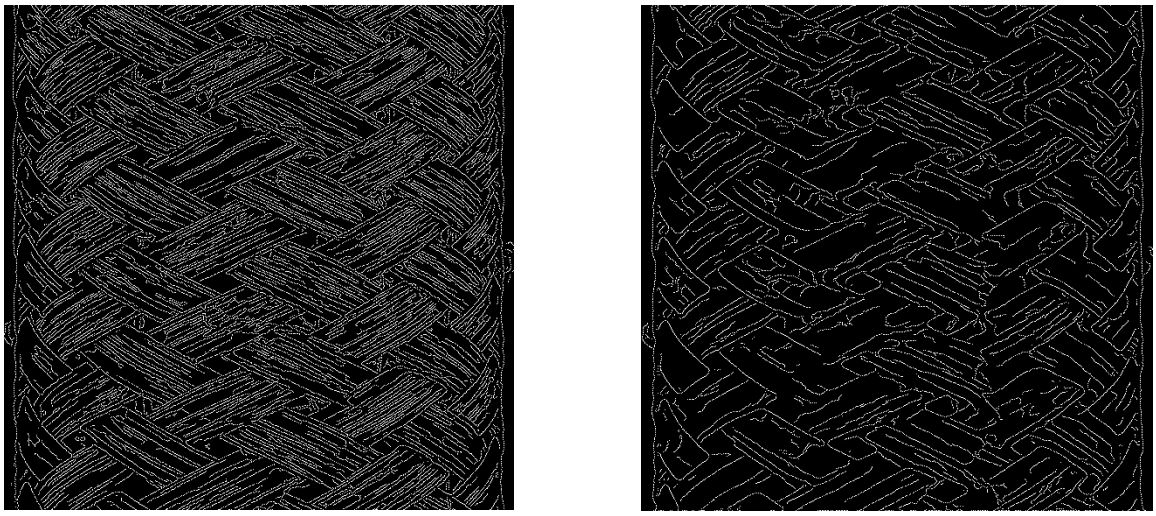

(a) (b)

Figure C-4: Images comparing the effect of using a median filter prior to the edge detection process. The size of the median filter has an effect on the detected edges, 5x5 median filter (a), and 17x17 median filter (b)

C.4 Results

To determine the effect that each of these processes had on the frequency spectrum of the images, the angular intensity plots can be compared. Figure C-5 show the effect of raw images and the previously discussed preprocessing options. Both the raw and edge detection images shown sharp symmetric peaks which is desirable for a proper braid angle measurement. The 13x13 median filter removes high frequency data by blurring features in the image, which results in a lower mean pixel intensity and a flatter peaks for the fiber directions.

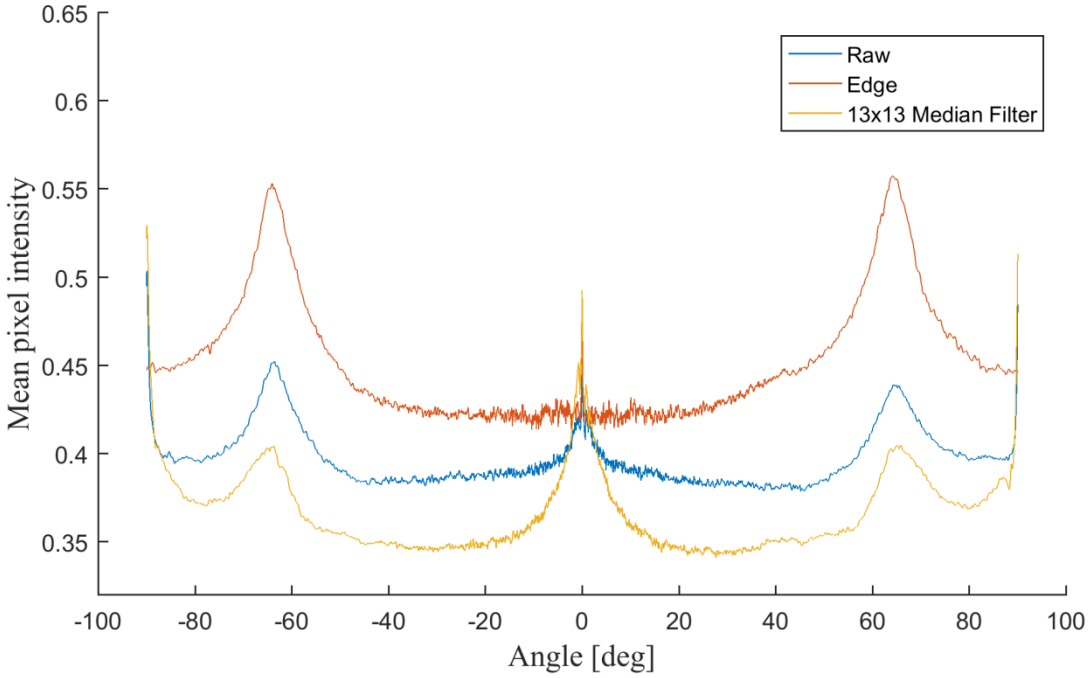

Figure C-5: Angular intensity plot of braid preforms comparing the raw image, Canny edge detection and median filtering.

To quantify the effect of these image preprocessing techniques, four images of a 63° braid preform were tested. These results are shown in Table C-1 which shows that the average measurement remains relatively unchanged, whereas for the median filter, the deviation significantly increases due to the removal of high frequency data.

Table C-1: Machine vision braid angle measurements for edge detection and median filtering preprocessing techniques.

	Machine vision braid angle [deg]		
	Raw image	Edge detection	13x13 Median filter
Mean	63.61	63.60	63.36
St. Dev.	0.40	0.49	0.87

The application of the median filter before the Canny edge detection causes nearly identical results as the edge image without median filtering. Changing the size of the median filter does not significantly change the frequency spectrum, which is shown in Figure C-6.

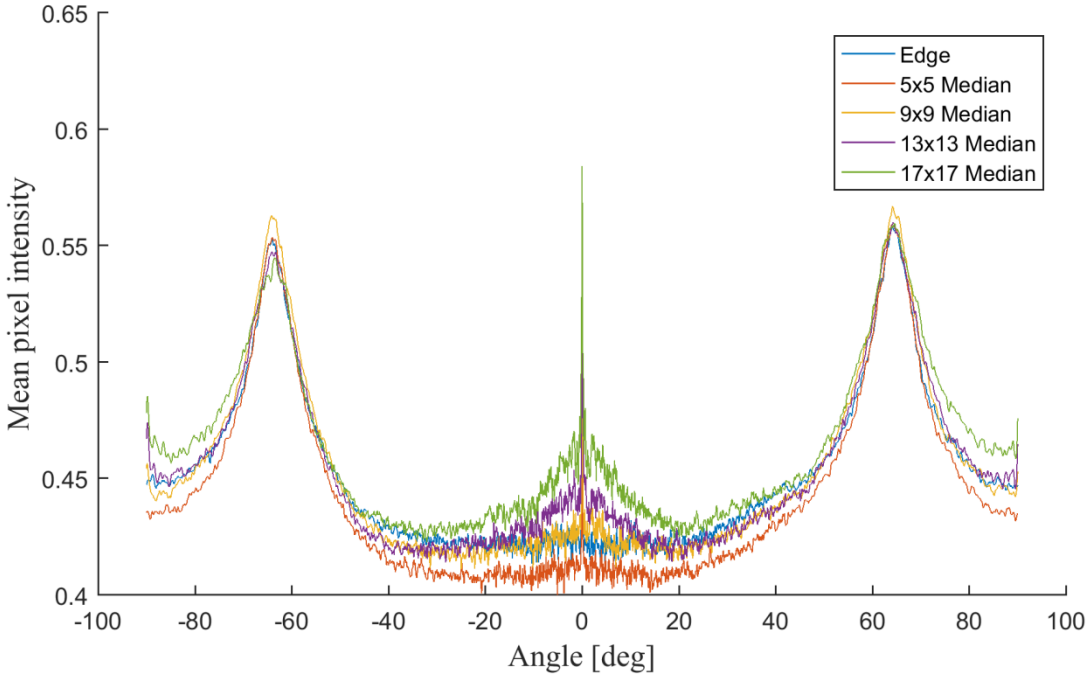

Figure C-6: Angular intensity plot showing the effect of combining Canny edge detection and median filtering. Changing the size of the median filter has little effect on the angular intensity of the frequency spectrum.

C.5 Conclusions

Image preprocessing was tested to improve the quality of the measurements by isolating relevant features for braid angle measurement. These methods were found to have a minimal impact on the braid angle measurement, as well as increase the deviation between consequent measurements. As a result, these image processing techniques were not included as a part of the image processing routine.

C.6 References

[1] R. Gonzalez and R. Woods, Digital Image Processing, Prentice Hall, 2001, .

[2] W. Burger and M. Burge, Digital Image Processing: An Algorithmic Introduction Using Java, New York, USA: Springer, 2008, .

Appendix D Braiding speed calibration

This appendix contains information relating to the calibration procedure and results of the braiding speed calibration required to convert from volts to rotational speed of the yarn carriers and from volts to linear speed of the mandrel.

D.1 Puller calibration

Calibration of the puller was done by determining the time taken for the mandrel to advance a distance of 300mm at different specified voltages. Each voltage was tested twice and all trials were randomized. Pulling tests were done in a fully loaded configuration which was done by fastening all of the braid yarns to the mandrel to include the force required to pull the yarns. The results shown in Figure D-1 show a linear trend which with a R^2 value of 0.9997.

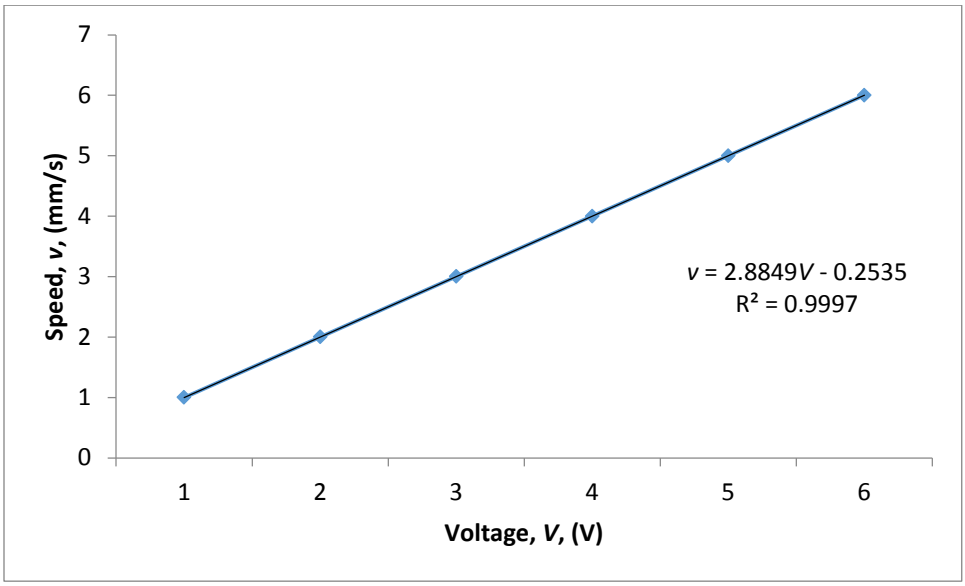

Figure D-1: Speed versus voltage relationship for the puller

D.2 Braider calibration

Calibration of the braider was done to determine the relationship between the supplied voltage and the rotational speed of the yarn carriers. This was done by determining the time taken for a yarn carrier to complete two revolutions around the track plate. Each voltage was tested twice in a random order. The results are shown in Figure D-2. Similar to the puller calibration, the yarns were fastened to the mandrel prior to starting the test to represent the expected braiding conditions. The results in Figure D-2 show a linear trend which with a R^2 value of 0.9999.

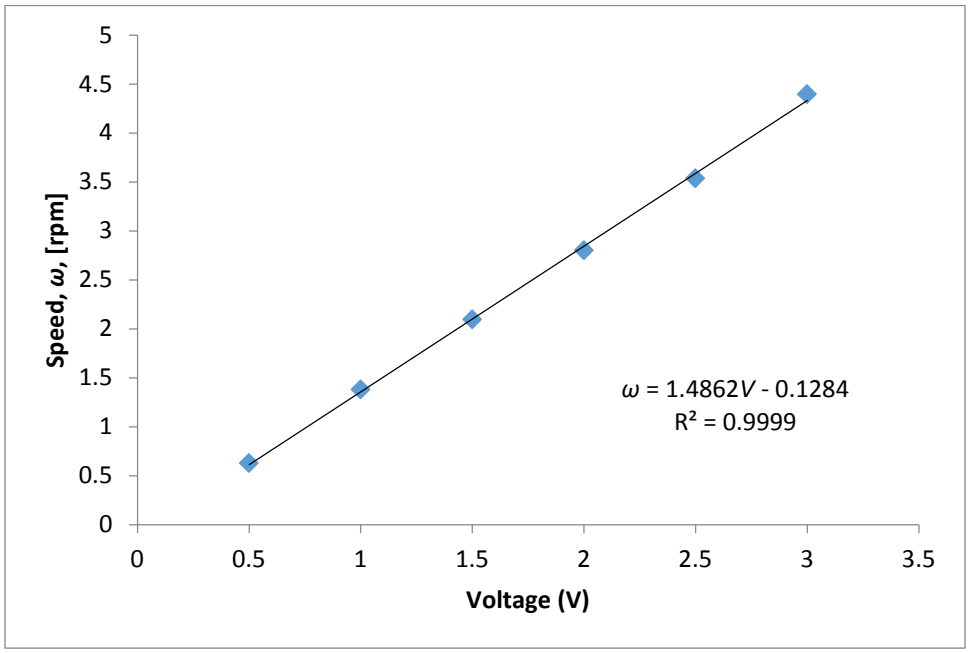

Figure D-2: Rotational speed versus voltage plot for the braiding machine